Alma Mater Studiorum – Università di Bologna

DOTTORATO DI RICERCA IN

Ingegneria Civile, Chimica, Ambientale e dei Materiali

Ciclo XXX

**Settore Concorsuale:** 09/D2

**Settore Scientifico Disciplinare:** ING-IND/24

# PURIFICATION OF ANTIBODIES THROUGH CONVECTIVE CHROMATOGRAPHY

Presentata da: **Eleonora Lalli**

Supervisore
**Cristiana Boi**

Co-Supervisore
**Giulio C. Sarti**

Coordinatore Dottorato
**Luca Vittuari**

*I hate tennis, hate it with all my heart, and still I keep playing, keep hitting all morning, and all afternoon, because I have no choice. No matter how much I want to stop, I don't. I keep begging myself to stop, and I keep playing, and this gap, this contradiction between what I want to do and what I actually do, feels like the core of my life.*

*-Andre Agassi*

# ABSTRACT

Downstream processing of immunoglobulin G is conventionally performed by bead-based column chromatography; affinity chromatography with Protein A is the most selective process in biotechnological industry for the purification of antibodies. However, this method suffers from several limitations, such as high pressure drops across the column, compaction of the granular porous bed and low diffusivity between the particles. In addition to fluid dynamic problems, the traditional process is affected by limitations related to the use of Protein A as affinity ligand. Materials activated with Protein A are very expensive, since the production cost of this recombinant protein is very high. Finally, ligand leakage causes contamination of the final product.

The aim of the present work was to overcome the limitations that affect the traditional process through the development of new convective chromatographic supports, like membranes and monoliths, functionalized with synthetic affinity ligands to be used instead of columns packed with Protein A beads.

The performance of regenerated cellulose membranes functionalized with two affinity ligands were studied; the commercial A2P ligand and the new recently synthesized HPTA were used to replace Protein A. Static and dynamic binding capacity and elution recoveries, were determined for the affinity membranes prepared, using pure solutions of IgG. Mixtures and complex solutions containing IgG were tested to determine ligands selectivity.

A processing method for the preparation of porous cellular ceramic monoliths was developed. Cellular $Al_2TiO_5$ and $Al_2TiO_5$-$Al_2O_3$ composites ceramics were obtained by emulsification of liquid paraffin in aqueous suspensions of mixed $Al_2O_3$ and $TiO_2$ powders, with subsequent burnout of the organic phase and two-step reactive firing.
The ceramic monolith were fully characterized to assess their use as novel chromatographic stationary phases, measuring porosity, axial dispersion coefficient and permeability; the surface was chemically modified to obtain functional groups to be used for ligand or direct protein immobilization.

# CONTENTS

## CHAPTER 4

## CHAPTER 5

**CHAPTER 9**

**Conclusions of Part II**

# INTRODUCTION

During the past decades, the production and purification of monoclonal antibodies (mAbs) have aroused an increasing interest, because these biological molecules play an important role in diagnostic and therapeutic treatment of infectious diseases, allergy, inflammation, autoimmune diseases, Alzheimer's syndrome, immunodeficiency, cancer and other illnesses. This is why monoclonal antibodies are very attractive as protein drug therapy [1-3].

The rapid diffusion of monoclonal antibodies and their rising importance are due not only to their successful application against many diseases, but also to the increasing acceptance by governmental institutions [3]. The development of the therapeutic monoclonal antibodies market started in the early 1980s; in particular, the first therapeutic product based on monoclonal antibodies was approved in 1986 for the prevention of kidney transplant rejection. Since then, the class of biopharmaceuticals based on these proteins has grown significantly: in fact, in November 2014, the products based on monoclonal antibodies approved in the United States and in Europe for the treatment of different diseases were 47. It is expected that nearly 70 monoclonal antibodies products will be on the market by 2020, because the current approval rate is almost four new products per year [4]. The antibody market share exceeded 80 billion $ in 2015 and it still growing, at the point that nowadays more than one third of the global market for biopharmaceuticals is covered by these important proteins [4, 5]. Moreover, a cancer therapy based on the use of monoclonal antibodies requires high daily dosages, in the range of grams rather than milligrams: as a result, the cost of the treatment is around 35,000 $ per patient per year [6, 7].

Because monoclonal antibodies became so important in the market of biopharmaceutical products, the focus must be placed on the production process of these proteins: there is an increasing interest in the rise of antibodies production process productivity.
The production process of monoclonal antibodies can be divided essentially into two parts: the first one is the fermentation step, or upstream, and second one is the purification step, or

downstream. Of course, both these two stages are composed of a variety of different and complex unit operations.

As far as the upstream is concerned, it is possible to state that the production of mAbs is not limited by the fermentation step, because the production yield has greatly improved and it is reasonable to expect it to rise up to 10 g/L in the near future [3, 8].

On the other hand, are still many issues related to the downstream processing of monoclonal antibodies: in fact, it is the purification itself that represents the bottleneck of the production process of mAbs. One of the main problems related to the purification process is represented by the relatively high costs: it is known that the downstream section accounts from 60% up to 80% of the total production costs, especially because of the strict requirements in term of purity and activity [9]. Nowadays, the downstream processing of monoclonal antibodies includes, among other unit operations, three chromatographic steps: one based on Protein A affinity chromatography for antibody capture, and two polishing steps, performed either by two ion-exchange columns or an ion-exchange and an hydrophobic interaction column [6, 10]. The Protein A step is the most expensive and accounts for 50-80% of the total downstream processing costs [11, 12].

Even though different technologies are available for the capture and purification of monoclonal antibodies, such as crystallization, aqueous two phase extraction and precipitation [13, 14], this step is traditionally largely based on affinity chromatography employing packed-bed columns with Protein A.

Affinity chromatography is a technique that exploits specific interactions that occur between the molecule that has to be recovered and an appropriate ligand, a natural or synthetic molecule immobilized on the stationary phase through a spacer arm (usually a small molecule that confers a certain mobility to the ligand and make it available for the target). With reference to antibodies, Protein A ligand can be used for the purification of a wide range of molecules because of its capability to bind the Fc region (constant fragment), which is the same for a specific class of antibodies.

The use of packed-bed columns with Protein A represents the most selective and diffuse process in biotechnological and biopharmaceutical industry for the purification of antibodies [8, 15], although many efforts are made to develop alternative technologies. Protein A affinity chromatography represents a unique combination of simplicity of operation, high selectivity and high binding capacity.

Although this technology is the most effective, it suffers from a few limitations, due to high pressure drops across the column, compaction of the granular porous bed and low diffusivity

between the particles of the chromatographic bed: these aspects imply long process time, low productivity and low ligand usage [8]. In addition to fluid dynamic problems, due to the type of stationary phase used, there are also limitations related to the use of Protein A as an affinity ligand. The production cost of this molecule is very high (because it is a recombinant protein), so the cost of the material activated with Protein A is high. Finally ligand leakage, due to proteolytic degradation, causes contamination of the final product [2, 16].

Anyway, more than 20 years experience with this kind of separation technique, led to a highly refined optimization of the process; Protein A leakages have been significantly decreased through genetic engineering, while dynamic binding capacity has been rising due to the improvements of the chromatographic supports. Moreover, contrary to common thinking, the biopharmaceutical industry is highly conservative: in fact, any minor change in a production process requires long evaluation, validation and standardization procedures to maintain FDA approval, usually leading to reduced production and additional costs in the short and mid terms [15]. These issues blocked the implementation of alternative technologies to Protein A affinity chromatography [12, 17]. In fact, it has been stated that Protein A affinity chromatography will be replaced only when a disruptive technology will be available on the market [17].

Among the alternative capture processes available, researchers are mostly interested in finding less expensive chromatographic processes as substitutes of Protein A packed columns. This leads to the study and development of convective chromatographic supports, like membrane and monoliths, of synthetic affinity ligands selective for monoclonal antibodies and a combination of these two elements [8, 18, 20].

The present work is related to the study and characterization of new synthetic ligands that were immobilized onto convective chromatographic materials, such as commercial cellulosic membranes and recently designed cellular ceramic monoliths, to produce innovative chromatographic supports to be used for the selective capture of monoclonal antibodies. The research activities were planned to determine the role and the influence that the main elements exert on the performance of the overall chromatographic material. The main components considered were:

1. the native convective support;
2. the spacer arm;
3. the affinity ligand.

This PhD thesis is divided into two parts: the first one concerns the study of the performance of cellulose membranes functionalized with affinity synthetic ligands. Static and

dynamic binding capacity, as well as elution recoveries, were determined for these chromatographic supports, using pure solutions of IgG. Mixtures and complex solutions containing IgG were tested to determine the selectivity of the ligands. The influence of the native support and of the spacer arm were taken into account as well.

The second part of this work regards the development and design of a new type of cellular ceramic monolith, that can be used, for the first time, as a stationary phase for chromatographic separations of proteins. The processing method was established, the structural features of the material were determined and preliminary protein adsorption tests were carried out, to prove the potentialities of this new material in the field of chromatographic separations.

# References

[1]   U. Langel, *Antibodies*, Chapter 25 of *Introduction to peptides and proteins*, CRC Press (2009) 343-354

[2]   L. Zamolo, M. Salvalaglio, C. Cavallotti, B. Galarza, C. Sadler, S Williams, S. Hofer, J. Horak, W. Lindner, *Experimental and theoretical investigation of effect of spacer arm and support matrix of synthetic affinity chromatographic materials for the purification of monoclonal antibodies*, Journal of Physical Chemistry B 114 (2010) 9367-9380

[3]   C. Boi, S. Dimartino, S. Hofer, J, Horak, S. Williams, G.C. Sarti, W. Lindner, *Influence of different spacer arms on Mimetic Ligand$^{TM}$ A2P and B14 membranes for human IgG purification*, Journal of Chromatography B 879 (2011) 1633-1640

[4]   D.M. Ecker, S.D.Jones, H.L. Levine, *The therapeutic monoclonal antibody market*, mAbs 7 (2015) 9-14

[5]   MarketsandMarkets, *Antibody production market by product analysis and global forecast to 2019*, May 2015

[6]   V. Girard, N.J. Hilbold, C.K.S. Ng, L. Pegon, W. Chahima, F. Rousset, V. Monchois, *Large-scale monoclonal antibody purification by continuous chromatography, from proccess design to scale up*, Journal of Biotechnology 213 (2015) 65-73

[7]   S.S. Farid, *Process economics of industrial monoclonal antibody manufacture*, Journal of Chromatography B 848 (2007) 8-18

[8]   C. Boi, *Membrane adsorbers as purification tools for monoclonal antibody purification*, Journal of Chromatography B (2007) 848, 19-27

[9]   C. Boi, V. Busini, M. Salvalaglio, C. Cavallotti, G.C. Sarti, *Understanding ligand-protein interactions in affinity membrane chromatography for antibody purification*, Journal of Chromatography A 1216 (2009) 8687-8696

[10]  A.A Shukla, B. Hubbard, T. Tressel, S. Guhan, D. Low, *Downstream processing of monoclonal antibodies - Applications of platform approaches*, Journal of Chromatography B 848 (2007) 28-39

[11]  B. Kelley, *Very large scale monoclonal antibody purification: tha case the conventional unit operations*, Biotechnology Progress 23 (2007) 995-1008

[12]  L. Blain, *Protein A: the life of a disruptive technology*, Bioprocess International 11(8) (2013) 29-38

[13] T.M. Przybycien, N.S. Pujar, L.M. Steele, *Alternative bioseparation operations: life beyond packed-bed chromatography*, Current Opinion in Biotechnology 15 (2004) 469-478

[14] M.E. Jorg Thommes, *Alternatives to chromatographic separations*, Biotechnology Progress 23 (2007) 42-45

[15] C. Boi, S. Dimartino, *Advances in membrane chromatography for the capture step of monoclonal antibodies*, Current Organic Chemistry 21(17) (2017) 1753-1759

[16] D. M. Yarmush, *Monoclonal Antibodies and Their Engineered Fragments*, Chapter 102 in *The Biomedical Engineering Handbook: Second Edition*, Ed. Joseph D. Bronzino; CRC Press LLC (2000)

[17] P. Gagnon, *Emerging challenges to Protein A: chromatin-directed clarification enables new purification options*, Bioprocess International 11(9) (2013) 44-53

[18] V. Orr, L. Zhong, M. Moo-Young, C.P. Chou, *Recent advances in bioprocessing application of membrane chromatography*, Biotechnology Advances 31 (2013) 450-465

[19] M.O. Herigstad, S. Dimartino, C. Boi, G.C. Sarti, *Experimental characterization of the transport phenomena, adsorption and elution in a protein A affinity monolithic medium*, Journal of Chromatography A 1407 (2015) 130-138

# CHAPTER 1

# Chromatography & Antibodies

## 1.1 Introduction

Chromatography is a largely used separation technique thanks to its high selectivity, versatility and efficiency; the scale-up of a process based on this separation method is easy, because it is based on a wide experience of applications in the biochemical industries. Chromatography is also known to be a very expensive process, this is why other technologies are gaining ground, such as precipitation, crystallization, aqueous two phase extraction [1, 2] and membrane based separations [3-7], but it is still very difficult to replace chromatography in the final separation stages, because it guarantees high levels of purity of the products that have to be recovered [8].

Chromatography can be defined as a separation technique of molecules in mixtures based on the different distribution that the components in the initial solution assume in two phases: the *stationary phase*, that is represented by the fixed bed through which the second phase, the *mobile phase*, flows. The solution containing the molecules that have to be separated is put in contact with the stationary phase and is moved through it by the mobile phase. The result is the separation of the components in the mixture because of the different interaction they have with the two main phases. Molecules whose interaction with the stationary phase is strong will be retained, so they will move through the stationary phase slower than molecules whose interaction with the stationary phase is weak.

The stationary phase can be arranged in two different ways giving rise to two chromatographic techniques, called respectively *column chromatography* and *thin layer chromatography*.

In the case of column chromatography, the granular stationary phase is put inside a holder, usually cylindrical, where it creates a porous bed through which the mobile phase can flow. In this case an important parameter is defined: the *retention time*, that represents the time needed by

a specific molecule to pass through the entire column, under the condition that the flow rate of the mobile phase is constant.

In the case of thin layer chromatography, the material constituting the stationary phase is put on a flat support creating a few hundred micrometers layer. The mobile phase and the components to be separated migrate upwards for capillarity. In this case a retention time is not defined, but the ratio between the path completed by the solute and the one completed by the front of the mobile phase is usually defined as a characteristic parameter. Both column chromatography and thin layer chromatography can be used as analytical techniques: the first one is quantitative, while the second one is qualitative. At industrial level, only column chromatography is used.

Chromatographic techniques can be classified according to the type of stationary phase and the various mechanisms that regulate the interactions between the initial mixture components and the stationary phase itself.

## 1.2 Chromatography for protein purification

The use of chromatography for proteins separation is advantageous for many reasons: there is a great number of possible chemical interactions, coming from the frequency and the distribution of amino acids in the protein chain, and different adsorbents materials are available. The separation can exploit many properties of proteins and adsorbers, but different parameters have to be firstly evaluated to select a particular technique: the composition of the solution that will be fed to the column, the chemical structure and the stability of the components, the electric charge at a certain pH value and the isoelectric point of the protein, the hydrophilic or hydrophobic behaviour and the dimension of the molecules [9]. However, more than one type of chromatographic technique is usually needed for the purification of a particular protein.

The next paragraphs will explain the mechanisms of the most used chromatographic techniques for protein purification; particular emphasis will be given to affinity chromatography, which represents the chromatographic application fulcrum of this PhD thesis.

### 1.2.1 Ion-exchange chromatography

Separations based on ion-exchange chromatography (IEX) are performed using columns packed with ion-exchange resins. The stationary phase, usually resin beads, used for IEX processes has immobilized charged groups on the surface. The mechanism of separation is based upon the reversible adsorption of charged molecules on the immobilized groups of opposite charge. Many biomolecules, such as amino acids and proteins, posses ionisable groups and the

fact that they present a positive or negative net charge on their surface, can be exploited to separate them from the mixtures in which they are contained. The net charge these compounds have depends on their isoelectric point and on the pH of the buffer they are dissolved in.

Applications of IEX are based on different steps: equilibration of the stationary phase, feeding of the sample, washing, elution and regeneration, as shown in Fig. 1.1.

During the equilibration step, the stationary phase is prepared for the desired start conditions, in which each charged group is associated to a counter-ion. The aim of second step, feeding of the sample, is to bind the target molecules: the buffer used in this step must have the same ionic strength and pH of the equilibration buffer. During the washing step, all unbound samples are removed from the surface. After that, a change in buffer composition used for the elution step causes the release of the molecules adsorbed on the surface of the stationary phase: normally, during the elution step, the ionic strength is increased to separate proteins, that desorb according to the number of charged groups on their surface. Finally, the regeneration step ensures that all proteins still bound are removed and the stationary phase, once the initial conditions are restored, is ready for the next cycle.



a)    b)

c)    d)
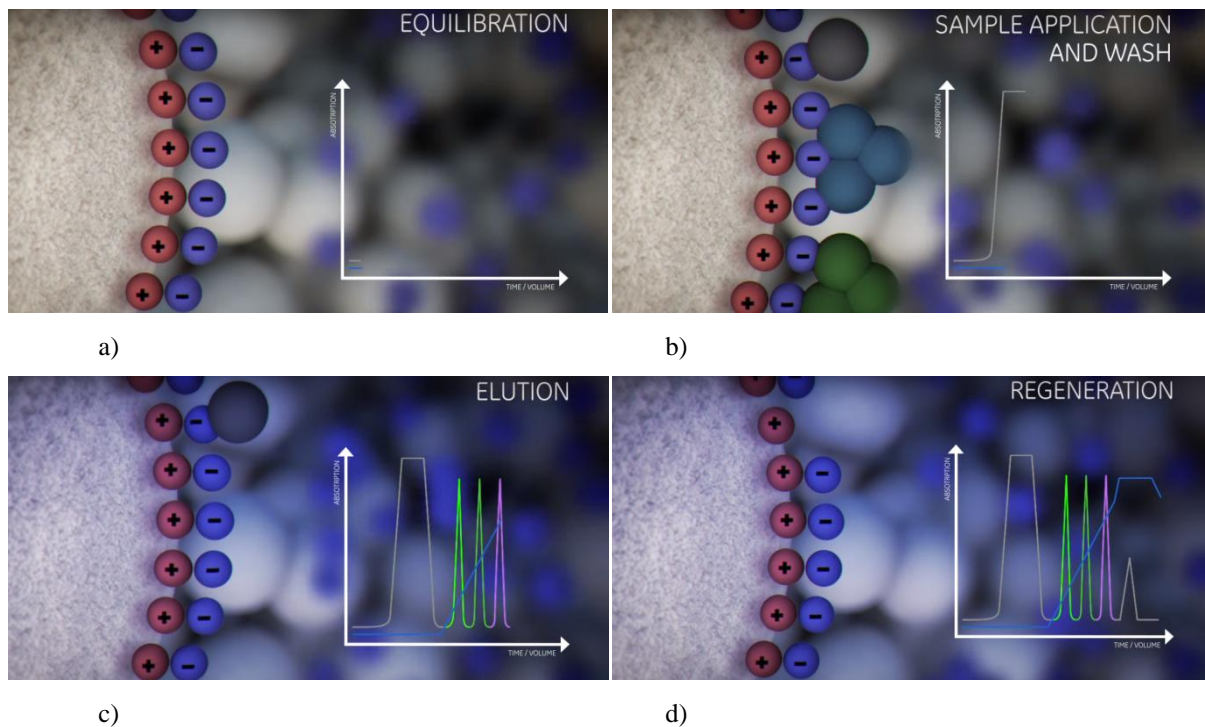
**Figure 1.1**    The Principles of Ion Exchange Chromatography [10]. a) equilibration step; b) sample feeding and washing steps; c) elution step; d) regeneration of the stationary phase.

## *1.2.2 Hydrophobic interaction chromatography*

Separation applications in hydrophobic interaction chromatography (HIC) are based on the reversible adsorption of biomolecules according to their hydrophobicity; the stationary phase used is an inert material that presents hydrophobic groups on the surface. A protein in a solution is surrounded by an extremely ordinate water film; the use of appropriate ions in the process buffer allows the hydrophobic groups on the surface of proteins to interact with those of the stationary phase.

Most part of HIC processes are performed on the steps shown in Fig. 1.2: equilibration, sample application, washing, elution and regeneration.
The aim of the equilibration step is to put the stationary phase into the desired start conditions and it is usually performed by adding salts to the equilibration buffer. According to the mechanism of this separation technique, proteins are bound to the surface of the stationary phase in presence of high salts concentration, during the second step of the process. The washing procedure ensures that the unbound material is removed from the stationary phase. A decrease of the buffer salts concentration is used to elute proteins: a gradient elution is the optimal procedure to separate proteins bound to the stationary phase. The regeneration step ensures to remove all compounds still bound as well as to recovery the full capacity of the stationary phase.



a)                                                                      b)

c)                                                                      d)
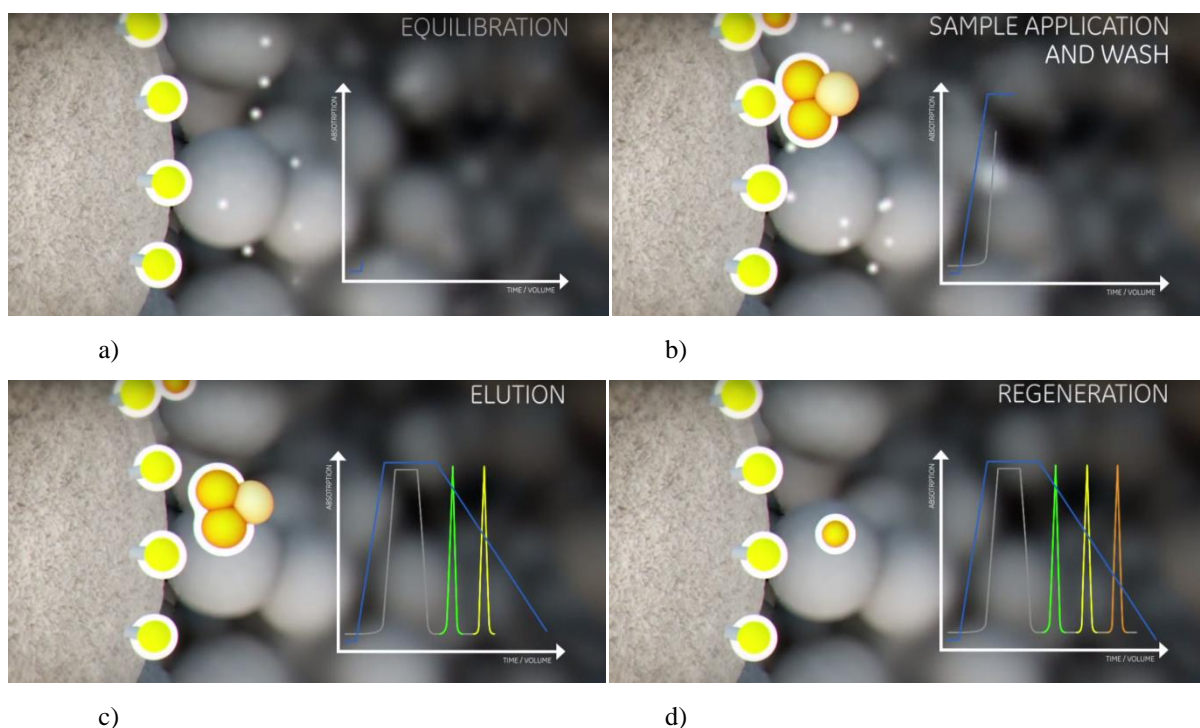
**Figure 1.2**    The Principles of Hydrophobic Interaction Chromatography [11]. a) equilibration step; b) sample feeding and washing steps; c) elution step; d) regeneration of the stationary phase.

### *1.2.3 Size exclusion chromatography*

Size exclusion chromatography (SEC), also called gel filtration chromatography, is a separation application that is usually performed with columns packed with porous beads: the stationary phase can be seen as a gel. The separation takes place thanks to differences in sizes of biomolecules that passes through the packed column. Among the other chromatographic techniques, SEC is the only non-adsorbent one, and it is mostly used for analytical purposes, rather than for industrial applications.

Fig. 1.3 shows the mechanism of separation of SEC applications. Mixtures of proteins of different size can be treated using this chromatographic operation, with the aim of separate the biomolecules according to their molecular weight. If a protein cannot diffuse inside the pores of the gel, because of its high molecular weight, it will exit the column faster than smaller molecules that can actually diffuse into the pores of the gel: access to the pores is limited by steric hindrance. If a molecule is smaller than the smallest pore of the gel, then, this molecule can access the total pore volume.
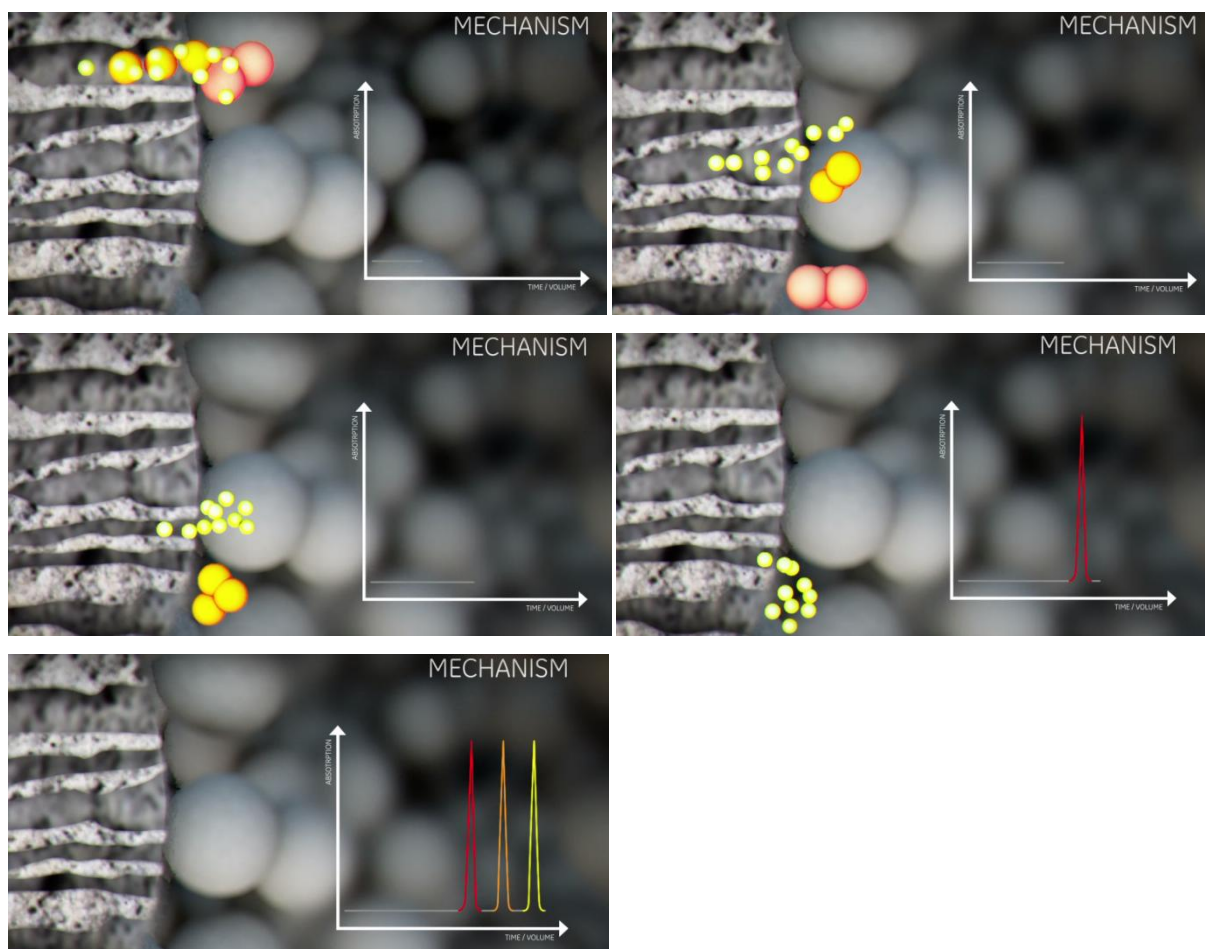


**Figure 1.3**     The Principles of Gel Filtration Chromatography [12].

## 1.2.4 Affinity Chromatography

Affinity chromatography (AC) is the most largely used operation for the purification and recovery of high valuable biomolecules, such as enzymes, hormones, vaccines, DNA and RNA fragments and monoclonal antibodies [13]. AC applications are based on a reversible specific interaction between the target biomolecule and a ligand that is immobilized on the surface of the stationary phase.

The affinity ligand is a molecule that has to be bound covalently to the surface of stationary phase; the chromatographic support should have a high density of reactive groups needed for the immobilization of the ligand, that has to be stable during the immobilization procedure as well as during the purification process. Important requirements for affinity ligands are: a) selectivity, they should interact with and bind only the target molecule, to ensure a high purity of the recovered compound; b) recovery, it must be as high as possible and it is guaranteed by the reversible binding with the target protein.

The main stages of AC are shown in Fig. 1.4.



a)  b)

c)  d)
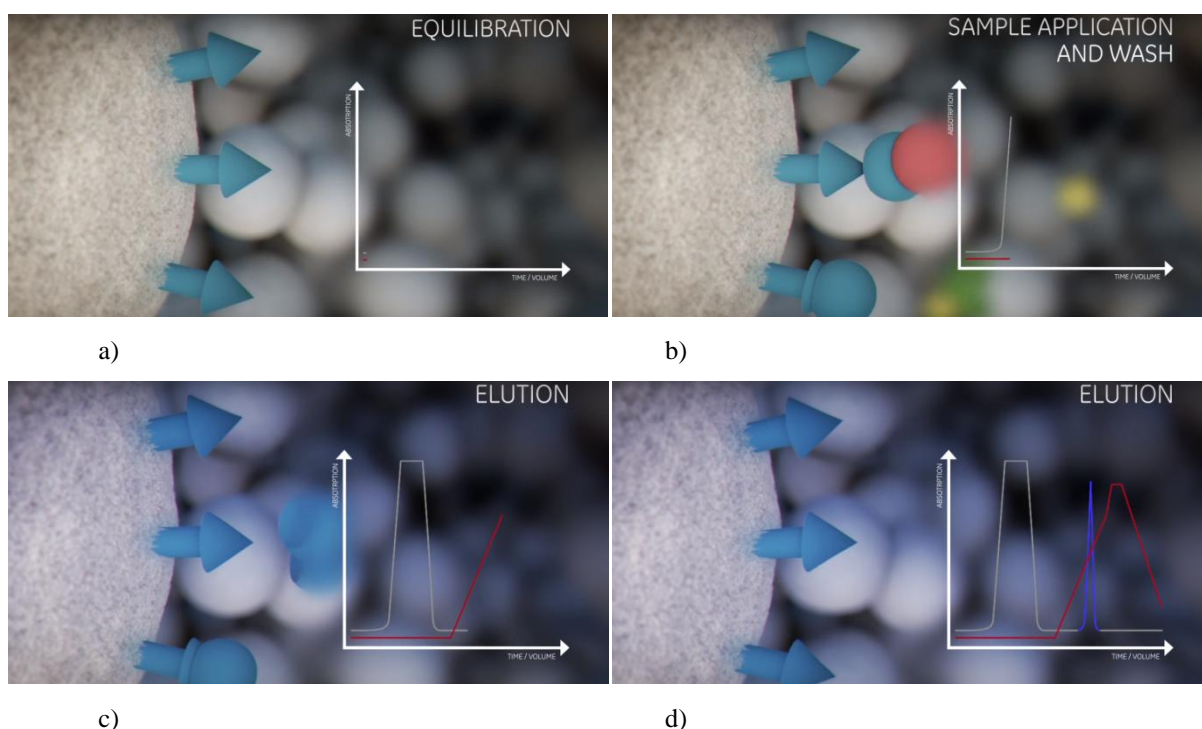
**Figure 1.4**  The Principles of Affinity Chromatography [14]. a) equilibration step; b) sample feeding and washing steps; c) and d) elution step.

The equilibration of the stationary phase is performed to have the desired start conditions. During the adsorption step, the target molecules are reversibly bound to the affinity ligand on the surface of the chromatographic support, while other biomolecules do not bind. Equilibration

buffer is the same used for sample application and washing, while the target compounds are eluted using a particular elution buffer. Elution can be specific or non-specific; specific elution introduces a competitor molecule for the binding site of the ligand; non-specific elution exploits changes in the pH or denaturing agents. In both cases the aim is to break the reversible binding between the ligand and the target protein.

### *1.2.4.1 Breakthrough curve*

The stages of an affinity chromatography process give a specific concentration profile exiting the chromatographic column, as shown in the chromatogram in Fig. 1.5.
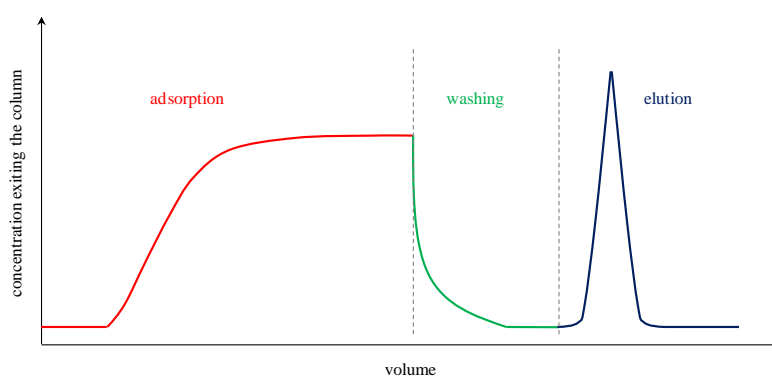


**Figure 1.5**    Qualitative concentration profile for a complete chromatographic affinity cycle.

The red part of the curve shown in Fig. 1.5 represents the so called *breakthrough curve*; this curve describes the concentration profile exiting the column as a function of time, or fed volume. Ideally, the concentration profile exiting the column is a step profile; in fact, when the concentration exiting the column becomes equal to the concentration in the feed solution there is the complete saturation of the stationary phase. Actually, the solute concentration profile increases gradually, because the saturation of the stationary phase requires a certain time, due to mixing phenomena, non-uniform flow distribution and slow adsorption kinetics [15].

The breakthrough curve gives many necessary information related to the process performance, such as the binding capacity of the column, the amount of product lost and the process time. A detail of a qualitative breakthrough curve is reported in Fig 1.6. At the beginning of the process, the exiting concentration is equal to zero, because the target protein in adsorbed in the column; once the stationary phase starts to saturate, the concentration increases until it reaches the value of the feed. From a qualitative point of view, the area beneath the breakthrough curve represents the amount of protein that is coming out of the column, so the lost amount of protein; the area between the breakthrough curve and the line corresponding to the feed

concentration (concentration = $c_0$) is the mass of protein adsorbed, from which is possible to evaluate the dynamic binding capacity of the chromatographic affinity support [16].
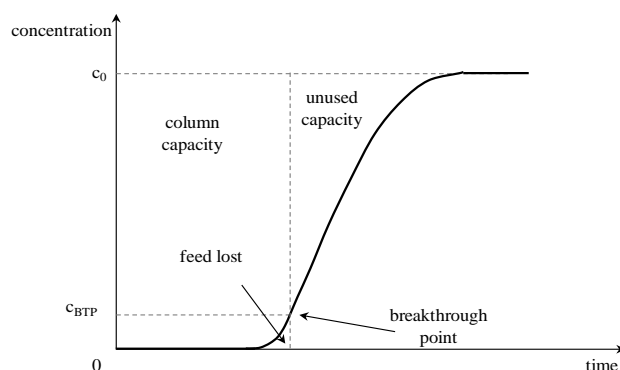


**Figure 1.6**    Qualitative breakthrough curve for a generic affinity chromatography process [17].

The position of the breakthrough curve depends on the column capacity and on the initial concentration of the solute in the feed solution. A higher binding capacity, at the same initial concentration, shifts the breakthrough curve to the right, while, at the same binding capacity, a decrease of the initial concentration makes the breakthrough curve move to the left.

In industrial processes the adsorption stage is stopped at the breakthrough point (BTP) to avoid the loss of a large amount of product, that is usually high valuable. At this point the concentration exiting the column is a particular fraction of the feed concentration (from 5 to 10 %) and it represents the right compromise between the amount of product lost and the unexploited binding capacity of the column. That is why it is extremely important to have chromatographic supports characterized by a high binding capacity and very steep associated breakthrough curves.

In the next paragraphs, the important role that affinity chromatography technique plays in the field of antibodies purification will be described: particular emphasis will be put on different chromatographic supports that can be used and on the influence that these have on the performance of the entire purification process.

## 1.3 Affinity chromatography for antibodies purification

### *1.3.1 Antibodies*

Antibodies, or immunoglobulins, are proteins produced by the immune system of the vertebrates to identify and neutralize foreign pathogens, such as antigens from bacteria and

viruses [18]. This large class of important proteins has merited increasing interest in the scientific community due to their extremely high level of diversity in the binding of target antigens [19]. Moreover, antibodies play an important role in many types of diseases such as cancers, infectious diseases, allergy, autoimmune diseases and inflammation, making them attractive as protein drug therapies [6, 18, 20].

Originally, the source of antibodies was antisera: the antibodies derived from such sera were limited in quantity and heterogeneous in quality. This class is now conventionally called the class of *polyclonal antibodies* [19]. Polyclonal antibodies are derived from different B-cell lines and they consist of antibodies against several epitopes, thus increasing the probability of eliminating the invading pathogen or malignant cell. These antibodies are typically produced by immunization of a suitable mammal followed by the purification from the mammal's serum to obtain antisera [18].

After the development of hybridoma technology, a potentially unlimited quantity of homogeneous antibodies with defined specificities and affinities became available: they are called *monoclonal antibodies* and are produced by a line of immune cells that are all clones of a single identical parent cell [18, 19]. With this method, it is possible to create specific monoclonal antibodies against almost any substance.

Monoclonal antibodies for a given antigen can be used for different purposes, such as the detection and quantitation of the antigen and purification by immunoprecipitation and affinity chromatography.

When monoclonal antibodies are produced in animals such as mice, they need to be humanized before use to avoid the recognition as foreign by human patients, otherwise they are rapidly removed from circulation or cause systemic inflammatory effects [18].

Monoclonal antibodies have gained increasing importance as reagents in diagnostic and therapeutic medicine, in the identification and determination of antigen molecules, in biocatalysis and in affinity purification and labelling of antigens and cells [19].

Five main classes of immunoglobulins have been identified in humans, and other animals: they include immunoglobulin G (IgG), A (IgA), M (IgM), D (IgD) and E (IgE). All antibody classes are monomeric, a part from IgA and IgM that are a dimer and a pentamer respectively. A monomeric antibody molecule structure is composed of four chains: two *light chains* and two *heavy chains*, as shown in Fig. 1.7. The chains are held together by disulfide bonds; the light and the heavy chain by inter-chain disulfides and the two heavy chains are held together by many disulfide bonds. The average molecular weight of the light chain is about 25

kDa, while that of the heavy chain goes from 50 kDa to 77 kDa [19]; usually the average molecular weight of IgG is 150 kDa.

The light chains are the same in all immunoglobulins and are composed of two different regions: the *variable region* and the *constant region*; the heavy chains are divided into variable and constant region too, but they are unique for each class of immunoglobulin. Variable regions are extremely differentiated, composed of different amino acids, and they allow the antibody to recognize a various number of different foreign molecules, called antigens. Recognition between an antibody and an antigen occurs according to the complementarity of the respective binding sites [21].
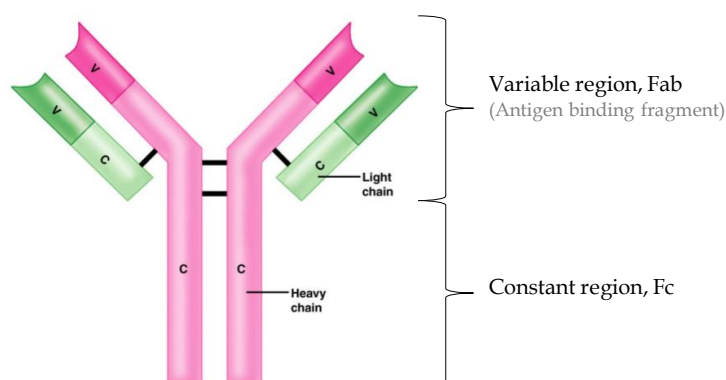


**Figure 1.7**     Structure of an immunoglobulin.

The constant fragment, the so called Fc moiety, of the antibody is exploited during the purification process of these proteins. In fact, the specific interaction between the constant region and Protein A allows the purification of a whole class of monoclonal antibodies with the same process, independently of their individual antigenic activity [21-23].

### *1.3.2 Traditional production and purification process*

Monoclonal antibodies are produced by recombinant mammalian cells as extracellular proteins; the most common expression vectors for antibodies are Chinese Hamster Ovary cells (CHO), but also murine lymphoid cell lines and murine hybridoma have been successfully used [21, 24]. Recent improvements in the production technology led to an increase of the productivity up to 10 g/L, and this shifted the pressure on the downstream processing, where the scale up for higher capacities is not straightforward [25].

The downstream process is composed of many different unit operations needed to obtain a final product with very high purity . It starts with cells harvest, which can be performed by centrifugation and/or microfiltration. In the last few years, centrifugation has been preferred

because it is a more standardized separation technique than microfiltration, that requires the optimization of the operating conditions according to feed solution variability [25].

The selective capture stage is represented by the affinity chromatography step; it allows the separation of the antibody from the contaminants present in the supernatant, while other unit operations are needed for the polishing step and for pathogens removal.

Affinity chromatography is traditionally carried out using columns packed with porous beads, functionalized with Protein A. At the moment, this step constitutes the most expensive among the other unit operations required for downstream processing; this is due to the high cost of Protein A resins that can vary from 10,000 to 20,000$ per litre of settled material [23] and it depends especially on the cost of Protein A.

Protein A is a 42 kDa protein and it is the most exploited ligand for the purification of monoclonal antibodies: it is produced by fermentation of recombinant *Staphylococcus aureus*. Bead-based affinity chromatography with Protein A is recognized as the most selective and diffused process in the biotechnological and biopharmaceutical industry, for the purification of antibodies [3]. Thanks to improvements of the chromatographic materials, the binding capacity of Protein A could reach 70 g of antibody per litre of resin [26, 27].

However, there are a few critical aspects related to the use of Protein A as affinity ligand; in fact, its production process is characterized by high costs, which imply the high cost of activated the chromatographic materials, as already stated. Moreover, a relevant problem is related to the possible loss of Protein A from the stationary phase, due to proteolytic degradation [20, 28]: this causes the contamination of the final product and damages the human body, since it is a strong pathogen. Beside the issues related to the use of this particular affinity ligand, mass transport limitations also affect the traditional purification process.

A scheme of the industrial process for production and purification of monoclonal antibodies is shown in Fig. 1.8.
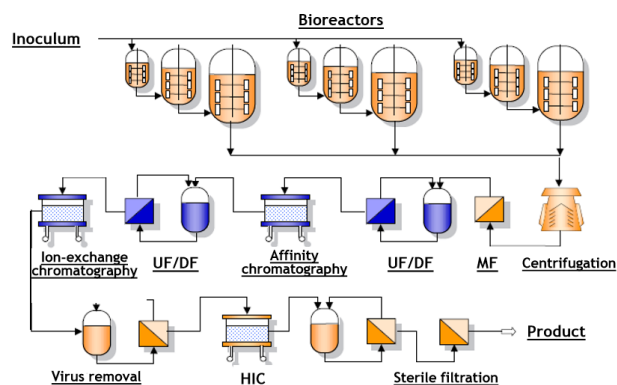


**Figure 1.8**    General scheme of the production process of antibodies [17].

## 1.4 Bead-based affinity chromatography

As already stated, the traditional process for the purification of antibodies is carried out using column packed with porous beads of the diameter of 50 - 100 μm on whose surface the affinity ligand (Protein A) is immobilized. In this process the prevailing mass transport mechanism is diffusion.

Such systems exhibit a quite good performance, but the long distances the solute has to diffuse through to interact with the ligand constitute an important limit of this strategy. On the other hand, the use of smaller particles, with greater superficial area and shorter diffusive distances, has the drawback of drastically increasing the pressure drops and, consequently, the operative costs to an extent that makes the separation process unprofitable [17].

High pressure drops, compaction of the packed bed and slow intraparticle diffusion lead to long process time, low productivity and poor ligand usage [3].

Another serious problem that affects resin-based affinity chromatography processes is channeling, that represents the formation of preferential paths for the flowing solution: this leads to a scarce bed utilization. Other problems are related to the radial and axial dispersion of the solutes inside the columns.

An alternative material that can be used to pack chromatographic columns is represented by perfusive particles: these are porous beads characterized by the presence of through pores, that allow convective transport; the small pores that help interconnecting the direct pores represent only a small fraction of the total pore volume. The use of perfusive affinity chromatography can overcome some of the limitations that affects the process performed using diffusive particles.

## 1.5 Convective affinity chromatography

Problems related to mass transport in packed columns can be overcome using porous chromatographic supports in which the main transport phenomenon is convection, that is by using membranes and monoliths as stationary phase.

Even though the affinity ligand is immobilized inside the pores of these materials, the convective flux through the matrix will transport the target molecules right close to the available binding sites, reducing the limitations due to poor ligand usage and low diffusion that characterize packed-bed columns.

A schematic drawing that summarizes the differences in terms of transport mechanisms between packed-bed chromatography and convective chromatography is shown in Fig. 1.9.
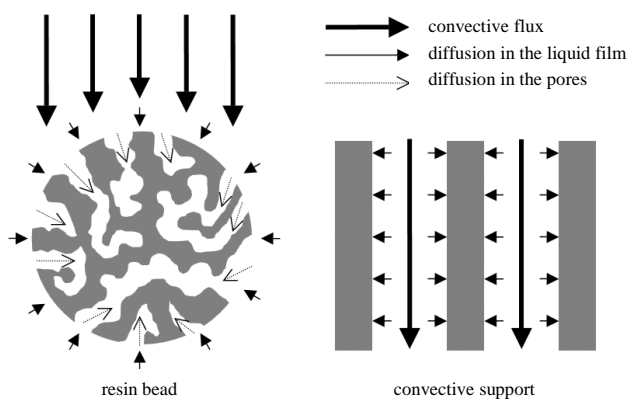


**Figure 1.9**  Transport mechanisms in resin-based chromatography and in convective chromatography [17].

### 1.5.1 Membranes

Membranes are traditionally produced as thin polymeric sheets; in an affinity membrane chromatography process, the column is filled with various overlapped porous layers to have a pore volume sufficient to perform the separation. Usually microfiltration membranes are used: the pores have an average diameter of 0.4 - 3.0 μm and the void fraction can vary from 0.6 to 0.8; membranes represent a less expensive chromatographic materials compared to beads.

The ligand, immobilized on the inner surface of the pores, is easily reached by the target molecules, because of the convective flux across the membranes: this avoids the limitations due to diffusion hindrance. Moreover, the use of membranes eliminates packing requirements, allows to register lower pressure drops, making the process less costly; in this way it is possible to work at higher flow rates, increase the mass transfer rates, reduce buffer consumption due to smaller unit dead volumes and so reduce the process time and the chance of biomolecules degradation, without varying the performance of the chromatographic material: in fact, the separation efficiency does not depend on feed flow rate over a wide range of values [3, 29].

Membrane chromatography is particularly indicated for the purification of large biomolecules (molecular weight higher than 150 kDa), like proteins, viruses and DNA fragments [30, 31]. Membranes provide a large available surface for the formation of the covalent bond with the ligand, while the these large molecules cannot enter the small pores of the beads in resins packed columns; in this case the total pore volume is not completely exploited and molecules adsorption takes place only on the outer surface of the beads [32, 33].

Many different studies have been carried out to demonstrate the superior performance of affinity membranes when compared to chromatographic beads [34-36]. The use of membranes functionalized with Protein A led to an increase of the binding capacity, with respect to Protein A beads, that demonstrates the high influence that the structure of the chromatographic support has on the performance of the process.

However, membranes are usually characterized by a lower specific area and an increase of this value may reduce the mechanical strength and lead to a non uniform pore size distribution.

### *1.5.2 Monoliths*

Monoliths are chromatographic materials produced as a continuous phase, in different shapes and geometries [37, 38]. Monoliths are considered as fourth generations chromatographic materials, after resins, gels and membranes and, recently, they became particularly attractive for the isolation and purification of large biomolecules [38, 39]. Their dimensions can vary from centimetres to nanometres, making their use possible even in the analytical field [37, 38, 40, 41]. These chromatographic supports are characterized by a high accessible surface area that easily traduces into great binding capacity; they are also characterized by high permeability, thanks to their high porosity, usually around 60% [42, 43].

Monoliths can be made of different materials, both ceramic and polymeric; they can differ in terms of geometry and pore dimension but their common characteristic is represented by high porosity and by the fact that the pores are well interconnected, forming a unique structure made of a dense channels network.

Usually, the specific area is lower for monoliths with respect to beads, but slightly higher than that of membranes.

### 1.6 Aim and structure of the work

The aim of this doctoral research project is to improve the affinity chromatographic step in the traditional purification process of antibodies, developing a new chromatographic support able to overcome the limitations that affects the purification process carried out using columns packed with porous beads, functionalized with Protein A.

To this aim membranes and monoliths were used as stationary phases and new synthetic affinity ligands, mimetic of Protein A, were characterized.

This work is divided into two parts: in the first one, *Affinity Membrane Chromatography*, the characterization of cellulose membranes functionalized with the new synthetic affinity ligands is described. The second part, *Ceramic Monoliths for Affinity Chromatography*, deals with the production, design and characterization of a new kind of ceramic material to be used as a novel chromatographic support.

# References

[1] T.M. Przybycien, N.S. Pujar, L.M. Steele, *Alternative bioseparation operations: life beyond packed-bed chromatography*, Current Opinion in Biotechnology 15 (2004) 469-478

[2] M. E. Jorg Thommes, *Alternatives to chromatographic separat3ions*, Biotechnology Progress 23 (2007) 42-45

[3] C. Boi, *Membrane adsorbers as purification tools for monoclonal antibody purification*, Journal of Chromatography B 848 (2007) 19-27

[4] V. Orr, L. Zhong, M. Moo-Young, C.P. Chou, *Recent advances in bioprocessing application of membrane chromatography*, Biotechnology Advances 31(2013) 450-465

[5] D.J Karst, F. Steinebach, M. Soos, M. Morbidelli, *Process performance and product quality in an integrated continuous antibody production process*, Biotechnology and Bioengineering 114 (2) (2017) 298-307

[6] C. Boi, S. Dimartino, S. Hofer, J, Horak, S. Williams, G.C. Sarti, W. Lindner, *Influence of different spacer arms on Mimetic Ligand$^{TM}$ A2P and B14 membranes for human IgG purification*, Journal of Chromatography B 879 (2011) 1633-1640

[7] C. Boi, C. Algeri, G.C. Sarti, *Preparation and characterization of polysulfone affinity membranes bearing a synthetic peptide ligand for the separation of murine immunoglobulins,* Biotechnology Progress 24 (2008) 1304-1313

[8] J.D. Henry, M.E. Prudich, W. Eykamp, T.A Hatton, K.P. Johnston, R.M Lemert, R. Lemlich, C.G. Moyers, J. Newman, H.A. Pohl, K. Pollock, M.P. Thien, *Alternative separation processes*, in R.H. Perry, D.W. Green, J. O. Maloney, Perry's *Chemical Engineers' Handbook*, 7$^{th}$ Ed.(1998) McGraw – Hill, Sidney, Australia

[9] R.K. Scopes, *Protein Purification – Principles and Practice*, 2$^{nd}$ Ed. (1987) Springer Verlag

[10] *The Principles of Ion Exchange Chromatography*, video available at http://www.gelifesciences.com/webapp/wcs/stores/servlet/catalog/en/GELifeSciences-it/applications/ion-exchange-chromatography-iex

[11] *The Principles of Hydrophobic Interaction Chromatography*, video available at http://www.gelifesciences.com/webapp/wcs/stores/servlet/catalog/en/GELifeSciences-it/applications/hydrophobic-interaction-chromatography-hic

[12] *The Principles of Gel Filtration Chromatography*, video available at http://www.gelifesciences.com/webapp/wcs/stores/servlet/catalog/en/GELifeSciences-it/applications/gel-filtration-gf

[13] F. Dechow, *Separation and Purification Techniques in Biotechnology*, Noyes Publication (1989) Park Ridge

[14] *The Principles of Affinity Chromatography*, video available at http://www.gelifesciences.com/webapp/wcs/stores/servlet/catalog/en/GELifeSciences-it/applications/affinity-chromatography-ac

[15] J. E. Kochan, Y.J. Wu, M.R. Etzel, *Purification of bovine immunoglobulin G via Protein G affinity membranes*, Industrial Engineering and Chemistry Research 35 (1996) 1150–1155

[16] F. H. Arnold, H.W. Blanch, C.R. Wilke, *Analysis of affinity separations I: predicting the performance of affinity adsorbers*, The Chemical Engineering Journal 30 (1985) B9–B23

[17] S. Dimartino, *Studio sperimentale e modellazione della separazione di proteine con membrane di affinità*, Tesi di Dottorato di Ricerca in Ingegneria Chimica dell'Ambiente e della Sicurezza XXI Ciclo, Facoltà di Ingegneria, Università degli Studi di Bologna, 2009

[18] U. Langel, *Antibodies*, Chapter 25 of *Introduction to peptides and proteins*, CRC Press (2009) 343-354

[19] D. M. Yarmush, *Monoclonal Antibodies and Their Engineered Fragments*, Chapter 102 in *The Biomedical Engineering Handbook: Second Edition*, Ed. Joseph D. Bronzino; CRC Press LLC (2000)

[20] L. Zamolo, M. Salvalaglio, C. Cavallotti, B. Galarza, C. Sadler, S Williams, S. Hofer, J. Horak, W. Lindner, *Experimental and theoretical investigation of effect of spacer arm and support matrix of synthetic affinity chromatographic materials for the purification of monoclonal antibodies*, Journal of Physical Chemistry B 114 (2010) 9367-9380

[21] K. Huse, H. J. Böhme, G. H. Scholz, *Purification of antibodies by affinity chromatography*, Journal of Biochemical and Biophysical Methods 51 (2002) 217-231

[22] A.A. Shukla, B. Hubbard, T. Tressel, S. Guhan, D. Low, *Downstream processing of monoclonal antibodies - Application of platform approaches*, Journal of Chromatography B 848 (2007) 28-39

[23] L. Blain, *Protein A: The life of a disruptive technology*, Bioprocess International 11 (2013) 29-38

[24] D.M. Ecker, S.D.Jones, H.L. Levine, *The therapeutic monoclonal antibody market*, mAbs 7 (2015) 9-14

[25] C. Boi, S. Dimartino, *Advances in membrane chromatography for the capture step of monoclonal antibodies*, Current Organic Chemistry 21(17) (2017) 1753-1759

[26] B. Kelley, *Very large scale monoclonal antibody purification: tha case the conventional unit operations*, Biotechnology Progress 23 (2007) 995-1008

[27] V. Natarajan, A.L. Zydney, Protein A chromatography at high titers, Biotechnology and Bioengineering 110 (2013) 2445-2451

[28] C. Boi, V. Busini, M. Salvalaglio, C. Cavallotti, G.C. Sarti, *Understanding ligand-protein interactions in affinity membrane chromatography for antibody purification*, Journal of Chromatography A 1216 (2009) 8687-8696

[29] S. Brandt, R.A. Goffe, S.B. Kessler, J.L. O' Connor, S. Zale, Membrane-based affinity technology for commercial scale purification, Nature Biotechnology 6 (1988) 779-782

[30] H. Yang, C. Viera, J. Fischer, M.R. Etzel, *Purification of a large protein using ion-exchange membranes*, Industrial & Engineering Chemistry Research 41 (2002) 1597–1602

[31] H.N. Endres, J.A.C. Johnson, C.A. Ross, J.K. Welp, M.R. Etzel, *Evaluation of an ion-exchange membrane for the purification of plasmid DNA*, Biotechnology and Applied Biochemistry 37 (2003) 259–266

[32] A. Zöchling, R. Hahn, K. Ahrer, J. Urthaler, A. Jungbauer, *Mass transfer characteristics of plasmids in monoliths*, Journal of Separation Science 27 (2004) 819–827

[33] J. Urthaler, R. Schlegl, A. Podgornik, A. Strancar, A. Jungbauer, R. Necina, *Application of monoliths for plasmid DNA purification. Development and transfer to production*, Journal of Chromatography A 1065 (2005) 93–106

[34] C. Boi, S. Dimartino, G.C. Sarti, Performance of a new Protein A affinity membrane for the primary recovery of antibodies, Biotechnology Progress 24 (2008) 640-647

[35] D. Yu, M.D. McLean, J.C. Hall, R. Ghosh, Purification of a human immunoglobulin G1 monoclonal antibody from transgenic tobacco using membrane chromatographic processes, Journal of Chromatography A 1187 (2008) 128-137

[36] Z. Ma, S. Ramakrishna, Electrospun regenerate cellulose nanofiber affinity membranes functionalized with Protein A/G for IgG purification, Journal of Membrane Science 319 (2008) 23-28

[37] A. Jungbauer, R. Hahn, *Polymethacrylate monoliths for the preparative and industrial separation of biomolecular assemblies*, Journal of Chromatography A 1184 (2008) 62-79

[38] A. Podgornik, N.L. Krajnc, *Application of monoliths for bioparticle isolation,* Journal of Separation Science 35 (2012) 3059-3072

[39] M.R. Etzel, *Layered stacks*, 213-234, Journal of Chromatography Library Vol 67, *Monolithic materials: preparation, properties and applications* (2003), Elsevier, Amsterdam, the Netherlands

[40] J. Sproβ, A. Sinz, *Monolithic media for applications in affinity chromatography*, Journal of Separation Science 34 (2011) 1958-1973

[41] G. Guiochon, *Monolithic columns in high-performance liquid chromatography*, Journal of Chromatography A 1168 (2007) 101-168

[42] S. Dimartino, O.M. Herigstad, C. Boi, E. Lalli, G.C. Sarti, *Experimental and theoretical analysis to assess the use of monolithic columns in process chromatography*, Chemical Engineering Transactions 49 (2016) 25-30

[43] M.O. Herigstad, S. Dimartino, C. Boi, G.C. Sarti, *Experimental characterization of the transport phenomena, adsorption and elution in a protein A affinity monolithic medium*, Journal of Chromatography A 1407 (2015) 130-138

# CHAPTER 2

# Materials and experimental apparatus

## 2.1 Introduction

Chapter 1 introduced the concept of chromatography, different chromatographic techniques for the purification of proteins and the key role of affinity chromatography for the capture of antibodies, such as Immunoglobulin G, that represents the target protein for the present work. Moreover, the concept of convective chromatography was presented as the innovative element of the research project for this PhD thesis: convective chromatography can be carried out using stationary phases such as membranes and monoliths, whose main mass transport mechanism is convection instead of diffusion, as it is for stationary phases such as beads.

This chapter describes the materials used as convective chromatographic supports, both membranes and monoliths, the proteins and the analytical techniques used for their characterization. Moreover, an important part of this chapter is dedicated to the description of the chromatographic cycle experiments: the experimental apparatus and the data elaboration will be presented.

## 2.2 Affinity membranes

Membranes represent one choice of stationary phase that can be used as convective chromatographic support. Good features for a chromatographic membrane are high porosity, high surface area and good mechanical properties; the porosity of the membrane plays a central role because it must ensure the accessibility to the total pore volume.
Moreover, it is important that the membrane material does not interact with proteins or contaminats, to avoid non-specific adsorption, or irreversible adsorption of the target protein, and to reduce membrane fouling.

Another significant feature the membrane should have is a high number of active sites available for the immobilization of the affinity ligand.

The next three paragraphs will describe in detail the main components of the chromatographic membrane used for the selective capture of Immunoglobulin G: the membrane support, the spacer arm and the affinity ligands.

### *2.2.1 Regenerated cellulose membranes*

The membrane support used in this research was made of regenerated cellulose. Cellulose is an organic compound, a polysaccharide consisting of a linear chain of several hundred to many thousands of β(1→4) linked D-glucose units. It is possible to cross-link these linear polymeric chains through (1→6) glycosidic bonds, as shown in Fig. 2.1. The structure and the void fraction of the cellulose membrane are tuned according to the degree of cross-linking. The -OH groups in position 2, 3 and 5 are active sites available to be functionalized with reactive groups, such as epoxy groups, to allow the immobilization of an affinity ligand.
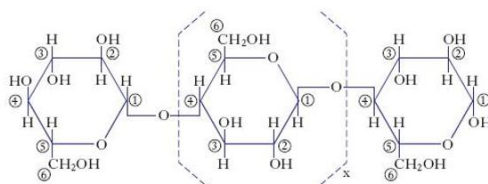


**Figure 2.1**   Cellulose structure.

Sartobind® Epoxy membranes, produced and kindly provided as a gift by Sartorius Stedim Biotech GmbH, were chosen as stationary phase for the preparation of affinity membranes. This matrix is made of regenerated cellulose activated with epoxy groups. The main properties of these membranes are reported in Table 2.1, while SEM images can be seen in Fig. 2.2.

**Table 2.1**   Sartobind® Epoxy membranes properties.

| Average Pore Size | Void Fraction | Thickness | Epoxy Group Density |
|---|---|---|---|
| [µm] | [%] | [µm] | [mol/cm$^2$] |
| 0.45 | 64 | 240 | $1.5 \cdot 10^{-6}$ |

The average pore size and epoxy group density are among the specifications provided by the manufacturer [1], while the membrane void fraction and thickness were experimentally

measured in our laboratory. The membrane thickness was measured using a micrometer (Absolute, Mitutoyo) and averaging the data over at least 10 points per membrane sheet, while the void fraction has been calculated by applying the method of moments. To this aim, independent chromatographic experiments were performed under non-binding conditions by feeding, at different flow rates, pulses of 10 and 100 μL of a 5% v/v acetone solution [2, 3]. Details related to the use of the method of moments for the characterization of porous materials can be found in paragraph 2.6.2.2.
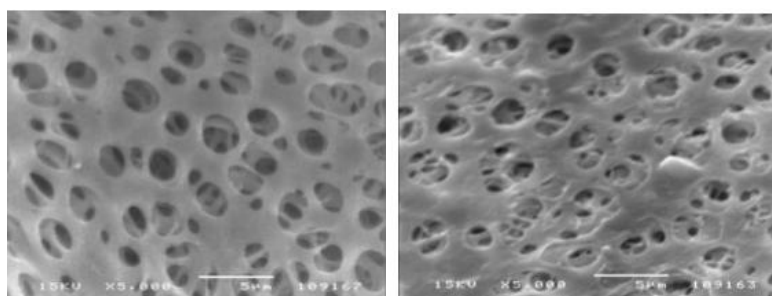


**Figure 2.2**    SEM images of Sartobind® Epoxy membranes: upper side on the left, lower side on the right. Analysis performed by the Membrane Technology Group, University of Twente.

### 2.2.2 Spacer arm

The spacer arm is usually a small molecule that is used to immobilize the affinity ligand on the surface of the membranes. Spacers usually consist of linear hydrocarbon chains with functionalities on both ends for easy coupling to the matrix and the ligand.

In the case of this research project, the complex spacer-ligand is synthesized first and then it is attached chemically to the membrane, following a specific immobilization protocol. In general, it is possible to immobilize the spacer arm on the support and then proceed with the immobilization of the ligand.

The choice of the spacer is very important because it has been demonstrated that the spacer arm can influence the performance of the whole chromatographic material, such as binding capacity, selectivity and protein recovery [4-7].

Moreover, it was shown that spacer arms of particular length and chemical composition can allow interactions between the affinity ligand and the matrix itself. These interactions can lead to a change in the conformation of the support in which the ligand, instead of being available for the capture of proteins, is adsorbed on the surface of the matrix [8].

For these reasons it is of great importance to investigate all the possible influences that this element has on the performance of the affinity material prepared.

In the present work, the spacer arm used to immobilize the affinity ligands on the membrane surface is 1,2-diaminoethane, also called 2LP, whose structure is reported in Fig. 2.3.
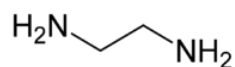


**Figure 2.3**     Structure of the spacer arm 2LP (1,2-diaminoethane).

### 2.2.3 Affinity Ligands

The affinity ligand is an important element of an affinity chromatographic support. Its role is fundamental, because it is responsible for the selective and reversible capture of the target protein.

Protein A is the most selective and exploited ligand for the purification of IgG, thanks to its great affinity for the constant fraction of this class of immunoglobulins. Also Protein G is largely exploited: it is expressed by Streptococcal bacteria and can capture immunoglobulins as Protein A does, but with differing binding specificities.

Due to some issues related to the use of Protein A, such as high production costs and possible leakage from the matrix, the interest of researchers and industries is now moving towards the use of synthetic ligands, in some cases mimetic of Protein A. This particular class of new ligands was developed studying the biological mechanisms involved in the recognition of IgG and often combining the use of molecular dynamic simulations and chemical synthesis.

Compared to Protein A, synthetic ligands have several advantages, such as reduced production costs and increased resistance to extreme pH values and ionic strength; they can also be designed to be selective for immunoglobulin classes that are not recognized by Protein A, such as human IgG$_3$. A huge advantage is the lower toxicity that synthetic ligands show, even if more studies need to be performed in this field: for this reason a possible release of ligands from the matrix causes a more contained risk compared to Protein A, which is a strong pathogen to the human body.

On the other hand, it is known that they are not perfectly able to mimic the Protein A interaction with the constant region of immunoglobulins, therefore, a lower selectivity might be expected [9].

As an alternative to Protein A and G, different classes of affinity ligands are available for the purification of IgG.

Among the synthetic ligands, A2P and B14 bio-mimetic ligands (mimetic Ligand[TM], ProMetic BioSciences, UK) and MEP HyperCel ligand (Pall, NY, USA) are the most popular. A2P ligand was developed to mimic the two amino acids of Protein A side chain, that play an important role

in the formation of the bond with IgG constant fragment [10]. The structure of B14 ligand is similar to that of A2P and it was designed to specifically bind $IgG_1$ [4]. MEP is a synthetic ligand able to purify antibodies even if it gives non-specific interactions with other proteins [11, 12]. These affinity ligands were successfully immobilized on both porous beads and membranes. Another important class of synthetic ligands is represented by peptide ligands: so far they were immobilized only on traditional chromatographic supports but it is expected that, thanks to their increasing development, their use on convective supports will be soon possible [13].

Among these: D-PAM (Xeptagen SpA, Italia) is a polypeptide that binds different classes of Immunoglobulins and it presents a higher selectivity with respect to Protein A [10, 12, 14]; HWRGWV, HYFKFD and HFRRHL ligands are mimetic of Protein A and were immobilized onto resins and characterized by the research group of Professor Carbonell [13].

In the present work, two different synthetic affinity ligands were immobilized on the surface of Sartobind® Epoxy membranes: the mimetic ligand A2P and a new ligand HPTA.

### 2.2.3.1 Mimetic Ligand$^{TM}$ A2P

The A2P ligand was developed by ProMetic BioSciences ltd. It represents the result of the selection made on combinatorial ligand libraries, where it is possible to find compounds specific for IgG binding. Molecular dynamic studies indicated the probability that this molecule could simulate the structure of two amino acids of Protein A, Phe 132 (phenylalanine) and Tyr 133 (tyrosine), which play a key role in the formation of the complex with IgG.

From a chemical point of view, A2P is a trichlorotriazine with 2 amino-phenols.

Fig. 2.4 shows the structure of the A2P synthetic ligand bond to the spacer arm through which it was immobilized on the surface of the membranes, the spacer arm 2LP (1,2-diaminoethane).
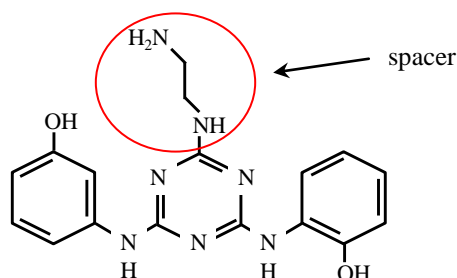


**Figure 2.4**    Chemical structure of A2P-2LP complex (molecular weight = 353.38 g/mol).

This ligand is commercial and many information related to its selectivity, binding and elution capacity, when immobilized on regenerated cellulose membranes, can be found in literature [5].

In the present work, this ligand was used as a benchmark to compare its performance to those of a new synthetic ligand, the ligand HPTA.

### *2.2.3.2 Ligand HPTA*

The HPTA ligand was recently designed, starting from the structure of A2P ligand, following the results obtained in the context of PRIN Project, in 2008 [15]; this project was carried out as a collaboration between the membrane research group of Università di Bologna and the group of Professor Cavallotti, Politecnico di Milano. The new ligand was then synthesized by Professor Giovenzana's group, at Università del Piemonte Orientale.

Using molecular dynamics combined with experimental activity and crystallographic studies it was possible to study the interaction between IgG and possible ligand molecules. This approach made it possible to find a new binding site for IgG that is more easily accessible than the usual binding site recognized by Protein A and to design and synthesize this new affinity ligand HPTA. Its structure is confidential, due to a current patent development; however in Fig. 2.5 it is possible to observe the secreted structure.

HPTA affinity ligand represents one of the innovative and challenging elements of the this research project, because it is not a commercial ligand and no data related to its performances can be found in literature.
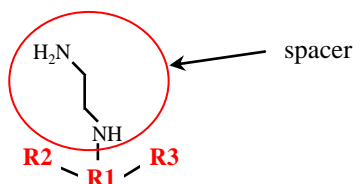


**Figure 2.5**    Chemical structure of HPTA-2LP complex (molecular weight = 332.17 g/mol).

## 2.3 Cellular ceramic monoliths

Monoliths were chosen as convective chromatographic materials, as an alternative to membranes. In particular, ceramic monoliths were produced and designed, before testing them as a novel chromatographic material.

The production and design of this material was carried out during the research period abroad, at the Department of Materials and Ceramics Engineering, Universidade de Aveiro, Portugal, under the supervision of Dr. Andrei Kovalevsky and Professor Jorge Frade.

### *2.3.1 Ceramic material*

The ceramic material used for the preparation of the monoliths is a composite material made of aluminium titanate and alumina, $Al_2TiO_5$-$Al_2O_3$; a SEM image of the structure of the monoliths produced is shown in Fig. 2.6.
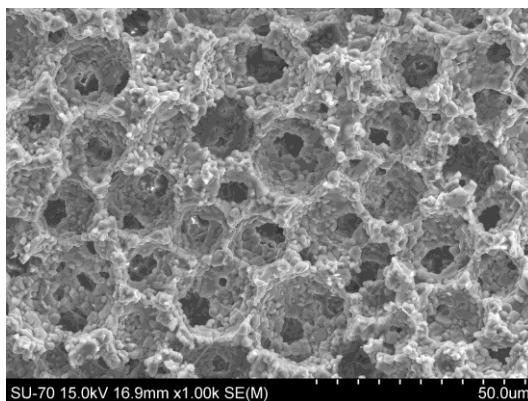


**Figure 2.6**     SEM image of the microstructure of the $Al_2TiO_5$-$Al_2O_3$ cellular ceramic monoliths.

These ceramic monoliths are highly porous materials, whose porosity can be tuned according to the manufacturing technique. Although aluminium titanate is very well known for its particular properties, that make its use interesting for several different applications, its use as a monolithic material in the field of filtration and separation applications requires a flexible and rational design, in order to give it the desired functionalities in terms of porous structure. The processing method for these new ceramic monoliths may take advantage of recent developments in the preparations of porous cellular ceramics through emulsification of ceramic suspensions [16-19]. Details on the processing method and design of the material are reported in Chapter 7.

## 2.4 Proteins and proteins mixtures

Different pure protein solutions and protein mixtures were used for the characterization of the affinity chromatographic supports. In particular, pure solutions of Immunoglobulin G (IgG), Bovine Serum Albumin (BSA) and lysozyme (LYS) were tested, as well as mixtures of the same three proteins in different combinations. Complex mixtures containing IgG, such as human serum, were also used. The aim was to determine the performance of affinity materials, of the chromatographic supports and of the spacers, such as binding capacity of IgG, selectivity and recovery of the target protein, together with non-specific adsorption.

All the samples used as feed solutions for adsorption tests were diluted to the desired concentration using 100 mM Phosphate Buffered Saline (PBS), pH 7.4.

### *2.4.1 Immunoglobulin G*

The pharmaceutical product Gammanorm was used as IgG source (pI ~ 7.4), purchased by Octapharma (Sweden). This product is sold in vials of 10 mL, the total protein concentration is 165 mg/mL and the minimum IgG content guaranteed is 95%. The real composition of this medication is reported in Table 2.2.

**Table 2.2**      Average composition of Gammanorm.

| IgG subclasses | Amount [%] |
|:---:|:---:|
| $IgG_1$ | 59 |
| $IgG_2$ | 36 |
| $IgG_3$ | 4.9 |
| $IgG_4$ | 0.5 |

The content of each vial was diluted using HPLC water and divided into 1 mL fractions, in order to have a protein concentration equal to 16.5 mg/mL. The so prepared aliquots were stored in the freezer at -18°C.

### *2.4.2 Bovine serum albumin*

Bovine serum albumin (BSA, pI ~ 4.7) is usually exploited for the preparation of protein concentration standards for laboratory experiments. It was used as a contaminant during adsorption tests, because this protein makes the purification of immunoglobulins particularly difficult, since it is the most abundant protein in blood plasma (its concentration can vary from 35 to 50 mg/mL).

It was purchased from Sigma-Aldrich (Milano) as a lyophilized powder of average molecular weight of 66 kDa and purity ≥ 96%.

### *2.4.3 Lysozyme*

Another protein considered as contaminant to be spiked in feed solutions for adsorption tests is lysozyme (LYS, pI ~ 11), which is an antimicrobial enzyme. This protein is mostly present in numerous animal and human secretions, such as tears and saliva, but it is also present in egg white in high concentrations. In a small part, lysozyme is also contained in serum (in concentrations below 10 μg/mL).

This particular functional protein was purchased from Sigma-Aldrich (Milano) as a lyophilized powder of average molecular weight of 14.3 kDa, protein content ≥ 90% and derived from chicken egg white.

### *2.4.4 Human serum*

Human serum was used as complex mixtures containing IgG.

Serum is obtained from plasma (that is the liquid part of the blood, yellow coloured, consisting of an aqueous solution of proteins, lipids, glucose, mineral salts and immunoglobulins) deprived from fibrinogen (a protein that intervenes in the coagulation process of blood). Serum is obtained by centrifugation of the coagulated blood, that removes the liquid part from the corpuscular fraction.

Human serum was purchased from Sigma-Aldrich (Milano).

## 2.5 Analytical techniques

Different analytical techniques, both quantitative and qualitative, were used for the characterization of protein solutions.

Among quantitative techniques, absorbance reading was used for pure protein solutions, while HPLC and Bicinchoninic Acid Assay (BCA) were used for protein mixtures.

Electrophoresis under denaturing conditions was used as a qualitative technique for the characterization of protein mixtures.

### *2.5.1 Absorbance measurements*

Absorbance reading is one of the simplest but, at the same time, most effective methods for the determination of protein concentration in pure solutions. This analytical technique is based on the ability of proteins to absorb radiations in the UV spectrum. Usually the wavelength used to perform the analysis is 280 nm, at which the proteins show a peak in the absorbance.

At low concentration values, the relation between the absorbance and the protein concentration in the solution is linear and can be described using Lambert and Beer law:

$$Abs_\lambda = \varepsilon_\lambda c\, H \qquad\qquad (2.1)$$

where $Abs_\lambda$ is the value of the absorbance read by the instrument at the wavelength $\lambda$, c is the concentration of the protein in solution, $H$ is the length of the optical path and $\varepsilon_\lambda$ is the proportional coefficient.

Although the absorbance is a pure number, the absorbance unit AU (Absorbance Unit) is usually used as unit of measure. The proportional coefficient expresses how easy the photons of the incident radiation interact with the molecule, and therefore it depends on the protein analyzed. Moreover, the proportionality coefficient depends on the buffer in which the protein is dissolved, therefore the pH and the ionic strength can modify the interaction of the photons with the biomolecule, because they alter the protein configuration.

The instrument used to measure the absorbance of pure protein solutions is a UV-vis Spectrophotometer (UV-1601 Shimadzu Italia, Milan, Italy), which has a length of the optical path equal to 1 cm.

### 2.5.2 Chromatographic analysis

Protein quantitation in the case of mixtures can be performed using the HPLC technique, High Performance Liquid Chromatography.

HPLC is a modern chromatographic technique in which, thanks to the use of high pressure values, the mobile phase flows through a column filled with a fine bead stationary phase. The instrument is usually composed of a pump system required for feeding the mobile phase, and an injector for the samples to be analyzed. The column is the main element of the instrument because here occurs the separation. Finally, a specific detector measures the amount of the effluent molecules, and the signal is recorded by a computer.

The HPLC instrument used for the experimental activity is composed of two modules: a Waters Alliance 2695 separation module equipped with a module 2487 dual-wavelength absorbance detector (Waters, Milan, Italy). Two different chromatographic columns were used in order to perform the HPLC analysis: for the determination of IgG concentration, a Protein A cartridge has been used (Applied Biosystems, PA ImmunoDetection® Sensor Cartridge for Perfusion Immunoassay™ Technology), while for protein mixtures (bovine and human serum, mixtures of IgG, BSA and LYS) an HPLC SEC column has been used (BioSuite™ 250, 4 μm, UHR SEC, Waters, Milan, Italy).

### 2.5.3 BCA colorimetric assay

BCA is a colorimetric method and consists in the use of a reagent, the bicinchoninic acid, that allows to determine the total protein content in the sample analyzed.

This method exploits the ability of proteins in alkaline environment to reduce $Cu^{2+}$ in $Cu^{1+}$ (biuret reaction); these two compounds react with the bicinchoninic acid to form a purple complex [20]. This complex shows an absorbance maximum value at 562 nm and the intensity of

the coloration can be considered almost proportional to the amount of protein present; the total protein content in the samples analyzed can be determined using a calibration curve, obtained using samples of BSA of known concentration.

The kit Pierce BCA Protein Assay, purchased from Thermo Fisher Scientific, was used to determine the total protein content of human serum samples, following the standard suggested protocol [21].

### *2.5.4 Electrophoresis*

The Electrophoresis is an analytical method based on the different velocity of migration of electrically charged particles immersed in a fluid by the effect of an electric field applied by a pair of electrodes.

Electrophoretic separation is carried out using a polymeric gel, made of polyacrylamide, which acts as a molecular sieve through which the various molecules must flow. The polyacrylamide gel consists of two parts: the stacking gel and the running gel; the first part represents the top of the gel containing the loading wells where the samples to be analyzed and a molecular marker are placed, while the second part is the portion of gel in which the electrophoretic run takes place. The percentage of polyacrylamide increases from the loading area of the wells to the bottom of the gel: the different pore distribution allows the separation of the fragments of proteins and only the smaller ones can reach the bottom of the gel, so the fragments of biomolecules are separated on the basis of their molecular weight.

SDS-PAGE (Sodium Dodecyl Sulphate - PolyAcrylamide Gel Electrophoresis) is the most commonly used technique among polyacrylamide-based gel electrophoresis techniques. SDS is an anionic detergent capable of breaking non-covalent interactions in proteins, which lose their three-dimensional structure and are denatured: so there are SDS-protein complexes, in a ratio of about one molecule of SDS for each two amino acid residues, characterized by a negative net charge which can be considered proportional to the mass of the protein itself; the negative charge gained by the formation of the bond with the sodium dodecyl sulfate is greater than the charge of the native protein, which is negligible.

Before performing the analysis, the protein sample is also treated with bromophenol blue, a colorant that shows the course of the electrophoretic rum. In this way it is possible to evaluate the presence of a given protein in the sample if the corresponding coloured band is visible in the gel.

IgG treated with SDS is denatured into the four chains: two light and two heavy chains, with a molecular weight respectively of 25 and 50 kDa. The presence of IgG in a sample treated with

SDS-PAGE is thus visible if there are coloured bands at the molecular weights of the light and heavy chains of IgG; other bands correspond to any pollutants present in the sample.

## 2.6 Chromatographic experiments and apparatus

Traditional chromatographic experiments were performed, both in batch and dynamic mode, to characterized the affinity chromatographic support prepared.

The experimental procedure is composed by the following steps:

- **Equilibration**: the starting working conditions of the affinity chromatographic material are set using a buffer solutions, PBS, which is the same buffer used to prepare the protein solution.
- **Adsorption**: in this stage, the protein solution is put in contact with the affinity chromatographic material and the target protein is captured by the affinity ligand immobilized on the surface of the stationary phase. On a laboratory scale, the chromatographic support is completely saturated, to exploit the total binding capacity of the material.
- **Washing**: the washing step is important because it allows to wash out the protein solution still present in the pores of the matrix and any protein non-specifically adsorbed on the support. The buffer used is the same used for the equilibration step.
- **Elution**: the buffer used in this phase of the chromatographic cycle is able to break the interactions between the affinity ligand and the adsorbed target protein, to recover the product of interest; in particular, a solution of 100 mM glycine, pH 2.8, was used as elution buffer.
- **Equilibration**: a final step of equilibration using PBS is needed to restore the initial conditions and make the chromatographic support ready for the next cycle.

Both for batch and dynamic experiments, the same chromatographic support was used for at least 3 subsequent cycles. After a specific number of chromatographic cycles, it is possible to add a step of regeneration, to restore completely the initial conditions of the affinity matrix, especially if the recovery of the protein during the elution step is not complete. For the regeneration of the material, a solution of 0.4 M NaOH is usually used to denature and desorb all proteins still bound to the affinity matrix.

*2.6.1 Batch experiments*

Batch experiments were carried out for membranes and monoliths according to the step described above, but following two different specific procedures, due to the different conformation of the chromatographic materials.

Membranes: for each adsorption test, two membrane discs of 1.5 cm diameter were used. The equilibration step was performed soaking the membranes in PBS for at least 15 min. The adsorption test was carried out by soaking the membrane discs in the protein solution of known concentration and kept under gentle agitation until equilibrium was reached (2 hours, time determined by kinetic studies; see Chapters 3 and 4). After the adsorption step, the membranes were first dabbed with paper to remove the excess of protein solution and then washed with PBS, keeping them under gentle agitation for 1 hour. The elution step was carried out by immersing the membranes in the glycine buffer for 1 hour, under gentle agitation.

Monoliths: in the case of monoliths, batch experiments were performed to check the activity of the epoxy groups on the surface (see Chapter 8), performing the only adsorption test using BSA solution of known concentration. The monolith was used in the form of small pieces and powder (small pieces crashed to powder). Both pieces and powder were put in contact with the protein solution for 24 hours.

In both cases, the protein concentration was determined at the beginning and at the end of the adsorption step (as well as at the end of the washing and elution steps in the case of membranes) using the appropriate analytical technique. In this way it was possible to calculate the amount of protein adsorbed, washed and eluted, therefore it was possible to calculate the binding capacity of the chromatographic materials.

*2.6.2 Dynamic experiments: FPLC*

Dynamic experiments were performed following the steps described in paragraph 2.6 and using appropriate column holders for membranes and monoliths (a description of the column holders will be given in paragraph 2.6.3).

The chromatographic columns were used on a Fast Protein Liquid Chromatography (FPLC) ÄKTA Purifier 100 (GE Healthcare, Milan, Italy).

This FPLC system is specially designed for small scale laboratory and research applications. The chromatographic unit consists of three modules, as shown in Fig. 2.7. From the bottom to the top they are:

− Pump system P-900, composed by two pairs of high performance piston alternating pumps, able to reach a flow rate of 100 mL/min and a maximum pressure of 100 bar.

− Monitor UV-900, a multiple wavelength absorbance detector able to simultaneously monitor three different wavelengths in the range of 190 to 700 nm.

− Monitor pH/C-900, a combined detector for in-line measurement of pH and conductivity.



**Figure 2.7**    Scheme of the FPLC ÄKTA Purifier.

Other components are present in the system, such as valves, a mixer, the chromatographic column, and others, as shown in Fig. 2.8. The pump system consists of 4 heads, two for the pair of pumps A and two for the pair B. Each pair of pumps works in parallel to ensure a constant flow. The pump system A can process two different lines, respectively line A1 and line A2; the same concerns the pumps B, which moves the solutions connected to lines B1 and B2. The choice between line 1 and 2 is determined by the position of a switch valve. Therefore, the chromatographic system can process up to 4 buffers, two of which can be fed simultaneously, one from the pump A and one from the pump B.
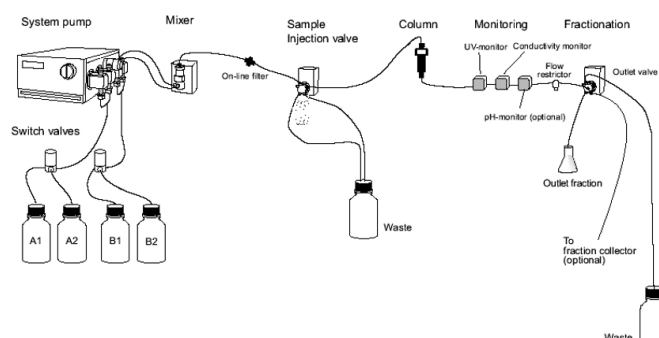


**Figure 2.8**    Scheme of the basic components of a FPLC ÄKTA Purifier.

A pressure damping device is placed after the pumps to contain the pressure swings associated with the alternating operation of the pistons. The lubrication of the pumps is ensured by a special retro-lubrication system, in which a service fluid flows in a closed circuit with a velocity proportional to that of the pumps. The service fluid is a 20% v/v ethanol solution in water.

The solutions from the two lines are homogenized in a magnetic mixer, filtered through a 2 μm pore size polypropylene filter and reach the injection valve. As shown in Fig. 2.9, the injection valve can assume three different positions. When the valve is in the Load position, the buffer coming from the pumps is fed to the chromatographic column. In this position, it is possible to load the sample from port 3 while the column is equilibrated. Between the ports 2 and 6 the sample container is placed, which can be a simple pipe of known volume (loop) or a superloop (see below in this same paragraph). When the valve moves to the Inject position, the sample is pushed to the chromatographic column by the buffer flow, while when the valve is in Waste position, the column is excluded from the circuit and the solution is collected in a waste tank. When a change of buffer is needed, this position is useful to wash the system volumes before the column.
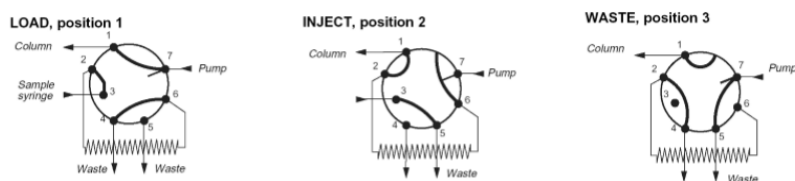


**Figure 2.9**    Positions associated to the injection valve.

After the injection valve, the solution flows towards the column, then it flows through the UV cell, the conductivity and pH measuring instruments. Before the outlet valve it is possible to insert a flow restrictor, an element that generates pressure drops and increases the pressure in the measuring instrument section. This is necessary to avoid the formation of air bubbles at the outlet of the column that could affect the measurements.
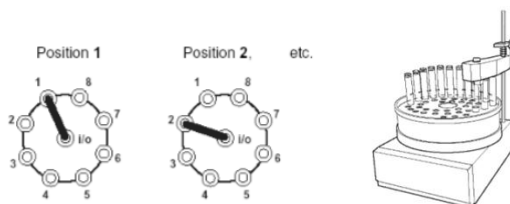


**Figure 2.10**   Positions associated to the outlet valve and fractions collector.

At the end of the circuit there is an eight-port valve; depending on the position of the outlet valve, it is possible to direct the flow to a special fractions collector (Fig. 2.10), or to other collectors elements, or to a waste tank.

As previously introduced, the protein sample can be fed to the column using a superloop, that allows to inject up to 150 mL. It consists of a pyrex glass tube with an internal piston that divides the tube into two regions (Fig. 2.11). In the region below the piston, the sample to be analyzed is loaded: this can be done using a syringe or a peristaltic pump. The region over the piston corresponds to the inlet of the buffer fed by the pumps, when the injection valve is in Inject position: the flow of the buffer allows the piston inside the tube to move downwards and so the sample is fed to the column.
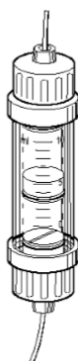


**Figure 2.11**   Scheme of the superloop.

Unicorn$^{TM}$ is the program used to operate the chromatographic unit and to process the results. It is presented to the user with a four-window structure:

− Manager: this window is the documents management system; it is divided into two columns, in the one on the left there are the working methods used to run the experiments, and in the column on the right there are the results of the tests;

− Method editor: in this window you can create, edit and save working methods;

− System control: this is the most important window; it allows to follow the results of real-time experiments and to modify the operating parameters manually and with immediate effect on the process;

− Evaluation: this window allows the elaboration of the results obtained. It is possible to normalize the curves, integrate the area underneath peaks, minimizing noise interference on the recorded signal. Results can also be exported to other programs such as worksheets or text files for further elaboration.

### *2.6.2.1 Data elaboration*

The elaboration of the results of the chromatographic cycle experiments is important to determine the amount of protein adsorbed, washed and eluted: these information are necessary to evaluate the performance of the affinity chromatographic support, because they allow to calculate the dynamic binding capacity and the recovery.

The system dispersion curve has to be determined to perform a correct elaboration of the data, because the external column volumes affect the separation process. The experiments aiming to the determination of the system dispersion curve are performed under non-binding conditions following the same steps of traditional chromatographic cycles.

In particular, these experiment were carried out using a solution of 0.4% v/v acetone in water, instead of using a protein solution. All the buffers used in the different stages of the cycle were replaced by demineralised water.

Looking at Fig. 2.12 and at Eq. (2.2) it is easy to understand that the mass of the protein that is fed to the column, $m_{fed}$, that corresponds to the starting concentration of the protein, $c_0$, times the volume of the protein solution fed during the adsorption phase, $V_{ads}$, can be divided into three parts: a first part is related to the mass of protein present in the whole chromatographic system volume, $m_{sys}$, a second part is associated to the mass of protein adsorbed by the affinity matrix, $m_{ads}$, and a third part corresponds to the mass of protein that is lost, exiting the system, $m_{out}$. The contribution given by $m_{sys}$ can be evaluated integrating the area beneath the y axis and the dispersion curve, while $m_{out}$ is calculated integrating the area below the breakthrough curve. The difference between the mass of the protein fed and these two contributions gives the amount of protein adsorbed in the column.

$$m_{fed} = m_{sys} + m_{ads} + m_{out} \tag{2.2}$$
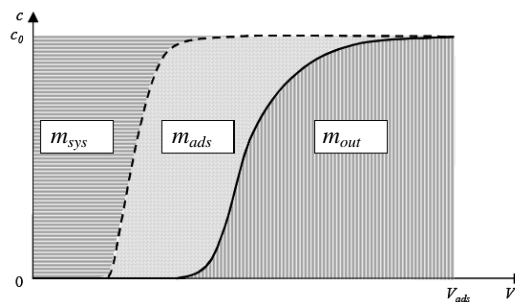


**Figure 2.12** Qualitative profile of the dispersion curve (dashed line) and the breakthrough curve (solid line) in the adsorption step.

The dynamic banding capacity at 100% breakthrough (when the affinity matrix is completely saturated), $DBC_{100\%}$, is represented by the ratio between the amount of protein adsorbed and the total volume of chromatographic support placed in the column:

$$DBC_{100\%} = \frac{m_{ads}}{V_{matrix}} \qquad (2.3)$$

The $DBC_{100\%}$ corresponds to the concentration of the protein in the stationary phase in equilibrium with the mobile phase, at the conditions at which the experiment was performed. This parameter depends especially on the affinity support used, but it can vary also as a function of the concentration of protein fed and on the flow rate of the feed solution.

If dynamic binding capacity data are reported according to the equilibrium concentration, it is possible to build the adsorption isotherm for the system considered. By interpolating the experimental data with a reasonable theoretical isotherm, such as that of Langmuir, it is possible to estimate important parameters such as maximum capacity under dynamic conditions, $DBC_{MAX}$, and the dissociation constant $K_d$. Details related to the procedure described will be exposed in Chapter 3 and 4.

Experimental data related to the washing step can be analysed in same way. At this stage, the washing buffer displaces the protein solution from the system's volumes, and part of the previously adsorbed protein may desorb from the support, either because it is bound non-specifically, and therefore through weak interactions, or due to the reversibility of the specific binding. The amount of protein exiting the column at this stage, $m_{wash}$, corresponds to the area below the washing curve and is composed by two contributions, one related to the protein mass present in the system volumes, $m_{sys}$, and the other equal to the mass of protein that desorbs from the support, $m_{des}$, as shown in Fig. 2.13 and by Eq. (2.4).

$$m_{wash} = m_{sys} + m_{des} \qquad (2.4)$$
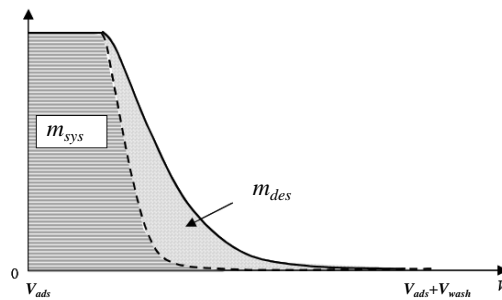


**Figure 2.13**   Qualitative profile of the dispersion curve (dashed line) and the breakthrough curve (solid line) in the washing step.

The mass of protein still bound to the affinity matrix after the washing step corresponds to mass of protein that should be theoretically recovered during the elution step:

$$m_{elu}^{theoretical} = m_{ads} - m_{des} \qquad (2.5)$$

The mass of protein that can be actually recovered during the elution step is instead determined by the integration of the area below the elution peak; since the amount of protein eluted is usually less than the mass of protein still bound after the washing step, the concept of recovery has to be introduced: it is defined as the ratio between the mass of protein actually eluted and the mass of protein that should have been eluted theoretically:

$$R = \frac{m_{elu}^{real}}{m_{elu}^{theoretical}} \qquad (2.6)$$

The recovery of protein during the elution step is a very important parameter used to evaluate the performance of the affinity chromatographic support: the role of the affinity ligand is crucial, because the binding between this element and the protein should be completely reversible.

### 2.6.2.2 Method of moments

The important theoretical tool of the method of moments can be used to determine fundamental structural characteristics of the chromatographic column: parameters such as porosity, axial dispersion coefficient and mass transport coefficient can be calculated.
This method was first introduced in the late '60s [22, 23], but it is still largely used [24, 25].

The method of moments was developed for chromatographic columns packed with porous beads; the theory that will be presented in this paragraphs derives from the one introduced to describe bead-based chromatography with some simplifications due to the fact the system used for this research project refers to convective chromatographic materials. Moreover, the method of moments was used, for the purposes of this PhD thesis, working under non binding conditions, with the aim of determine the void fraction and the axial dispersion coefficient of the porous chromatographic support used.
The complete and general theory related to method of moments can be found in literature [22, 23].

The definition of the n-th moment of the concentration profile of an effluent peak exiting a chromatographic column after a pulse injection is:

$$M_n = \int_0^\infty c(t)t^n dt \qquad (2.7)$$

the n-th absolute or normalized moment is:

$$\mu_n = \frac{M_n}{M_0} = \frac{\int_0^\infty c(t)t^n\,dt}{\int_0^\infty c(t)\,dt} \tag{2.8}$$

and the n-th absolute central moment is:

$$\overline{\mu}_n = \frac{\int_0^\infty c(t)(t-\mu_1)^n\,dt}{\int_0^\infty c(t)\,dt} \tag{2.9}$$

It is important to calculate the first moment $\mu_1$ and the second central moment $\overline{\mu}_2$ to determine the porosity and the axial dispersion coefficient of porous supports; the statistical meaning of this two moments are respectively the average value $\mu$ and the variance $\sigma^2$ of the distribution that coincides with the output peak. From a practical point of view, these moments represent the retention time of the injected sample and the enlargement of the front of the solutes related to the efficiency of the chromatographic column.

In particular, the expressions used to calculate $\mu_1$ and $\overline{\mu}_2$ are the following:

$$\mu_1 = \frac{M_1}{M_0} = \frac{\int_0^\infty f(t)t\,dt}{\int_0^\infty f(t)\,dt} \tag{2.10}$$

$$\overline{\mu}_2 = \frac{\int_0^\infty f(t)(t-\mu_1)^2\,dt}{\int_0^\infty f(t)\,dt} \tag{2.11}$$

A simplification of the method of moments is given by the HETP method (method of the Height Equivalent to a Theoretical Plate). To make sure that this method can be applied, it is strictly necessary that the effluent peak can be approximated to a Gaussian distribution: only in this case the retention time, that is the first moment, coincides with the time corresponding to the maximum height of the peak, and the second moment can be evaluated starting from the width of the peak in correspondence to the inflection points. Unfortunately, it is not always possible to approximate the peaks to a Gaussian distributions, so the method of moments is the tool used for the calculation of the characteristic column parameters.

When the method of moment is used referring to a convective chromatographic system under non-binding conditions, the expressions of the first and second moment can be written as follows:

$$\mu_1 = \frac{L_{TOT}}{v} \varepsilon \tag{2.12}$$

$$\overline{\mu}_2 = 2 L_{TOT} \frac{D_L}{v^3} \varepsilon^2 \tag{2.13}$$

where $L_{TOT}$ is the total length of the chromatographic column, $v$ is the superficial velocity, $\varepsilon$ is the void fraction, or porosity, and $D_L$ is the axial dispersion coefficient.

Form the experimental point of view, the method of moment was applied to peaks exiting the chromatographic column (both using membranes and monoliths) after performing pulse injections of small volumes of different tracers, under non-binding conditions, using the FPLC. In particular, to avoid non-specific interactions between the tracers and the chromatographic materials, such as electrostatic and hydrophobic, experiments under non-binding conditions were carried out diluting each tracer in a 20 mM phosphate buffer containing 250 mM sodium chloride and 5% v/v ethanol.

Pulse injections of 10 and 50 µL were performed several times to ensure the reproducibility of the results, for the following tracers: acetone (5% v/v), glycine (400 mM), arginine (8 mg/mL), dextran sulfate sodium salt (4000Da, 8 mg/mL), LYS (4 mg/mL) and BSA (4 mg/mL), in order to cover a wide range of molecular weights. Injections were performed at four different flow rates: 1, 2.5, 5 and 7.5 mL/min.

Moreover, measuring the first moment, contributions from extra column volumes were taken into account, performing the same injections to the empty column holder.

### 2.6.3 Convective modules

Chromatographic materials, membranes and monoliths, have to be place inside specific modules, or column holders.

The next two paragraphs will present a description of the modules used.

#### 2.6.3.1 Membrane column holder

The column holder used in the case of membranes is shown in the picture below, and it can be used with 5 membranes discs of 2.6 cm diameter.

This module is made of stainless steel, a material that guarantees high mechanical strength. The column holder is composed of a female part, in which the membranes, the frits and the o-rings are placed, and a male part with a thread zone that ensure the closure of the module.



**Figure 2.12**   Membranes module and its equipment.

The inner parts of the cell, those in direct contact with the membranes, present many knurlings, designed to improve the inlet flow distribution and to facilitate the collection of the effluent solution. Moreover, to further improve the flow distribution and to prevent the membranes from being in direct contact with the rigid surfaces of the cell, important cell equipments are used: they are called frits, discs made of a mixture of PTFE and PEEK.

In addition, to ensure the hydraulic seal of the cell, two o-rings are used; the order of the elements to be placed in the module is the following: frit - o - ring - membranes - frit - o - ring.

This membrane module was the subject of many studies at the Membrane Research group of the University of Bologna: the aim of the design was to ensure the correct flow distribution and the appropriate degree of compression of the membranes [26, 27].

### *2.6.3.2 Monoliths column holder*

Dynamic experiments were carried out using small cylindrical ceramic columns, diameter of approximately 1 cm but of different lengths, placed inside an adjustable length plastic holder provided by BIA Separations (Ljubljana, Slovenia): this cell was designed to be used with commercially available convective interaction media (CIM) monolithic columns, sold by the same producer.

For this reason, it was necessary to optimize the configuration of this column holder, to use it with the ceramic monoliths produced (refer to Fig. 2.13). To do so, the ceramic stationary phase, casted in the shape of a cylinder, 1.2 cm diameter and 8 cm length approximately, was first polished to remove defects that affected the external surface and cut into cylinders of the desired

dimensions. The samples were then placed inside a rigid plastic ring, and then into the holder, to ensure the hydraulic seal of the cell. Between the ceramic monolith and the rigid plastic ring, thin layers of parafilm and silicon were used to prevent the monolith to move inside the holder and to guarantee the hydraulic seal.

The original polymeric frits at the inlet and at the outlet of the cell were kept, to ensure an optimal flow distribution across the ceramic columns.



a)                                   b)
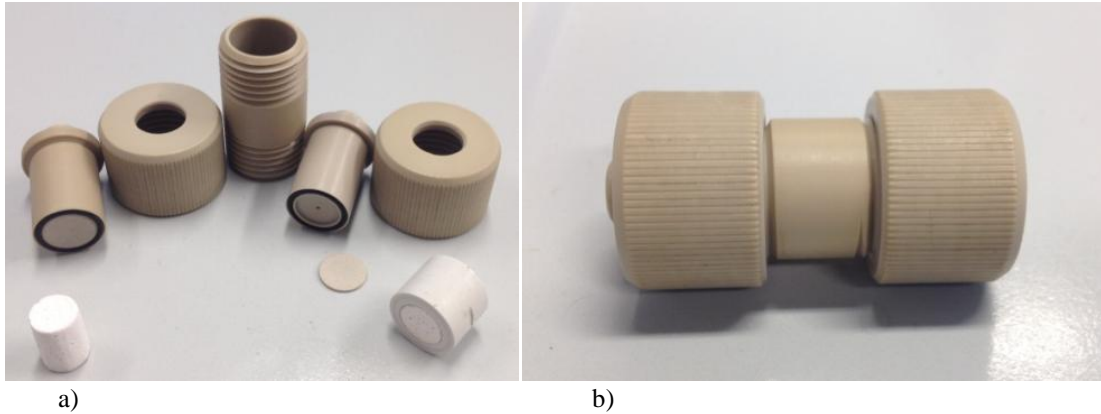
**Figure 2.13** Monoliths module and its equipment; a) module disassembled with a monolithic column on the left and a monolithic column inside the plastic ring on the right; b) module assembled.

# References

[1]    http://microsite.sartorius.com/en/biotechnology/laboratory/products_applications/membrane_adsorbers/literature/pdfs/Manual_Sartobind-Epoxy-Sheet_SL-6113-e05041.pdf (accessed on 09 October /2017); Sartobind® Epoxy Sheet

[2]    G. Guiochon, A. Felinger, D.G. Shirazi, A.M. Katti, *Fundamentals of Preparative and Nonlinear Chromatography*, Elsevier 2nd ed., San Diego (2006)

[3]    M.O. Herigstad, S. Dimartino, C. Boi, G.C. Sarti, *Experimental characterization of the transport phenomena, adsorption, and elution in a protein A affinity monolithic medium*, Journal of Chromatography A 1407 (2015)130-138

[4]    C. Boi, S. Dimartino, S. Hofer, J, Horak, S. Williams, G.C. Sarti, W. Lindner, *Influence of different spacer arms on Mimetic Ligand$^{TM}$ A2P and B14 membranes for human IgG purification*, Journal of Chromatography B 879 (2011) 1633-1640

[5]    C. Boi, V. Busini, M. Salvalaglio, C. Cavallotti, G.C. Sarti, *Understanding ligand-protein interactions in affinity membrane chromatography for antibody purification*, Journal of Chromatography A 1216 (2009) 8687-8696

[6]    C. Boi, S. Dimartino, G.C. Sarti, *Modelling and simulation of affinity membrane adsorption*, Journal of Chromatography A 1162 (2007) 24-33

[7]    L. Zamolo, M. Salvalaglio, C. Cavallotti, B. Galarza, C. Sadler, S Williams, S. Hofer, J. Horak, W. Lindner, *Experimental and theoretical investigation of effect of spacer arm and support matrix of synthetic affinity chromatographic materials for the purification of monoclonal antibodies*, Journal of Physical Chemistry B 114 (2010) 9367-9380

[8]    W.L. DeLano, M.H. Ultsch, A.M. de Vos, J.A. Wells, *Convergent solutions to binding at a protein-protein interface*, Science 287 (2000) 1279-83

[9]    C. Boi, S. Dimartino, *Advances in membrane chromatography for the capture step of monoclonal antibodies*, Current Organic Chemistry 21(17) (2017) 1753-1759

[10]   C. Boi, *Membrane adsorbers as purification tools for monoclonal antibody purification*, Journal of Chromatography B 848 (2007) 19-27

[11]   L.N. Lund, P. Gustavsson, R. Michael, J. Lindgren, L. Norskov-Lauritsen, M. Lund, G. Houen, A. Staby, P.M.St. Hilaire, *Novel peptide ligand with high binding capacity for antibody purification*, Journal of Chromatography A 1225 (2012) 158-167

[12]   A.C.A. Roque, C.S.O. Silva, M.A. Taipa, *Affinity-based methodologies and ligands for antibody purification: advances and perspectives*, Journal of Chromatography A 1160 (2007) 44-55

[13] W.S. Kish, A.D. Naik, S. Menegatti, R.G. Carbonell, *Peptide-Based affinity adsorbents with high binding capacity for the purification of monoclonal antibodies*, Industrial & Engineering Chemistry Research 52 (2013) 8800-8811

[14] J. Horak, S. Hofer, C. Sadler, S. Williams, W. Lindner, *Performance evaluation of Mimetic LigandTM B14-triazole-FractoAIMS adsorbents for the capture of human monoclonal immunoglobulin G from cell culture feed*, Analytical and Bioanalytical Chemistry 400 (2011) 2349-2359

[15] G.C. Sarti, J.B. Nagy, N. Elvassore, C. Cavallotti, Final report on PRIN project, *Sviluppo di cromatografia a membrana per la purificazione di biomolecole*, 2008

[16] N. Vitorino, J.C.C. Abrantes, J.R. Frade, *Cellular ceramics processed by paraffin emulsified suspensions with collagen consolidation*, Materials Letters 98 (2013) 120–123

[17] M.F. Sanches, N. Vitorino, J.C.C. Abrantes, J.R. Frade, J.B. Rodrigues Neto, D. Hotza, *Effects of processing parameters on cellular ceramics obtained by paraffin emulsified suspensions*, Ceramic International 40 (2014) 9045–9053

[18] N. Vitorino, C. Freitas, A.V. Kovalevsky, J.C.C. Abrantes, J.R. Frade, *Cellular $MgAl_2O_4$ spinels prepared by reactive sintering of emulsified suspensions*, Materials Letters 164 (2016) 190–193

[19] M.F. Sanches, N. Vitorino, C. Freitas, J.C.C. Abrantes, J.R. Frade, J.B. Rodrigues Neto, D. Hotza, *Cellular ceramics by gelatin gelcasting of emulsified suspensions with sunflower oil*, Journal of the European Ceramic Society 35 (2015) 2577–2585

[20] P.K. Smith, R.I. Krohn, G.T. Hermanson, A.K. Mallia, F.H. Gartner, M.D. Provenzano, E.K. Fujimoto, N.M. Goeke, B.J. Olson, D.C. Klenk, *Measurement of protein using bicinchoninic acid*, Analytical Biochemistry 150 (1985) 76-85

[21] Thermo Scientific, Pierce™ BCA Protein Assay Kit, User Guide

[22] M. Kubin, *Theory of the chromatography. II. Effect of the external diffusion and of the adsorption on the sorbent particle*, Collection of Czechoslovak Chemical Communications 30 (1965) 2900–2907

[23] E. Kučera, *Contribution to the theory of chromatography : Linear non-equilibrium elution chromatography*, Journal of Chromatography 19 (1965) 237–248

[24] K. Miyabe, G. Guiochon, *Measurement of the parameters of the mass transfer kinetics in high performance liquid chromatography*, Journal of Separation Science 26 (2003) 155–173

[25] H. Hong, A. Felinger, K. Kaczmarski, G. Guiochon, *Measurement of intraparticle diffusion in reversed phase liquid chromatography*, Chemical Engineering Science 59 (2004) 3399–3412

[26] F. Morselli, *Caratterizzazione di membrane di affinità per IgG umana*, Master Thesis Università di Bologna, Academic Year 2007-08

[27] S. Dimartino, *Studio sperimentale e modellazione della separazione di proteine con membrane di affinità*, Tesi di Dottorato di Ricerca in Ingegneria Chimica dell'Ambiente e della Sicurezza XXI Ciclo, Facoltà di Ingegneria, Università degli Studi di Bologna, 2009

# PART I


# Affinity Membrane Chromatography

# CHAPTER 3

# Membrane activation and characterization

## 3.1 Introduction

This chapter provides information related to the experimental protocols used for the modification of the cellulose membranes; moreover, details regarding the experiments carried out to characterize the affinity chromatographic membranes will be given.

## 3.2 Membranes modification

As introduced in Chapter 2, the affinity membranes are composed of three fundamental elements, the cellulosic matrix, the spacer arm and the affinity ligand. It is appropriate to evaluate the influence that each element has on the binding capacity and the selectivity, usual parameters chosen to express the efficiency of an affinity chromatographic material, to study the performance of the convective chromatographic support. Therefore, protein adsorption experiments were carried out using the native Sartobind® Epoxy membranes, the cellulosic membranes modified with only the spacer arm 2LP and complete affinity membrane, that is the membrane with the complex ligand-spacer (both A2P ligand and HPTA ligand).

For all the three type of material tested (native membranes, 2LP-membranes and A2P/HPTA-membranes) it is necessary an endcapping of the unreacted epoxy groups. Indeed, after the immobilization of the spacer arm or of the affinity ligands, part of the epoxy groups on the surface might still be active and might cause a non-specific interaction with the target protein or other proteins during the adsorption experiments. This is particularly true in the case of the native membrane support, that require an endcapping of all the epoxy groups before use it as a control during the experiments. Therefore, a study of the endcapping strategy was indeed performed modifying the native cellulose membrane with different reagents.

The immobilization procedures for ligands and the spacer arm were adapted from the protocol described by C. Boi *et al*. [1].

### *3.2.1 Endcapping strategies*

Different chemical reagents were tested with the goal of obtaining an optimal deactivation of the residual epoxide groups of the cellulosic membranes. Treatments with 2-ethanolamine, 2-mercaptoethanol and acidic hydrolysis are the principal strategies suggested in the literature for endcapping of epoxy activated matrices [2, 3], and for each case a different reaction mixture was prepared. It is useful to remind that the membranes were cut into discs of 1.5 cm diameter and 2.6 cm diameter to use them in batch and dynamic tests respectively.

**2-ethanolamine**: this encapping solution was prepared mixing 2-ethanolamine in ethanol at a concentration of 0.1 M.

**2-mercaptoethanol**: in this case, a solution of 5 mol-equivalents (with respect to the initial density of epoxy groups on the support) of 2-mercaptoethanol in water was prepared.

**Acidic hydrolysis**: a solution of sulphuric acid at a concentration of 0.5 M in water, with a volume equal to 20 times the volume of the membrane sheets, was prepared.

The membrane discs were first equilibrated in ethanol (or water, according to the endcapping procedure) then suspended in the prepared solution and the mixture was gently shaken overnight at 50 °C, for a total of 15 hours. To remove the excess blocking agent the membrane supports were then washed using ethanol and water for several subsequent times (usually 30 minutes in ethanol, 30 minutes in water, at least twice). It was observed that the use of a sonicator to carry out the washing steps, after the endcapping procedure, improved the matrix performances [4]. Figure 3.1 reports chemical modification that occurred to the support as a consequence of the three different endcapping procedures.
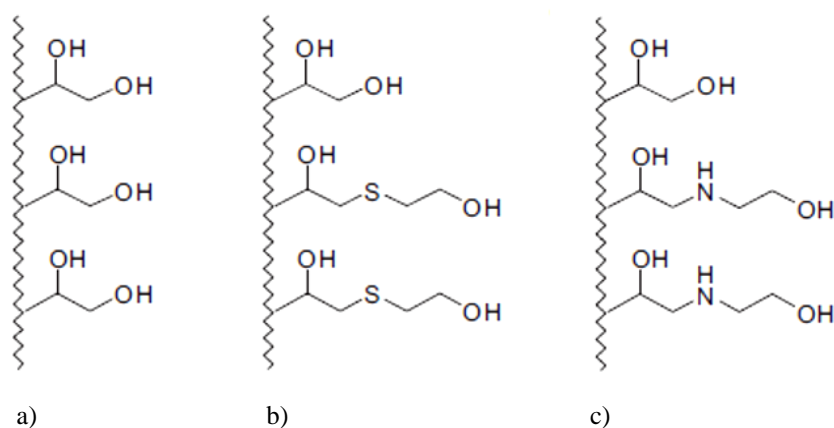


**Figure 3.1** Endcapping strategies for epoxy activated supports via: a) acidic hydrolysis, b) 2-mercaptoethanol and c) 2-ethanolamine (c) [3].

### 3.2.2 Spacer arm immobilization

It is useful to remind that the 2LP membranes were prepared to study the possible interaction of the spacer arm with the target protein (IgG) or with other proteins during the adsorption tests. Therefore, the preparation of this type of membrane aimed to the immobilization of the 1,2-diaminoethane, trying to deactivate all possible residual functional groups on the supports, that could non-specifically interact with proteins.

To do so, the epoxy activated matrix discs were first suspended in ethanol, to ensure they were completely wet. The membranes were then soaked in a solution of 10 mol-equiv. (with respect to the density of epoxy groups on the support) of the spacer arm 2LP (1,2-diaminoethane) in ethanol. This modification was carried out under gentle shaking at 50°C for 15 hours, in a thermostatic bath. The membranes were then washed several times with ethanol and water (30 minutes in ethanol, 30 minutes in water, at least twice) to remove the 2LP not bound to the surface but still present in the pores of the matrix.

The unreacted epoxy groups on the membranes were endcapped using a solution of 2-ethanolamine or 2-mercaptoethanol, in the appropriate concentration: the membranes were kept at 50°C for 15 hours and finally washed with ethanol and water for several times. In this case, an additional endcapping strategy needed to be adopted to deactivate the free amine groups of the spacer. This procedure was carried out by suspending the membranes discs into pure acetone at room temperature for 24 hours and keeping them under gentle agitation. Subsequently, the membranes were rinsed with water many times.

Actually, the two endcapping procedures in the case of 2LP-membranes, were carried out also in the reversed order (first the endcapping of the amine groups and second of the epoxy groups), with the aim of optimizing the performances of the support.

In Fig. 3.2 it is possible to observe a schematic drawing of the reaction sequence for the preparation of 2LP-membranes.



2LP modification     2-mercaptoethanol endcapping     acetone endcapping

a)

b)
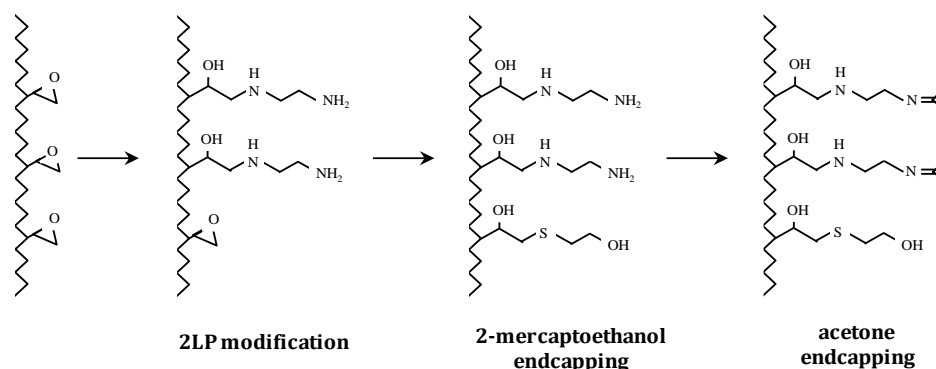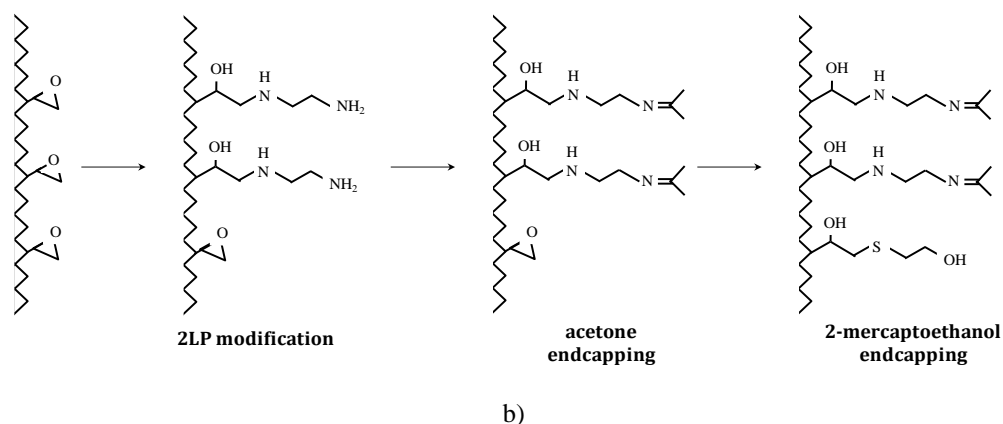
**Figure 3.2**    Chemical structure of 2LP-membranes; a) the endcapping of the residual epoxy groups was performed using 2-mercaptoethanol and the endcapping of the amine groups using pure acetone; b) the two encapping strategies were performed in the reversed order.

### 3.2.3 Complex ligand-spacer immobilization

Fort the affinity membrane preparation, the same protocol described in paragraph 3.2.2 was used to immobilize A2P and HPTA ligands.

The membranes were soaked in a solution of 10 mol-equiv. of the complex ligand-2LP, after a short equilibration step in ethanol, and kept at 50°C for 15 hours using a thermostatic bath. Only difference was on the volume of ethanol needed to dissolve the complex ligand-spacer that was higher for HPTA ligand, due to its lower solubility. In particular, 2 mL of ethanol were used to dissolve 37 mg of ligand A2P needed to modify two membranes discs of 1.5 cm diameter, while 8 mL of ethanol were used to dissolve 35.2 mg of HPTA needed to modify the same membrane surface.

After immobilization, the membranes were washed using ethanol and water (30 minutes in ethanol, 30 minutes in water, at least twice), and subjected to the endcapping procedure using solutions of 2-ethanolamine or 2-mercaptoethanol in the appropriate concentration, as described in paragraph 3.2.1: this step was carried out at 50°C for 15 hours. Finally, the affinity membranes were thoroughly rinsed with ethanol and water using an ultrasonic bath, to completely remove any trace of endcapping agent and make the membranes ready for chromatographic experiments.

The affinity membranes were stored at 4°C in a solution of 20% ethanol in water.

A schematic drawing of the A2P/HPTA-membranes is shown in Fig. 3.3, while in Fig. 3.4 there are pictures of the membranes taken before and after the A2P/HPTA immobilization. The images give a qualitative indication of the success of the immobilization procedure.

a)                                        b)
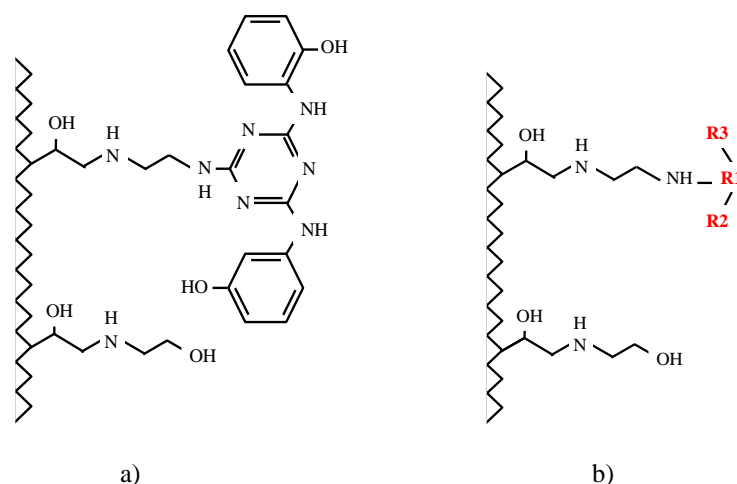
**Figure 3.3**    Schematic drawing of the chemical structure of the membranes after the immobilization of a) A2P ligand and b) HPTA ligand; in both cases the endcapping of the residual epoxy groups was performed using 2-ethanolamine.



a)            b)            c)
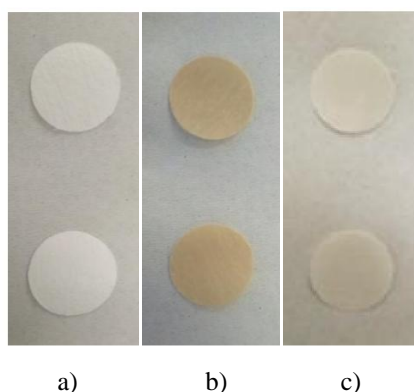
**Figure 3.4**    Pictures of the membrane sheets a) before ligand immobilization, b) after A2P immobilization and c) after HPTA immobilization.

## 3.3 Experimental characterization

In the following paragraphs, all the experiments performed to determine the performance of the activated supports will be described.

The experiments were designed as to determine the influence of all the affinity membrane components (i.e. membrane matrix, spacer arm and ligand) on the overall performance of the activated material. To do so, different batch and dynamic chromatographic cycles were performed using pure protein solutions as well as mixtures.

Preliminary kinetic studies were carried out to set the operating conditions to be adopted during batch adsorption experiments.

Finally, adsorption and desorption isotherms were constructed for both affinity ligands: in this context, the theory related to adsorption isotherms will be also presented.

### 3.3.1 Kinetic studies

During preliminary batch adsorption experiments, the affinity membranes are immersed in a solution at known concentration of the target protein, and kept under gentle mixing until equilibrium is reached. Kinetic adsorption studies are needed to determine the time required to reach equilibrium between the protein in solution and the protein adsorbed on the membrane surface. Analogous kinetic studies are needed for the elution step.

A2P-membranes were used to perform adsorption and desorption kinetic studies. In particular, 4 small membrane discs of 1.5 cm diameter were first equilibrated in 100 mM PBS, pH 7.4, and then soaked into 5 mL of IgG solution in PBS, at an initial concentration of 0.75 mg/mL. At fixed times of 1, 2, 3, 4, 5, 10, 20, 30, 45, 60, 75, 90, 120 and 130 minutes, a small volume of 100 μL was taken from the IgG solution and analyzed using the HPLC equipped with the Protein A column.

The membranes were then washed using 5 mL of PBS and the concentration of IgG in the solution was measured using the HPLC.

Finally, the four A2P-memrane discs were immersed into 5 mL of elution buffer, 100 mM glycine, pH 2.8, and kept under gentle agitation for 150 minutes. At fixed times of 1, 2, 3, 4, 5, 10, 20, 30, 45, 60, 75, 90, 105, 120, 140 and 150 minutes a volume of 100 μL was taken from the solution and analyzed using the same technique.

This way, it was possible to determine the time needed to reach equilibrium during the adsorption and desorption steps, therefore, the operating conditions that has to be adopted to perform batch experiments. Moreover, it was assumed that the same conditions could be applied to HPTA affinity membranes, since the chemical structures of the two ligands are closely related.

### 3.3.2 Influence of the native membrane and endcapping procedures

Adsorption tests have been performed employing native Sartobind® Epoxy membranes and pure protein solutions, to understand the extent of the contribution to protein adsorption of the epoxy groups, present on the surface of the cellulosic membranes. In other words, in these experiments no modification protocols have been used and the biomolecules that bind to the membranes are those captured by the active epoxy groups.

In particular, the protein species that were considered for the experiments were IgG, BSA and lysozyme. All feed solutions that were prepared had a concentration of about 0.5 mg/mL.

Two membrane discs of 1.5 cm diameter were equilibrated in 5 mL of PBS for 15 minutes; then, they were immersed in 2 mL of the protein solution and kept under gentle

agitation for 2 hours. The membranes were washed for 1 hour using 5 mL of PBS and the elution step was performed for 1 hour using 2 mL of the elution buffer.

Protein concentration was determined by absorbance reading at 280 nm.

The same experimental procedure was applied to optimize the endcapping strategy and determine the blocking reagent that gave the lowest amount of protein adsorbed. In particular, contaminant proteins as BSA and lysozyme were used to prepare pure protein solutions at a concentration of 0.5 mg/mL: adsorption experiments were carried out using membranes treated with acidic hydrolysis, 2-mercaptoethanol and 2-ethanolamine.

### 3.3.3 Influence of the spacer arm

Membranes modified with 2LP spacer were employed to perform batch chromatographic experiments, using IgG and BSA solutions at a concentration of 0.5 mg/mL. In particular, membranes were prepared first performing the endcapping of the epoxy and then that of the amine groups, and viceversa, to determine which of the two procedures allowed to obtain the lowest amount of protein adsorbed, that means the lowest interaction between the support and the proteins.

The best configuration was used to perform dynamic adsorption experiments using pure IgG solutions (0.5 mg/mL); the experiments were performed with the FPLC, placing 5 membrane discs of 2.6 cm diameter inside the column holder, as described at the end of Chapter 2. As common for this type of characterization, the system dispersion curve was obtained in independent experiments, under non-binding conditions, to calculate the contribution of the system dead volumes and mixing effects on the dynamic binding capacity (paragraph 2.6.2.1).

In this case, the system dispersion curves were measured by feeding a solution of IgG in PBS (at a concentration of 0.5 mg/mL and at a flow rate of 1 mL/min) using the membranes that were completely saturated during previous adsorption tests, to ensure experimental non-binding conditions.

System dispersion curves were compared with the breakthrough curves registered in experiments performed at a constant flow rate of 1 mL/min. The curves were integrated and the amount of IgG adsorbed was calculated as a difference between the IgG adsorption curve and the system dispersion curve (paragraph 2.6.2.1). Moreover, the amount of IgG adsorbed by 2LP-membranes was compared to the amount adsorbed by A2P-membranes: the aim was to find a correlation between the non-specific adsorption given by the spacer arm and the incomplete recovery of IgG that was observed for A2P membranes during the elution step.

## 3.3.4 Characterization of affinity membranes

Affinity membranes prepared with A2P and HPTA ligands were characterized through batch and dynamic experiments, using pure protein solutions, as well as mixtures containing IgG and other proteins, such as BSA and lysozyme added as contaminant, and using human serum. The adsorption experiments were carried out following the standard procedures summarized in Table 3.1 and 3.2; membranes were subjected to different endcapping protocols. Details and results related to all the experiments performed are reported in Chapter 4.

**Table 3.1**     Operating conditions used to carry out batch experiments.

| Step | Buffer | Volume [mL] | Time [h] |
|---|---|---|---|
| Equilibration | 100 mM PBS pH 7.4 | 5 | 0.25 |
| Adsorption | IgG/BSA/LYS (0.50 mg/mL) in 100 mM PBS pH 7.4 | 2 | 2 |
| Washing | 100 mM PBS pH 7.4 | 5 | 1 |
| Elution | 100 mM glycine pH 2.8 | 2 | 1 |

**Table 3.2**     Operating conditions used to carry out dynamic experiments.

| Step | Buffer | Volume [mL] |
|---|---|---|
| Equilibration | 100 mM PBS pH 7.4 | 15 |
| Adsorption | IgG/BSA (0.50 mg/mL) in 100 mM PBS pH 7.4 | 40 |
| Washing | 100 mM PBS pH 7.4 | 30 |
| Elution | 100 mM glycine pH 2.8 | 25 |

## 3.3.5 Adsorption and desorption isotherms

Adsorption and desorption isotherms were obtained, for A2P and HPTA membranes, using solutions of pure IgG at different concentrations. The batch experiments were performed using two membranes discs of 1.5 cm diameter for each IgG concentration value. The affinity membranes were immersed in the protein solutions until equilibrium was reached, then they were washed with PBS and finally eluted with glycine. The protein concentration was determined by absorbance reading at 280 nm, and the static binding capacity was calculated by a mass balance for every solution. Moreover, the membranes were tested for three subsequent cycles without intermediate regeneration.

The isotherms obtained for A2P ligand were compared to literature data [5].

All the data related to these experiments were analyzed using the Langmuir model. This model was developed at the beginning of the last century to describe the adsorption of a gas onto

solid surfaces [6]; although the model was developed for other applications, it is still largely used and in literature the adsorption of a biomolecule onto an affinity support is often described by the Langmuir model [7-9].

The Langmuir model assumes that the interaction between a protein in solution and a ligand immobilized on a solid surface is monovalent, that the binding is reversible and that there are no interactions between adsorbed molecules. It is also assumed that the support is homogeneous and that adsorption occurs on one layer of material only. Under these assumptions the following reaction can be written:

$$P + L \leftrightarrow PL \tag{3.1}$$

where *P* represents the protein, *L* the affinity ligand and *PL* the complex composed by the ligand and the adsorbed protein.

The mass balance associated with Eq. (3.1) for the protein adsorbed on the membrane can be written as the sum of two elements: one related to the protein-ligand complex formation reaction, adsorption reaction, and one for the desorption reaction. Since the formation of the protein-ligand complex directly depends on the protein interaction with the support, it seems reasonable to suppose that the rate of adsorption reaction depends linearly with the concentration of protein in solution. Moreover, since a biomolecule cannot interact with a binding site already occupied by other proteins, the rate of adsorption must also be proportional to the concentration of free binding sites. Combining these two effects, the following second order equation can be written:

$$R_a = k_a c(q_{max} - q) \tag{3.2}$$

where $R_a$ is the rate of the adsorption reaction, $k_a$ is the kinetic constant for the adsorption reaction, *c* is the generic concentration of the protein, *q* is the corresponding concentration of protein immobilized onto the support and $q_{max}$ is the ligand concentration, corresponding to the maximum binding capacity of the membrane.

Similar considerations can be made for the desorption reaction, whose rate is supposed to be proportional to the concentration of protein adsorbed on the membrane:

$$R_d = k_d q \tag{3.3}$$

where $R_d$ represents the rate of the desorption reaction and $k_d$ the corresponding kinetic constant.

At equilibrium, the rate of the adsorption reaction and the rate of the desorption reaction are equal, thus:

$$k_a c(q_{max} - q) = k_d q \tag{3.4}$$

equation from which it is possible to obtain the concentration of protein adsorbed, that represents the adsorption isotherms according to the Langmuir model:

$$q = \frac{q_{max} c}{K_d + c} \qquad (3.5)$$

$K_d$ is the dissociation constant and it represented by the ratio between the desorption kinetic constant and the adsorption kinetic constant:

$$K_d = \frac{k_d}{k_a} \qquad (3.6)$$

$$q = \frac{q_{max} c}{K_d + c}$$

# References

[1]   C. Boi, V. Busini, M. Salvalaglio, C. Cavallotti, G.C. Sarti, *Understanding ligand-protein interactions in affinity membrane chromatography for antibody purification*, Journal of Chromatography A 1216 (2009) 8687-8696

[2]   C. Boi, S. Dimartino, S. Hofer, J. Horak, S. Williams, G.C. Sarti, W. Lindner, *Influence of different spacer arms on Mimetic Ligand A2P and B14 membranes for human IgG purification*, Journal of Chromatography B 879 (2011) 1633-1640

[3]   J. Horak, S. Hofer, W. Lindner, *Optimization of a ligand immobilization and azide group endcapping concept via "Click Chemistry" for the preparation of adsorbents for antibody purification*, Journal of Chromatography B 878 (2010) 3382-3394

[4]   F. Brienza, *Preparation and characterization of affinity membranes for IgG purification*, Master Thesis, Università di Bologna, Academic Year 2014-15

[5]   C. Boi, S. Dimartino, G.C. Sarti, *Modelling and simulation of affinity membrane adsorption*, Journal of Chromatography A 1162 (2007) 24-33

[6]   I. Langmuir, *The constitution and fundamental properties of solids and liquids. Part I. Solids*, Journal of the American Chemical Society 38 (1916) 2221-2295

[7]   T.C. Beeskow, W. Kusharyoto, F.B. Anspach, K.H. Kroner, W.D. Deckwer, *Surface modification of microporous polyamide membranes with hydroxyethyl cellulose and their application as affinity membranes*, Journal of Chromatography A 715 (1995) 49-65

[8]   K.H. Gebauer, J. Thömmes, M.R. Kula, *Breakthrough performance of high-capacity membrane adsorbers in protein chromatography*, Chemical Engineering Science 52 (1997) 405-419

[9]   A. Tscheliessnig, R. Hahn, A. Jungbauer, *In situ determination of adsorption kinetics of proteins in a finite bath*, Journal of Chromatography A 1069 (2005) 23-30

# CHAPTER 4

# Experimental results and discussion

## 4.1 Introduction

This chapter will present the results related to the characterization of affinity membranes modified with two different synthetic ligands for the selective capture of IgG. The affinity ligands used were the A2P ligand and the HPTA ligand and they were immobilized onto the cellulosic membranes through the spacer arm 2LP.

As already pointed out in this thesis, the ligand A2P was the subject of different literature works; for this work, it was used as a benchmark to evaluate the reproducibility of the data that can be found in literature, and to compare its performance to those of the new recently designed ligand HPTA. In fact, the data related to the HPTA ligand that will be shown in this chapter are the first ever obtained.

The aim of this chapter is twofold: on the one hand it is important to show the results of the characterization of a completely new ligand that might improve the performance of affinity membranes; on the other hand, it is interesting to understand how the performance of an affinity support do not depend only on the affinity ligand, but they might also depend on the other elements the support is made of, such as the spacer arm and the matrix itself.

The results of the chromatographic characterization will be presented following the same structure of the previous chapter, were all the experiments performed were described and explained.

## 4.2 Kinetic studies

Kinetic studies were the first experiments carried out, using A2P-membranes, to determine the time needed to reach the equilibrium during batch adsorption and desorption experiments. A summary of the operating conditions can be found in Table 4.1, while the results are shown in Fig. 4.1.

**Table 4.1** Operating conditions used to carry out the kinetic studies for A2P-membranes; endcapping performed with 2-ethanolamine.

| Step | Buffer | Volume [mL] | Time [min] |
|---|---|---|---|
| Equilibration | PBS 100 mM pH 7.4 | 10 | 20 |
| Adsorption | IgG (0.75 mg/mL) in PBS 100 mM pH 7.4 | 5 | 130 |
| Washing | PBS 100 mM pH 7.4 | 5 | 77 |
| Elution | Glycine 100 mM pH 2.8 | 5 | 150 |



a)          b)
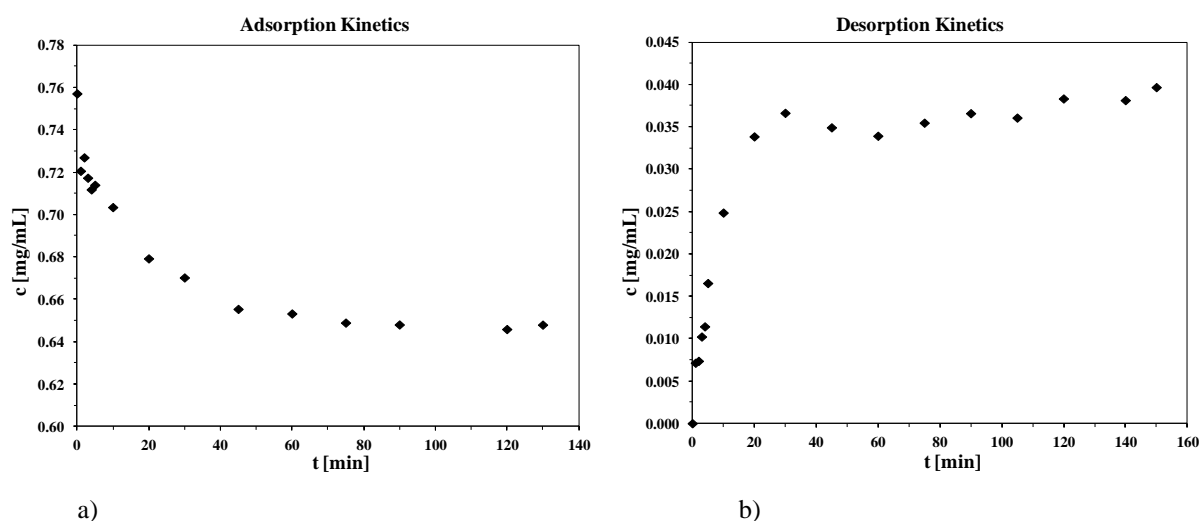
**Figure 4.1** a) Adsorption and b) desorption kinetics for A2P-membranes.

From the plot regarding the adsorption kinetics, it is clear that during this stage, equilibrium was widely reached after 120 minutes; for this reason, all batch experiments were performed leaving the membranes inside the protein solution for two hours. As far as the desorption kinetics is concerned, it was concluded that equilibrium was reached after one hour: from the plot it is clear that the plateau is not well defined and that already after 30 minutes the concentration of IgG in the elution buffer presented an oscillatory trend around an average value, that remained approximately constant till the end of the experiment. It was decided not to perform the elution step longer than one hour, during batch experiments, not to denature the proteins due to strong acid conditions.

The explanation for the oscillatory trend in the elution step has to be traced back to the analytical technique used. In fact, the HPLC equipped with the Protein A column was used: in the case of acid samples, the reproducibility of the analysis was not ensured because Protein A could not bind properly to IgG (due to the low pH of the elution samples). For this reason, there is no evident plateau in Fig. 4.1b and, moreover, the amount of IgG eluted was underestimated.

About this, in Table 4.2 some details regarding the amount of protein adsorbed and desorbed as a function of time can be found.

**Table 4.2**    Amount of IgG adsorbed and desorbed as a function of time during kinetic studies.

| Time [min] | Adsorption | | Desorption | |
|:---:|:---:|:---:|:---:|:---:|
| | $m_{ads}$ [mg] | $q_{ads}$ [mg/mL] | $m_{elu}$ [mg] | $q_{elu}$ [mg/mL] |
| 0 | - | - | - | - |
| 1 | 0.183 | 1.076 | 0.036 | 0.210 |
| 2 | 0.152 | 0.893 | 0.038 | 0.256 |
| 3 | 0.198 | 1.165 | 0.052 | 0.304 |
| 4 | 0.224 | 1.318 | 0.057 | 0.338 |
| 5 | 0.214 | 1.259 | 0.081 | 0.480 |
| 10 | 0.261 | 1.539 | 0.120 | 0.705 |
| 20 | 0.368 | 2.167 | 0.160 | 0.944 |
| 30 | 0.406 | 2.395 | 0.172 | 1.016 |
| 45 | 0.469 | 2.763 | 0.165 | 0.972 |
| 60 | 0.478 | 2.815 | 0.161 | 0.948 |
| 75 | 0.495 | 2.916 | 0.167 | 0.985 |
| 90 | 0.498 | 2.937 | 0.172 | 1.012 |
| 105 | - | - | 0.170 | 1.000 |
| 120 | 0.506 | 2.985 | 0.178 | 1.050 |
| 130 | 0.499 | 2.940 | - | - |
| 140 | - | - | 0.177 | 1.046 |
| 150 | - | - | 0.183 | 1.078 |

The table above shows data related to the amount of IgG adsorbed and desorbed as a function of time, as well as the binding and elution capacity ($q_{ads}$ and $q_{elu}$) expressed as the mass of IgG adsorbed, or eluted, per mL of membrane (that can be easily calculated knowing the number of membranes, their thickness and diameter). These data give a preliminary indication of the performance of A2P-membranes: in fact, the equilibrium binding capacity reached after 130 minutes was 2.94 mg/mL, while the recovery of IgG after 150 minutes of elution step was 36.69% (calculated as the ratio between the mass eluted and the mass adsorbed).

This low value of IgG recovered, as already stated, is related to the analytical method employed, that underestimates the amount of protein in all the elution samples.

After drawing these conclusions, all the elution samples collected from the subsequent experiments were: 1) analyzed by UV measurements (in the case of pure proteins); 2) diafiltered to remove the elution buffer from the proteins, using Microcon® Centrifugal Filters. In this case, after removing the elution buffer, IgG on the filter was washed with PBS, performing the same

filtration using the micro centrifuge. Finally, recovered IgG on the filter was suspended in PBS that allowed us to analyze the samples with HPLC using the Protein A analytical cartridge: the analyses performed with this method were more accurate and reproducible.

Apart from the preliminary data regarding the performance of the A2P-membranes, the kinetic studies were useful to estimate the operating conditions for batch experiments.

## 4.3 Influence of the native membrane

The study of the performance of affinity membranes started with the investigation of the influence of the plain supports, such as the native Sartobind® Epoxy membranes without modification. The aim was to understand if the membrane support was responsible for non-specific interactions with proteins.

Therefore, control experiments were carried out in batch by testing pure protein solutions of IgG, BSA and lysozyme, at a fixed concentration of 0.5 mg/mL; IgG was the target protein, while BSA and lysozyme were chosen as contaminant proteins, since they have different isoelectric point with respect to IgG and they can be found in blood serum in significant quantities.

Three subsequent cycles were performed, without regenerating the membranes.

The results are presented in Table 4.3.

**Table 4.3** Binding capacity of the native membranes.

|  | Affinity cycle | $q_{ads}$ [mg/mL] |
|---|---|---|
| **IgG** | I | 0.38 |
|  | II | ~0.00 |
|  | III | ~0.00 |
| **BSA** | I | 0.37 |
|  | II | 0.27 |
|  | III | ~0.00 |
| **LYS** | I | ~0.00 |
|  | II | ~0.00 |
|  | III | ~0.00 |

The results obtained in terms of binding capacities show explicitly that all the considered proteins exhibit some sort of interaction with the support. In particular, BSA seems to be the biomolecule that binds more significantly to the unmodified membranes. These results were expected, since the epoxy groups are very reactive and Sartobind® Epoxy membranes are

specially designed to bind proteins, such as BSA. Therefore, to understand the effect of the cellulosic support, it was necessary to deactivate the epoxy groups with an endcapping step and repeat the adsorption test.

### *4.3.1 Endcapping procedures*

An optimization of the endcapping strategy was performed to completely exclude the influence of the native membranes as well as the endcapping agent on non-specific adsorption.

There are a number of blocking agents suggested in literature for deactivate epoxy groups when they are present on cellulosic supports [1, 2]. The choice of 2-ethanolamine was dictated by previous experience, as well as by other published works [3]; however, other authors identified this blocking agent to be responsible for a relevant amount of non-specific binding and a reduced adsorption of immunoglobulin [2]. In light of this, it was decided to test the efficacy of two different endcapping strategies, acidic hydrolysis and 2-mercaptoethanol and to compare their performance with that of 2-ethanolamine.

Three subsequent cycles were performed for membranes endcapped with the three blocking agents and all feed solutions were prepared at a concentration of 0.5 mg/mL.
The results are presented in Table 4.4.

**Table 4.4** Results of the optimization of the endcapping strategy.

| Blocking agent | Contaminant used | Affinity cycle | $q_{ads}$ [mg/mL] |
|---|---|---|---|
| Acidic hydrolysis | BSA | I | 0.11 |
| | | II | ~0.00 |
| | | III | ~0.00 |
| | LYS | I | 0.18 |
| | | II | ~0.00 |
| | | III | ~0.00 |
| 2-mercaptoethanol | BSA | I | ~0.00 |
| | | II | ~0.00 |
| | | III | ~0.00 |
| | LYS | I | ~0.00 |
| | | II | ~0.00 |
| | | III | ~0.00 |
| 2-ethanolamine | BSA | I | 0.40 |
| | | II | 0.80 |
| | | III | 0.44 |

Looking at the results shown, it is evident that both acidic hydrolysis and 2-mercaptoethanol are superior to 2-ethanolamine. Indeed, the amount of BSA that binds to the ethanolamine-endcapped supports is more than two times greater than that adsorbed onto the plain supports (Table 4.4). This result demonstrates the strong influence that the positive charges introduced by 2-ethanolamine have on the binding of the negatively charged BSA molecules. On the other hand, endcapping with acidic hydrolysis and 2-mercaptoethanol appears to be very efficient, with both methods the quantities of adsorbed impurities are drastically reduced. Hence they seem to be very promising for future adsorption tests with the complete affinity membrane. Nonetheless, since the use of sulphuric acid could damage the ligand molecules immobilized on the matrix [4], only 2-mercaptoethanol was studied further as an alternative to 2-ethanolamine.

Since it was demonstrated that an efficient endcapping procedures avoids interactions between the contaminant proteins and the support, it is possible to conclude that the native membranes are not responsible for non specific adsorption; the only interaction that can occur is between the proteins and the epoxy groups on the surface of the membranes, but these active groups can be easily deactivated with an appropriate blocking agent. Therefore, the investigation of the membrane performance moved towards the next element of interest: the spacer arm.

## 4.4 Influence of the spacer arm

The influence of the spacer arm on affinity membrane performance has been reported in the literature [2, 6, 7]. In previous works it was demonstrated that the spacer arm influences significantly relevant properties like binding capacity, selectivity and recovery [3, 5, 8]. However, no systematic investigation was performed to experimentally inspect the behavior of the spacer arm by itself, its effect on non-specific binding and, therefore, on protein recovery.
To this aim, the effect of the spacer 1,2-diaminoethane (2LP) immobilized onto cellulosic membranes with respect to protein binding was investigated: 2LP-membranes were tested for adsorption with pure protein solutions, both in batch and in dynamic chromatographic cycles.

### 4.4.1 Batch experiments

As described in Chapter 3, the preparation of 2LP-membranes followed two different protocols, related to the order in which the endcapping of epoxy and amine groups was performed, after the spacer immobilization. Batch adsorption experiments were performed for both types of 2LP-membranes, using solutions of IgG and BSA, at a concentration of 0.5 mg/mL. Two subsequent cycles were carried out, without regenerating the membranes.

**Table 4.5**     Results of the adsorption experiments for 2LP-membranes; a) endcapping of epoxy groups first and of amine groups second; b) endcapping of amine groups first and of epoxy groups second.

a)

|  | Affinity cycle | $q_{ads}$ [mg/mL] |
|---|---|---|
| **BSA** | I | 0.960 |
|  | II | 0.810 |
| **IgG** | I | 0.400 |
|  | II | 0.253 |

b)

|  | Affinity cycle | $q_{ads}$ [mg/mL] |
|---|---|---|
| **BSA** | I | 1.120 |
|  | II | 0.680 |

The results (Table 4.5) clearly show that 2LP-membranes are responsible for a non-negligible adsorption of proteins, especially BSA; this is even more relevant in the case the endcapping protocol of amine groups is performed before that of the epoxy groups, Table 4.5b.

However, to further investigate the role of the spacer arm, dynamic experiments were also performed. In this case, only 2LP-membranes prepared performing the endcapping of the epoxy groups first, and of the amine groups second, were used, since they showed a lower amount of BSA non-specifically adsorbed.


### *4.4.2 Dynamic experiments*

Dynamic adsorption experiments were performed using a chromatographic apparatus, an AKTA Purifier 100, at a constant flow rate of 1 mL/min. Experiments were performed with new membranes for obtaining the breakthrough curves, and with saturated membranes for obtaining the system dispersion curves.

A typical result is shown in Fig. 4.2, were both breakthrough curve and system dispersion curve are reported. The area between the system dispersion curve and the breakthrough curve is not negligible and represents the contribution of the 2LP spacer to IgG non-specific adsorption. For the example reported in Fig. 4.2, the value of IgG non-specific adsorption was calculated as 0.77 mg/mL, and it was of the same order of magnitude in all experiments performed. The 2LP membranes were subsequently washed with PBS and eluted with 0.1 M glycine pH 2.8, but the IgG adsorbed was not removed with the elution buffer.

The value of IgG non-specifically adsorbed is of the same order of magnitude of that obtained performing batch experiments.
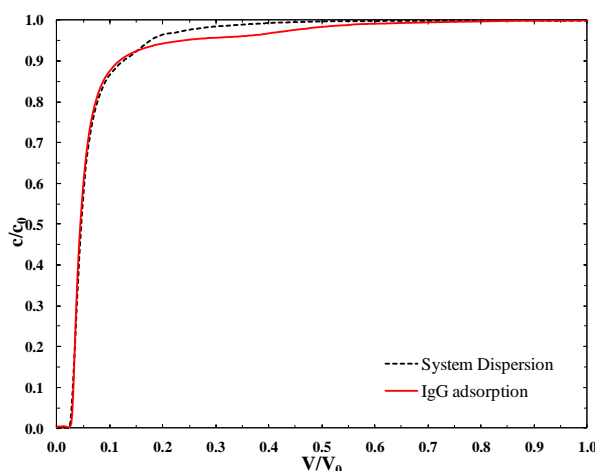
**Figure 4.2**    Comparison between system dispersion curve and IgG breakthrough curve for 2LP-membranes.

To conclude, the 2LP-membranes were able to interact with proteins, since they adsorbed both IgG and BSA. The spacer arm is responsible for non-specific adsorption and for irreversible adsorption of the target protein, either in batch and dynamic experiments: this affects the selectivity of the affinity chromatographic support, that is usually traced back to the ligand only, as well as the recovery during the elution step.

In analyzing the performances of the two affinity ligands, A2P and HPTA, that will be presented in the next paragraphs, the non-specific interaction of 2LP need to be taken into account.

The part of the work related to the study of the spacer arm performance is published in the paper *Effect of the spacer arm on non-specific binding in membrane affinity chromatography*, MRS Communications [9].

## 4.5 A2P ligand

Affinity membranes modified with the A2P ligand were characterized through batch and dynamic adsorption tests, using pure protein solutions as well as mixtures. Encapping of epoxy groups was performed both with 2-ethanolamine and 2-mercaptoethanol.

The results presented are those of preliminary tests, performed to optimize the immobilization protocol, the experimental conditions and the analytical techniques. It has to be considered that only 1 gram of ligand was available to perform the characterization and that only results of representative experiments will be presented. However, the results obtained confirmed those of previous experiments carried out by the membrane research group of the University of Bologna, that used to work with the A2P ligand.

A2P-membranes performance will be compared to those of HPTA-membranes, even if the results are only indicative, due to the small amount of ligand available.

### 4.5.1 Batch experiments

#### 4.5.1.1 Pure protein solutions

The first set of experiments performed to characterize A2P affinity membranes were carried out using pure solutions of IgG and BSA, at a concentration of approximately 0.5 mg/mL. Each experiment was performed using a membrane set composed of two membranes of the diameter of 1.5 cm. Three subsequent cycles were carried out, without regenerating the membranes.

The aim of the preliminary tests using IgG was to evaluate the binding capacity of the affinity membranes and to compare the results to literature available data [3, 5]. Moreover, BSA was employed as a pure contaminant protein, to assess the possible non-specific interactions with the ligand, or the support in general.

Finally, the performance of A2P-membranes endcapped with 2-ethanolamine and 2-mercaptoethanol were compared. Table 4.6 shows the results obtained.

**Table 4.6**   Preliminary adsorption experiments for A2P-membranes, using pure protein solutions: IgG and BSA at a concentration of 0.5 mg/mL; endcapping performed with 2-ethanolamine (#1) and with 2-mercaptoethanol (#2, #3).

| Experiment | | Affinity cycle | $q_{ads}$ [mg/mL] | Recovery [%] |
|---|---|---|---|---|
| **#1** | **IgG** | I | 1.74 | 47.9 |
| | | II | 1.32 | 45.0 |
| | | III | 1.20 | 39.2 |
| **#2** | **IgG** | I | 2.02 | 61.5 |
| | | II | 1.05 | 55.3 |
| | | III | 0.71 | - |
| **#3** | **BSA** | I | 1.09 | 65.7 |
| | | II | - | - |
| | | III | - | - |

Experiments sets #1 and #2 showed a good amount of IgG adsorbed and an average value for the protein recovery during the elution step of 44% and 58% respectively. The amount of IgG adsorbed decreases with the increase of the subsequent cycle number : this result, together with the low recovery, demonstrates that part of the IgG is irreversibly adsorbed. This could be

ascribed to the ligand itself, or, as discussed in the previous paragraphs, by the spacer arm used to immobilize A2P on the membranes.

Experiment set #3 shows that, at least during the first cycle, BSA was captured by the support; this non-specific interaction can be traced back both to the ligand and the spacer arm, for which it was already demonstrated the ability to bind BSA (paragraph 4.4).

Since these were only preliminary data, the experimental plan continued with the aim of clarifying the issues related to the selectivity of A2P ligand, performing batch adsorption tests using mock protein mixtures.

### 4.5.1.2 Protein mixtures

A2P membranes were tested using mixtures of IgG and BSA; the solution had a composition of 0.5 mg/mL of IgG and 0.2 mg/mL of BSA. The obtained results are presented in Table 4.7. Unfortunately, due to experimental errors it was not possible to measure the amount of BSA adsorbed during the first chromatographic cycle.

**Table 4.7** Preliminary adsorption experiments for A2P-membranes, using mixtures of IgG and BSA at a concentration of 0.5 mg/mL and 0.2 mg/mL respectively; endcapping performed with 2-mercaptoethanol.

| Affinity cycle | IgG | | BSA |
|:---:|:---:|:---:|:---:|
| | $q_{ads}$ [mg/mL] | Recovery [%] | $q_{ads}$ [mg/mL] |
| I | 1.47 | 28.0 | - |
| II | 1.69 | 7.8 | 1.08 |
| III | 0.36 | 28.1 | 0.72 |

If the results of Table 4.7 are compared to those of Table 4.6 it is possible to say that the amount of IgG adsorbed does not seem to depend on the presence of BSA in the solution. However, the IgG recovery is drastically decreased and, at the same time, the amount of BSA adsorbed is of the same order of magnitude of the experiment carried out using pure proteins, even if the concentration of BSA in that case was 0.5 mg/mL.

The concentration of all the samples of these experiments were performed by HPLC analysis in a different set up according to the samples to be analyzed. Protein A column was used to measure the concentration of IgG and a SEC column to measure BSA concentration; IgG concentration had to be measured separately, since the peaks of BSA and IgG in the SEC chromatogram were not completely resolved. Performing the analysis using two different column, some errors might have occurred in the estimation of the concentration of the two

species. For this reason, to better understand the obtained results, it was important to examine the samples by SDS-PAGE electrophoresis.

In particular, this qualitative technique was used only for the elution samples.

The resulting SDS-PAGE gel is shown in Fig. 4.3: the picture shows the results of the analysis of the elution samples of the three chromatographic cycle.



| | |
|---|---|
| 1 | MW marker |
| 2 | elution I |
| 3 | elution II |
| 4 | elution III |
| 5 | IgG (0.05 mg/mL) |
| 6 | BSA (0.05 mg/mL) |
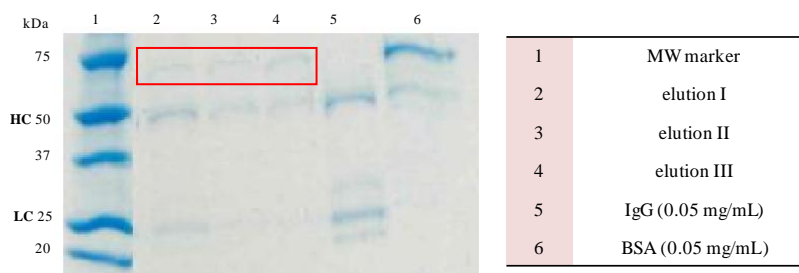
**Figure 4.3**    SDS-PAGE gel image obtained from the analysis of the eluted samples of experiments with a mixture of IgG and BSA at a concentration of 0.5 mg/mL and 0.2 mg/mL respectively; A2P-membranes endcapped with 2-mercaptoethanol.

The light and the heavy chains of IgG are visible in lanes from 2 to 5; the intensity of these bands in lanes 2, 3 and 4 is decreasing, due to a decrease in the concentration of IgG eluted. As already discussed for pure protein solution, this can be explained by the possible irreversible binding between the protein and the ligand and/or the spacer arm.

As far as the selectivity is concerned, the presence of BSA in all elution samples is clear (pointed out in the red rectangle), due to the bands in correspondence of 60-70 kDa. This confirms the HPLC results and shows that the ligand is not very selective.

### 4.5.2 Dynamic experiments

Dynamic experiments were carried out using the FPLC by feeding a solution of 0.5 mg/mL IgG in PBS; with the aim of determining the dynamic binding capacity for A2P membranes. As customary, the system dispersion curve was obtained and it was compared to the IgG breakthrough curve, as shown in Fig. 4.4.

Unfortunately, due to experimental problems occurred during the elution step, it was not possible to calculate the amount of IgG eluted; that is also the reason why Fig. 4.4 shows only the adsorption phase.
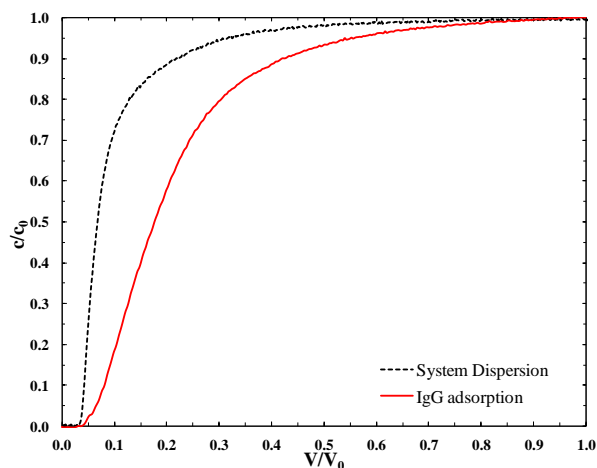
**Figure 4.4**   Comparison between system dispersion curve and IgG breakthrough curve for A2P-membranes.

The amount of IgG adsorbed was calculated as 3.37 mg/mL. This value can be compared to the amount of IgG adsorbed during the batch experiments performed with pure IgG solutions discussed above: the highest value obtained was 2.02 mg/mL (first cycle of experiment #2 in Table 4.10). Such a great difference was quite unexpected, since dynamic experiments usually give results similar to those of batch tests [3, 10]: in particular, batch experiments allow to reach the maximum value of adsorbed protein. So, this result could be an indication of the fact that equilibrium was not reached during the batch adsorption step. It is possible that increasing the duration of the adsorption stage during batch experiments the amount of IgG captured would increase.

However, this is the result of a single experiment and cannot be considered representative; more tests must be done to verify the reproducibility of the data obtained.

## 4.6 HPTA ligand

Affinity membranes modified with the HPTA ligand were characterized through batch adsorption tests, using pure protein solutions as well as mixtures. Encapping of epoxy groups was performed with both 2-ethanolamine and 2-mercaptoethanol.

Preliminary tests were performed to optimize the immobilization protocol, the experimental conditions, the analytical techniques used and to assess the HPTA ability to bind the protein of interest, IgG. It has to be considered that only 1.25 grams of HPTA ligand were available to perform the characterization; this is the reason why it was not possible to perform dynamic adsorption experiments. However, even if a small amount of ligand was available, the obtained results gave good indications concerning the performance of the affinity membranes.

## 4.6.1 Batch experiments

### 4.6.1.1 Pure protein solutions

The results of batch tests using pure protein solutions, IgG and BSA, are reported in Table 4.8 and 4.9. In the first table, the results related to HPTA-membranes endcapped with 2-ethanolamine are presented, while in the second table the results obtained analyzing HPTA-membranes endcapped with 2-mercapoethanol are reported.

**Table 4.8**   Preliminary adsorption experiments for HPTA-membranes, using pure protein solutions: IgG and BSA at a concentration of 0.5 mg/mL and 0.25 respectively; endcapping performed with 2-ethanolamine.

| Affinity cycle | IgG | | BSA |
|:---:|:---:|:---:|:---:|
| | $q_{ads}$ [mg/mL] | Recovery [%] | $q_{ads}$ [mg/mL] |
| I | 1.14 | - | 0.15 |
| II | 1.02 | - | ~0.00 |
| III | 0.73 | - | ~0.00 |

Looking at the results reported in Table 4.8, it has to be considered that HPTA-membranes endcapped with 2-ethanolamine were already used for other chromatographic cycles, after which any regeneration was performed: for this reason the recovery was not taken into account and the binding capacity for these membranes was obviously reduced, with respect to new membranes (for example, HPTA-membranes endcapped with 2-mercaptoethanol, Table 4.9).

Anyway, the matrix selectivity with respect to IgG appears to be quite good: BSA was adsorbed only during the first chromatographic cycle and its binding capacity is about eight times lower than that exhibited by IgG. Clearly, the amounts of protein adsorbed are low for both membrane sets, because much of the free binding sites on the membranes lost their functionality or were irreversibly saturated due to the previous chromatographic experiments. Therefore this is more a qualitative indication of the matrix selectivity, rather than a quantitative one. In addition, it has to be remembered that the BSA concentration in protein solution was half of the IgG concentration, and this factor undoubtedly played a role in determining the lower adsorption of BSA onto the matrix.

About the recoveries, they were not taken into consideration because the membranes were already used for other chromatographic experiments.

**Table 4.9** Preliminary adsorption experiments for HPTA-membranes, using pure protein solutions: IgG and BSA both at a concentration of 0.5 mg/mL; endcapping performed with 2-mercaptoethanol.

|  | Affinity cycle | $q_{ads}$ [mg/mL] | Recovery [%] |
|---|---|---|---|
| **IgG** | I | 2.20 | 62.62 |
|  | II | 1.40 | 76.48 |
|  | III | 1.09 | 71.63 |
| **IgG** | I | 1.79 | 69.3 |
|  | II | 1.14 | 76.6 |
|  | III | 1.07 | 75.9 |
| **BSA** | I | 1.22 | 91.3 |
|  | II | 0.01 | - |
|  | III | 0.27 | - |

Considering the results reported in Table 4.9, it is clear that for new membranes, the amount of IgG adsorbed was obviously higher, with respect to the used membranes, discussed above. Moreover, comparing these results with those of A2P-membranes, it is clear that the binding capacity for the new ligand is slightly higher, but, more important, the recovery of IgG obtained is much higher. This represent a very promising result for this new HPTA ligand, even if the recovery did not reach 100% and even if the ligand was immobilized using the 2LP spacer, that was found to cause non-specific adsorption.

However, even HPTA-membranes presented interactions with BSA of the same order of magnitude of that observed for A2P-membranes. This can be due to the ligand itself or to the spacer arm; for sure, since the 2LP spacer is the only element in common of the two affinity supports (apart from the cellulose matrix for which it was excluded any influence on the overall performances), it can be considered responsible for part of the non specific adsorption, as well as for the irreversible binding of IgG, that prevents from obtaining a complete recovery.

These preliminary results indicated a rather satisfactory performance of the HPTA-membranes, especially as far as the IgG recovery is concerned; moreover, the non-specific adsorption was quite limited.

### *4.6.1.2 Protein mixtures*

To investigate the selectivity of the HPTA-membranes, different batch experiments using protein mixtures were performed. In particular, IgG and BSA mixtures and IgG and lysozyme mixtures were employed, as well a more complex solution, such as human serum. The experiments were carried out following the standard procedure for batch tests.

**IgG & BSA**

      The results regarding the batch tests performed with HPTA-membranes endcapped with 2-ethanolamine are shown in Table 4.10. Two different sets of membranes were used, identified as experiment #1 and #2, to verify the reproducibility of the obtained data.

**Table 4.10**   Preliminary adsorption experiments for HPTA-membranes, using mixtures of IgG and BSA at a concentration of 0.5 mg/mL and 0.2 mg/mL respectively; endcapping performed with 2-ethanolamine.

| Experiment | Affinity cycle | IgG | | BSA |
|---|---|---|---|---|
| | | $q_{ads}$ [mg/mL] | Recovery [%] | $q_{ads}$ [mg/mL] |
| | I | 1.50 | 45.3 | 0.94 |
| #1 | II | 1.42 | 29.7 | 0 |
| | III | 1.36 | 27.5 | 0 |
| | I | 1.52 | 44.0 | 0.25 |
| #2 | II | 0.84 | 35.6 | 0.32 |
| | III | 0.49 | 34.5 | 0.48 |

      The results show a good amount of IgG adsorbed, even if slightly lower than the values obtained in the experiments with pure protein solutions. Moreover, the membranes still present a certain amount of BSA adsorbed. The most evident result is represented by the percentage of IgG recovered, that is significantly lower if compared to the results of pure protein solutions. It is possible that the BSA presence in solution, even if in small amounts, might have an important influence on the elution capacity of the ligand.

      Fig. 4.5 and 4.6 show the results of SDS-PAGE analysis for all the elution samples are reported.

Both for experiment #1 and #2 the presence of BSA in the elution samples is clear, and pointed out by the red frame. IgG concentration can be qualitative estimated as well: the intensity of the bands in correspondence of 50 and 25 kDa (heavy and light chains, respectively) decreases by increasing the cycles number. Moreover, apart from the first cycle, for which the IgG content is higher, for the second and third elution samples, the intensity of the bands identifying IgG and BSA are very similar. Thus, it can be deduced that, after the first cycle, the amount of protein of interest which is eluted is comparable to that of the eluted contaminant.
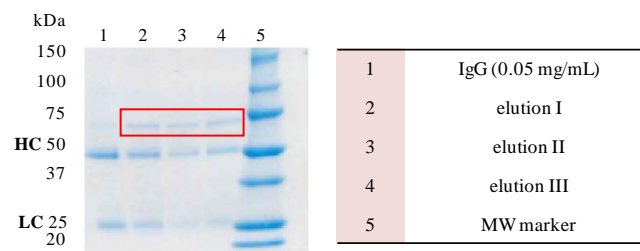
**Figure 4.5** SDS-PAGE gel image obtained from the analysis of the eluted samples of experiment #1 with a mixture of IgG and BSA at a concentration of 0.5 mg/mL and 0.2 mg/mL respectively; HPTA-membranes endcapped with 2-ethanolamine.
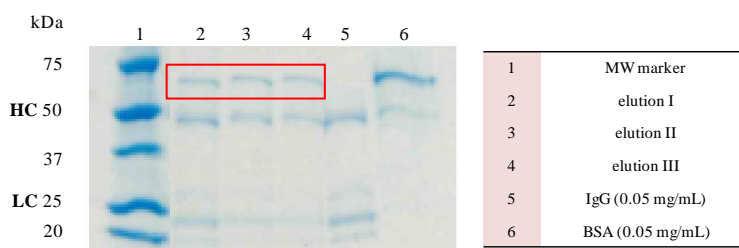


**Figure 4.6** SDS-PAGE gel image obtained from the analysis of the eluted samples of experiment #2 with a mixture of IgG and BSA at a concentration of 0.5 mg/mL and 0.2 mg/mL respectively; HPTA-membranes endcapped with 2-ethanolamine.

Similar experiments were performed in the case of HPTA-membranes endcapped with 2-mercaptoethanol and the results are summarized in Table 4.11.

In this case, it was witnessed a further decrease both of the amount of IgG adsorbed and of the target protein recovery, while the entity of the non-specific adsorption remained almost unchanged.

**Table 4.11** Preliminary adsorption experiments for HPTA-membranes, using mixtures of IgG and BSA at a concentration of 0.5 mg/mL and 0.2 mg/mL respectively; endcapping performed with 2-mercaptoethanol.

| Affinity cycle | IgG | | BSA |
|:---:|:---:|:---:|:---:|
| | $q_{ads}$ [mg/mL] | Recovery [%] | $q_{ads}$ [mg/mL] |
| I | 1.29 | 33.3 | 0.89 |
| II | 1.28 | 23.7 | 0.46 |
| III | 0.63 | 34.9 | 0.08 |

However, as discussed in paragraph 4.5.1.2, the analysis of BSA concentration was affected by experimental errors, due to the use of two different columns to estimate the

concentration of the two proteins in the mixture. For this reason, recovery data for BSA were not taken into account.

Fig. 4.7 shows the obtained SDS-PAGE gel for the analyzed elution samples.
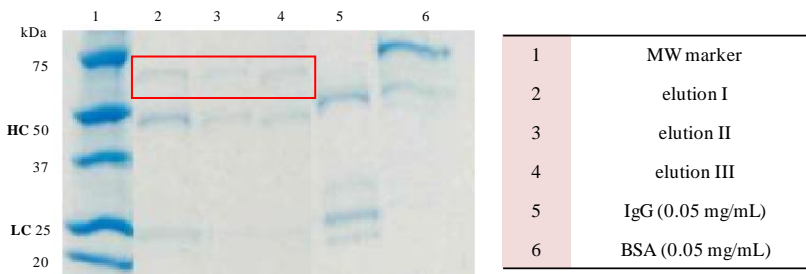


**Figure 4.7**    SDS-PAGE gel image obtained from the analysis of the eluted samples of experiments with a mixture of IgG and BSA at a concentration of 0.5 mg/mL and 0.2 mg/mL respectively; HPTA-membranes endcapped with 2-mercaptoethanol.

Comparing the outcomes of the electrophoresis with what was found previously from the trials with protein mixtures (regarding HPTA-membranes endcapped with 2-ethanolamine), it is evident that the quantities of immunoglobulin eluted are lower for all cycles: this result is also comparable to that obtained in the case of A2P-membranes tested with the same mixture. Moreover, similarly to what was observed earlier, BSA is present in all the eluted samples; in particular, except for the first cycles of both sets for which the IgG content seems higher, for all the others the intensity of the band corresponding to BSA is almost identical to those indicating the presence of IgG.

Looking again at Table 4.16, the adsorption capacities for IgG and BSA indicate clearly that not only the endcapping protocol with 2-mercaptoethanol had no positive effect on the matrix selectivity and elution capacity, but rather it made them slightly worse. In fact, as far as HPTA-membranes endcapped with 2-mercaptoethanol is concerned, the amount of captured IgG is in general lower or comparable to that determined earlier for the matrices endcapped with 2-ethanolamine, whereas the opposite can be claimed for BSA.

Furthermore, the behaviour of the membranes modified with A2P is basically the same as those containing HPTA: quite low antibody binding capacities with respect to the values measured for pure solutions, and a considerable binding of impurities. As for the IgG recoveries, the A2P and the HPTA membrane sets exhibit a similar elution performance, which is however slightly lower than that detected for the case of the 2ethanolamine-endcapped matrices.

Another set of experiments was performed using mixtures of IgG and BSA; in the case of experiment #3 the concentration of BSA was increased from 0.2 mg/mL to 0.75 mg/mL, reaching a higher value with respect to IgG concentration, that was kept at 0.5 mg/mL.

What is clear looking at the results in Table 4.12 is that the increase in the BSA concentration caused a significant decrease of the amount of IgG both adsorbed and eluted. As a consequence, the amount of BSA adsorbed increased importantly.

**Table 4.12**   Preliminary adsorption experiments for HPTA-membranes, using mixtures of IgG and BSA, respectively at a concentration of 0.5 mg/mL and 0.25 mg/mL (#1, #2), and at a concentration of 0.5 mg/mL and 0.75 mg/mL (#3); endcapping performed with 2-mercaptoethanol.

| Experiment | Affinity cycle | IgG | | BSA |
|---|---|---|---|---|
| | | $q_{ads}$ [mg/mL] | Recovery [%] | $q_{ads}$ [mg/mL] |
| #1 | I | 1.23 | 38.35 | 0.70 |
| | II | 0.97 | 42.43 | 0.40 |
| | III | 0.66 | 33.94 | 0.52 |
| #2 | I | 0.39 | 0 | 0.23 |
| #3 | I | 1.00 | 20.60 | 1.02 |
| | II | 0.36 | 44.52 | 1.75 |
| | III | 0.32 | 26.76 | 0.63 |

These results demonstrate that the selectivity of HPTA-membranes is not optimal and non-specific adsorption, that can be traced back to the ligand or to the spacer arm, is still an issue. Moreover, the more the contaminant protein is captured by the support, the less the target protein is adsorbed and eluted. This leads to think that the BSA binding is irreversible and causes a significant decrease in the number of active sites available for IgG binding.

More evidence in support of the previously shown results are reported in Fig. 4.8.
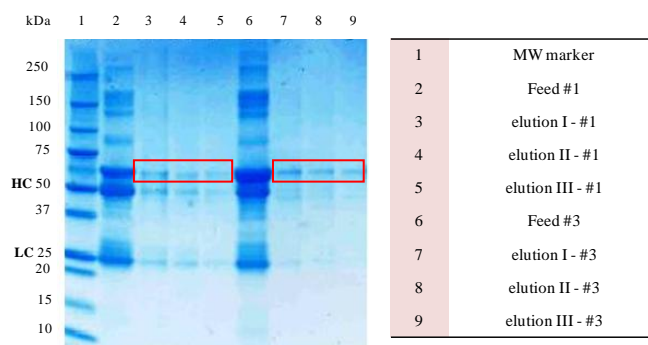


**Figure 4.8**   SDS-PAGE gel image obtained from the analysis of the eluted samples of experiments with a mixture of IgG and BSA at a concentration of 0.5 mg/mL and 0.25/0.75 mg/mL respectively; HPTA-membranes endcapped with 2-mercaptoethanol.

Looking at Fig. 4.8, it is evident that IgG is present in all elution samples and that its concentration decreases going from the first to the third cycle of both experiments, due to a decrease of the bands intensity. BSA is also present in all elution samples, especially in those of experiment #3, performed using a higher BSA initial concentration.

In light of all the results presented, it is possible to conclude that the 2LP spacer arm and/or the ligands were the main causes of non-specific binding and poor elution performances. What, however, was confirmed, is the marginal role played by the blocking agent which, at this point, can be considered irrelevant with respect to the other two factors.

### IgG & LYS

The second mixture used to investigate the selectivity of the HPTA-membranes was composed of IgG and lysozyme, with a composition of 0.5 mg/mL of IgG and 0.2 mg/mL of LYS. The results the three chromatographic cycles performed are reported in Table 4.13, while qualitative SDS-PAGE results are shown in Fig. 4.9.

It can be noticed that the adsorption of the antibody onto the membranes is evidently higher than that observed for the previously studied case of a mixture of IgG and BSA and it is comparable to the best result obtained for pure IgG solutions. Clearly, lysozyme did not compete for the ligand binding sites, and did not even bind to any residual active epoxy groups. The latter observation suggests that actually 2-ethanolamine worked quite well as blocking agent, except for its side-effect of introducing a positive charge onto the support (that interacts with BSA). A marginal reduction of IgG binding from one cycle to the following is still observed and again it may be caused by the combined effect of ligand inefficient IgG binding reversibility and spacer non-specific and irreversible adsorption. Indeed, the recovery values determined for IgG are quite lower than those observed for pure protein solutions.

**Table 4.13** Preliminary adsorption experiments for HPTA-membranes, using mixtures of IgG and LYS at a concentration of 0.5 mg/mL and 0.2 mg/mL respectively; endcapping performed with 2-ethanolamine.

| Affinity cycle | IgG | | LYS |
|:---:|:---:|:---:|:---:|
| | $q_{ads}$ [mg/mL] | Recovery [%] | $q_{ads}$ [mg/mL] |
| I | 2.29 | 58.7 | ~0.0 |
| II | 1.91 | 58.0 | ~0.0 |
| III | 1.79 | 47.5 | ~0.0 |

| | |
|---|---|
| 1 | MW marker |
| 2 | elution I |
| 3 | elution II |
| 4 | elution III |
| 5 | IgG (0.05 mg/mL) |
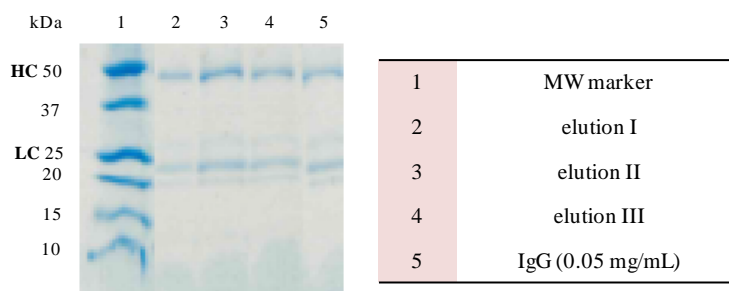
**Figure 4.9**  SDS-PAGE gel image obtained from the analysis of the eluted samples of experiment with a mixture of IgG and LYS at a concentration of 0.5 mg/mL and 0.2 mg/mL respectively; HPTA-membranes endcapped with 2-ethanolamine.

However, it can be pointed out that lysozyme has much less influence on the behaviour of the affinity matrix with respect to BSA. This fact may be the consequence of a greater affinity of BSA for the ligand binding sites, and its higher tendency to form hydrogen bonds with the spacer [11, 12], as well as a lower isoelectric point that allows this impurity to bind also to the endcapped epoxy groups.

**Human Serum**

The last mixture used for the characterization of the HPTA-membranes was human serum. Human serum was diluted ten times using PBS before performing these batch experiments.

The total amount of protein present in the feed samples was determined by the BCA colorimetric method. The analysis performed on freshly purchased human serum allowed to measure a total protein content equal to 57 mg/mL approximately, while the same analysis performed on the samples used for the adsorption tests showed a reduction in the total amount of protein, that was found equal to 20 mg/mL approximately.

However, the results obtained with this colorimetric assay have to be considered indicative values of the total protein content, since the calibration curve for the assay was obtained using BSA, as described in Chapter 2, while the samples of interest are complex protein mixtures.

Two sets of HPTA-membranes were used to perform two separate experiments, of three chromatographic cycles each. The results obtained in terms of IgG adsorbed and recovered, as well as impurities adsorbed, are shown in Table 4.14.

**Table 4.14** Preliminary adsorption experiments for HPTA-membranes, using human serum diluted ten times using PBS; endcapping performed with 2-mercaptoethanol.

| Experiment | Affinity cycle | IgG | | Impurities |
| --- | --- | --- | --- | --- |
| | | $q_{ads}$ [mg/mL] | Recovery [%] | $q_{ads}$ [mg/mL] |
| #1 | I | 0.142 | 70.63 | 1.089 |
| | II | 0.086 | 93.84 | 2.225 |
| | III | 0.176 | 34.58 | 2.155 |
| #2 | I | 0.037 | 100 | 1.192 |
| | II | 0.058 | 100 | 1.441 |
| | III | 0.169 | 36.58 | 3.835 |

The amount of adsorbed IgG is significantly lower than the values obtained in the case of the other binary mixtures employed. An increase of the amount of IgG adsorbed on the support during the third cycle for both sets was registered, as opposed to what was expected.

The recovery values of immunoglobulins are high and in a few cases greater than the values obtained from binary mixtures tests. During the third cycle a decrease in the IgG recovery, to a value of 35% for both sets, was measured.

The amount of adsorbed impurities did not follow a specific trend during the subsequent chromatographic cycles, and these values were found much higher than those of adsorbed IgG. The recovery of impurities was always measured approximately zero.

As for binary synthetic mixtures, also in this case the feed and elution samples were analyzed using the electrophoretic technique; the results can be found in Fig. 4.10.
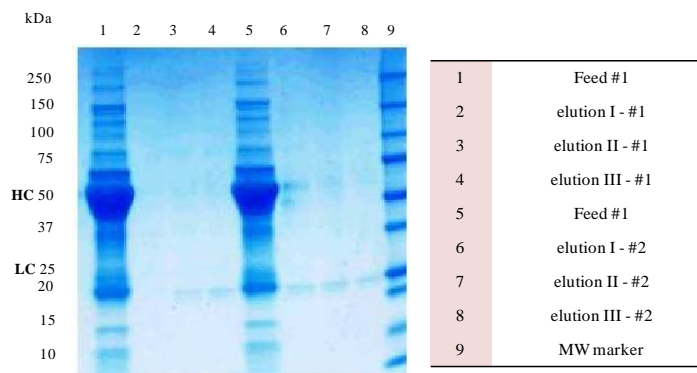


**Figure 4.10** SDS-PAGE gel image obtained from the analysis of the eluted samples of experiment with human serum diluted with PBS; HPTA-membranes endcapped with 2-mercaptoethanol.

Looking at the picture above, it is clear the presence of IgG in the two feed samples, in which the bands corresponding to the light and heavy chains are quite intense. IgG is also present in the elution samples: in this case, the bands of the light chain are clearly visible, while heavy

CHAPTER 4

chain bands are difficult to identify, probably due to the very low concentration that characterized the elution samples.

In lanes 1 and 5, another characteristic band can be seen, corresponding to a molecular weight of about 65-70 kDa: this band demonstrates the presence of BSA. In the elution samples, however, BSA band is only appreciated for the first chromatographic cycle of experiment #2. Thus, it can be concluded that the elution samples are more rich in IgG, rather than in BSA: this result agrees with those in Table 4.14.

Finally, comparing the lanes containing the feed solutions with the lanes containing the elution samples, it is clear that any of the bands corresponding to the other proteins in the human serum are present in the elution samples, apart from IgG and BSA. This can be considered as an additional proof of the key role of the spacer arm, that was found responsible for the non-specific adsorption of both IgG and BSA. Thus, if the ligand is responsible for non-specific adsorption too, it shows interactions only with BSA among the possible contaminant proteins.

## 4.7 Adsorption and desorption isotherms

With the purpose of completing the characterization of A2P and HPTA affinity membranes, other batch trials were performed for each membrane type. All membranes utilized in these set of experiments were endcapped with 2-ethanolamine.

Different chromatographic cycles, without intermediate regeneration, were performed, setting the initial concentration of pure IgG in PBS at different values: the Langmuir model was used to obtain the adsorption isotherms for both HPTA-membranes and for A2P-membranes. In particular, the results obtained with the HPTA-membranes were compared to literature isotherm data [5].

Fig. 4.11 shows the adsorption isotherms obtained, and the corresponding values of the Langmuir parameters: static binding capacity ($q_m$) and dissociation constant ($K_d$) for three subsequent adsorption cycles.
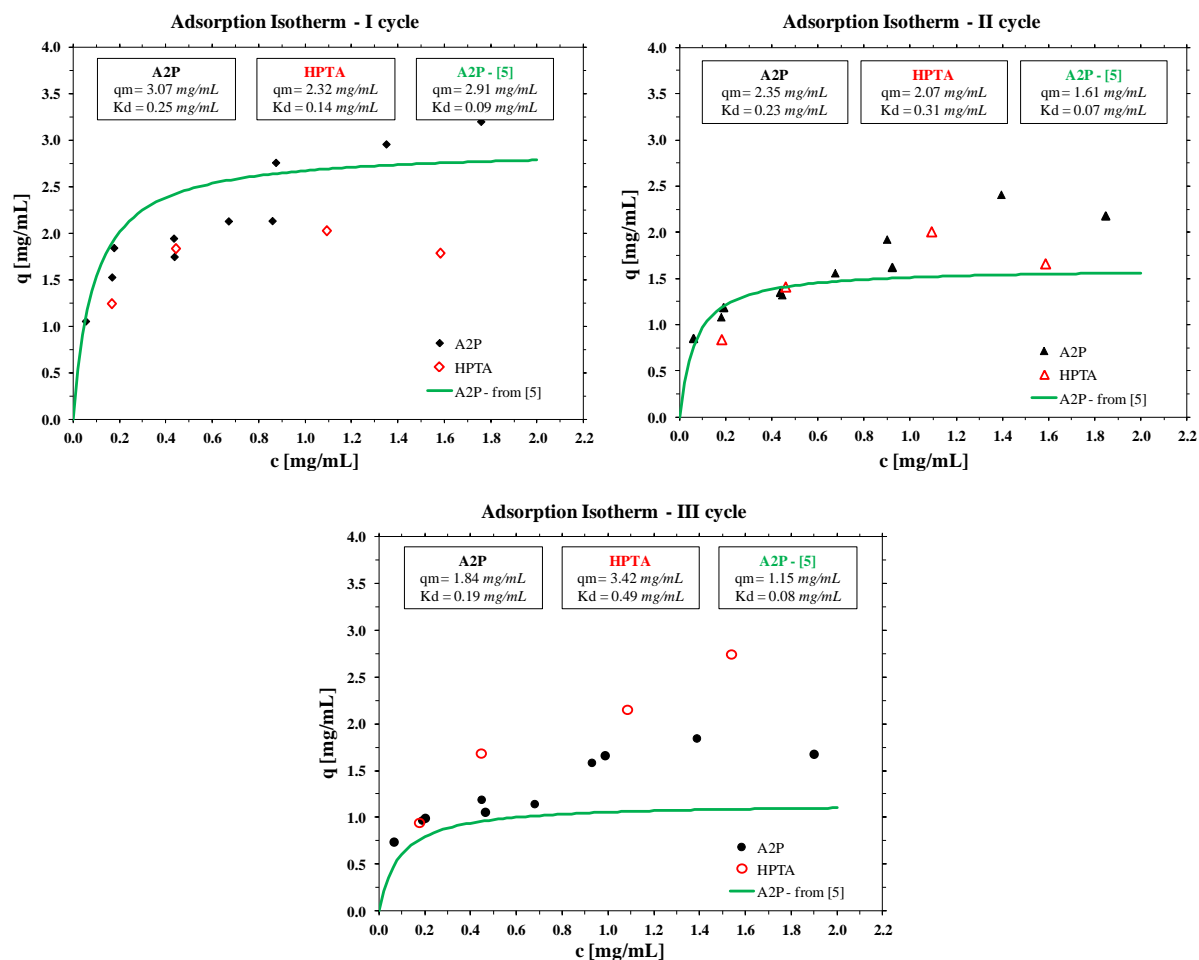
**Figure 4.11** Three subsequent adsorption isotherms for A2P-membranes, HPTA-membranes and Langmuir isotherm for A2P-membranes from literature [5].

It is apparent that the A2P-membranes isotherm obtained compares well with the Langmuir isotherm from literature, and that the experimental data are consistent. This is particularly true for the first cycle.

Moreover, comparing the performances of A2P and HPTA ligands, it can be immediately recognized that the membranes modified with A2P possess a larger static binding capacity than those functionalized with HPTA. Nonetheless, the decrease of adsorption capacity between the first and the second cycle is more accentuated for the A2P-membranes.

The sensible drop of the binding capacity for the supports modified with A2P is very likely related to the low recoveries that were measured in previous works and are well known from the literature [3, 5]. The formation of irreversible bonds is indeed a direct cause of the reduction of the available ligand binding sites during subsequent affinity cycles.

To prove this speculation, it is interesting to finally compare the elution performance of the two affinity membranes, that is reported in Fig 4.12.
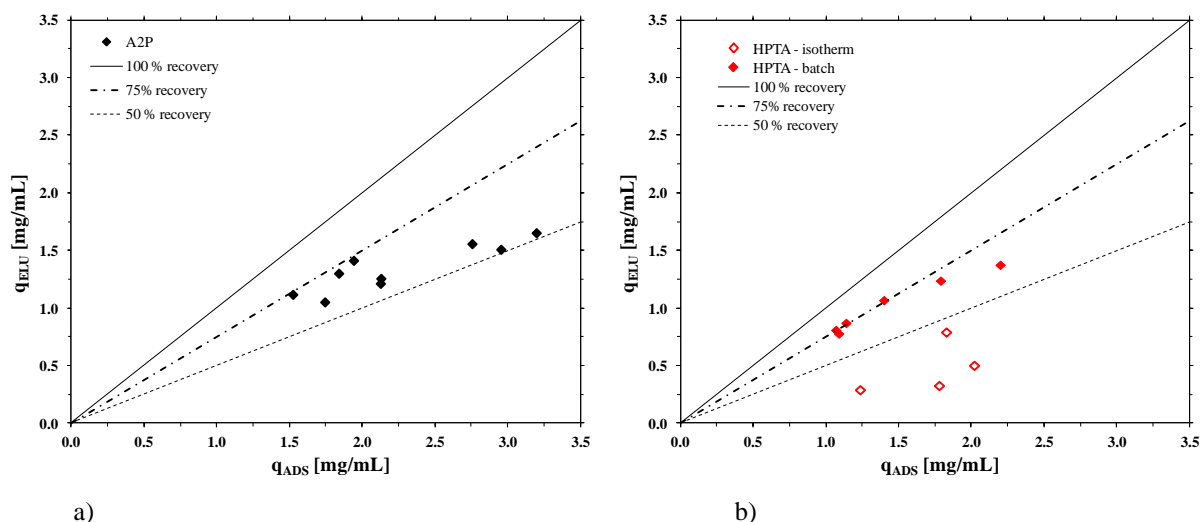
**Figure 4.12** Values of IgG recovery: a) A2P-membranes first cycle isotherm; b) HPTA-membranes first cycle isotherm and other batch chromatographic tests.

In the plot in Fig. 4.12a, it can be observed that the amount of IgG recovered with the elution varies from 50 to 75%; these values are in agreement with those found in the previous experimentation: average IgG recovery for A2P-2LP membranes was found equal to 62% [3]. On the other hand, looking at Fig. 4.12b it is clear that the average recovery value for HPTA-membranes is around 75%; unfortunately, IgG concentration of the elution samples of one data set was determined by HPLC analysis using the Protein A column, without removing the elution buffer and suspending the protein in PBS. For this reason, the measurement of the concentration of IgG was affected by experimental error and the results were greatly underestimated.

# References

[1] G.T. Hermanson, A.K. Mallia, P.K. Smith, *Immobilized Affinity Ligand Techniques*, [ed.] Academic Press, Inc., San Diego (CA - USA). 1992

[2] J. Horak, S. Hofer, W. Lindner, *Optimization of a ligand immobilization and azide group endcapping concept via "Click Chemistry" for the preparation of adsorbents for antibody purification*, Journal of Chromatography B 878 (2010) 3382-3394

[3] C. Boi, S. Dimartino, S. Hofer, J. Horak, S. Williams, G.C. Sarti, W. Lindner, *Influence of different spacer arms on Mimetic Ligand A2P and B14 membranes for human IgG purification*, Journal of Chromatography B 879 (2011) 1633-1640

[4] Private communication

[5] C. Boi, S. Dimartino, G.C. Sarti, *Modelling and simulation of affinity membrane adsorption*, Journal of Chromatography A 1162 (2007) 24-33

[6] L. Zamolo, V. Busini, D. Moiani, D. Moscatelli, C. Cavallotti, *Molecular dynamic investigation of the interaction of supported affinity ligands with monoclonal antibodies*, Biotechnology Progress 24 (3) (2008) 527-539

[7] L. Zamolo, M. Salvalaglio, C. Cavallotti, B. Galarza, C. Sadler, S. Williams, S. Hofer, J. Horak, W. Lindner, *Experimental and theoretical investigation of effect of spacer arm and support matrix of synthetic affinity chromatographic materials for the purification of monoclonal antibodies*, Journal of Physical Chemistry B 114 (2010) 9367-9380

[8] C. Boi, V. Busini, M. Salvalaglio, C. Cavallotti, G.C. Sarti, *Understanding ligand-protein interactions in affinity membrane chromatography for antibody purification*, Journal of Chromatography A 1216 (2009) 8687-8696

[9] E. Lalli, G.C. Sarti, C. Boi, *Effect of the spacer arm on non-specific binding in membrane affinity chromatography*, MRS Communications (2018) 1-6

[10] S. Dimartino, *Studio sperimentale e modellazione della separazione di proteine con membrane di affinità*, Tesi di Dottorato di Ricerca in Ingegneria Chimica dell'Ambiente e della Sicurezza XXI Ciclo, Facoltà di Ingegneria, Università degli Studi di Bologna, 2009

[11] R. Fang, X.J. Leng, X. Wu, Q. Li, R.F. Hao, F.Z. Ren, H. Jing, *Intermolecular hydrogen bond between protein and flavonoid and its contribution to the stability of the flavonoids* (2012) Guang Pu Xue Yu Guang Pu Fen Xi, Vol. 32, 108 - 120

[12] R.W. Hemingway, J.J Karchesy, *Chemistry and Significance of Condensed Tannins*, [ed.] Plenum Press, New York (NY - USA) 1989

# CHAPTER 5

# Modelling of breakthrough curves

## 5.1 Introduction and state of the art

A part of the characterization and process implementation of affinity membranes is related to modelling of breakthrough curves for membrane chromatographic systems. As introduced in Chapter 1, membrane chromatography is a promising process that can be used for the purification of different biological molecules as valid alternative to the traditional chromatography performed using columns packed with porous beads. To understand the overall separation mechanisms and to optimize equipment design, it is paramount to study the mass transport of solutes through the porous medium by adopting model-based approaches to predict the performance of such systems.

Several mathematical models have been developed to describe the transport phenomena and simulate chromatographic processes, most of them originate from the model proposed by Thomas [1, 2]. The Thomas model describes heterogeneous ion exchange chromatography in a packed bead column for a system with negligible axial dispersion and negligible dispersion in the external column volumes [1]. This simple model admits an analytical solution that gives a first estimate of the adsorption behaviour, when dispersion is not a relevant phenomenon. Therefore, to better describe adsorption chromatography a more complete model, like the general rate model, which accounts for all mass transfer contributions, is necessary [3].

Indeed, the mathematical description of membrane adsorption chromatography is simpler than the one needed for packed column chromatography, since it requires only a unique porosity and simplifications according to the relevant characteristic times are in order. The first mathematical model proposed for membrane adsorption [3] is based on partial differential equations that have to be solved simultaneously in both time and space. This model extends the theory related to membrane affinity chromatography to the study of extra-column effects in the membrane system that are relevant when the membrane column volume is of the same order of magnitude of the

extra-column volumes. This situation is quite common in preparative scale systems where small membrane units, with non-negligible void volumes, are in use.

Moreover, in the field of membrane adsorption, a general rate model that includes convection and axial dispersion, mass transport from the mobile phase to the stationary phase, pore diffusion and surface diffusion within the stationary phase, adsorption and desorption kinetics has been developed [4]. Since the solution of this type of models requires a considerable computational time, several simplified forms have been developed, such as the lumped kinetic model and the lumped pore model [5, 6]. These models are generally good to describe the system for which they have been developed and validated, however, since the lumped parameters often lose completely their physical meaning, they cannot be used equally well to describe other experimental systems and they are not appropriate for scale-up purposes.

Other type of models are based on empirical approaches but their use out of the range of experimental data is not allowed, so they cannot be used for process scale-up [7]. The zonal rate model [8, 9] separates the effects of hydrodynamics and binding by dividing the entrance and elution hold-up volumes, as well as the membrane unit, into virtual zones that are represented as a network of CSTRs and PFRs. This model can be applied to axial and radial membrane chromatography processes and it can be used for scale-up purposes.
Moreover, there are models that combine the zonal rate model and computational fluid dynamics [10, 11] to better describe the hydrodynamics inside the membrane chromatographic unit.

Since mathematical models have to be effective simulation tools, reliable for prediction, optimization and scale up purposes, they must be based on physical and chemical principles and theories: they should be as simple as possible and able to describe the physical phenomena related to the process [12]. A considerable number of models for membrane chromatography belong to this class of physical models, because they are based on the theory and the fundamental equations of mass transport inside porous media. However, they differ according to the process they describe, as well as according to the hypothesized mechanisms. In the field of frontal affinity chromatography there are works [13, 14] that aim at the development of a transport model that considers pore diffusion, external film resistance, finite kinetics rate and column dispersed flow. Numerical methods can be used to solve the model equations. Different physical models study the effect of model parameters on the shape of the breakthrough curves [15], while other works deal with the accurate study of the adsorption mechanism [16, 17], describing the interaction between the ligand and the target molecule using the Freundlich adsorption equation.

This chapter discusses the effects of dispersion, that can occur both during transport of solutes inside the column and in the ancillary equipment: respectively, axial dispersion and system dispersion. The dispersion contribution to the mass transport mechanism is taken into account by the dispersion coefficient: it is an important parameter and it can be easily determined through experimental tests that are independent from the process under investigation.

The drive for this modelling work originates from the publication of a paper [18] that deals with the modelling of membrane chromatography. The authors sustain that the use of polydispersed chromatographic membranes leads to dispersed breakthrough curves, due to unequal flow through unequally sized pores. The purpose of the authors is to develop a mathematical model based on a theory of polydispersed pores that can predict the breakthrough curves by knowing the membrane pore size distribution. Indeed the use of accurate models on the microscopic scale will bring to a detailed description of the phenomena involved, however this approach is not necessary to simply obtain the prediction of breakthrough curves, that can be easily described with physical models based on the continuum equation using the appropriate parameters.

This literature work does not take into account the dispersion phenomenon and does not consider works that have already been published, such as the physical models for membrane chromatography developed by Etzel *et al*. [3] and by Dimartino *et al*. [12]. These models are adequate for the description of every single step and phenomenon related to a membrane chromatographic process. In particular, the use of the axial dispersion coefficient, as an important parameter of the model, is sufficient for the prediction of breakthrough curves in the case of a generic chromatographic membrane, without the need of hypothesizing polydispersed membranes.

In support for this last statement a new simplified model was developed. The purpose was first, to theoretically calculate the dispersion coefficient starting from the construction of the breakthrough curve for a polydispersed membrane; second, to validate the model using its results as input for a physical model for membrane chromatography [12]; third, to finally prove the inefficacy of polydispersed membrane hypothesis, as well as the incompleteness of the theory that derives from it.

## 5.2 Model development

A general mathematical model suitable for the entire chromatographic cycle should take into account the relevant kinetic and transport phenomena occurring inside the membrane

column in all process stages. However, to demonstrate the importance of the dispersion coefficient it is sufficient to consider only the adsorption stage with negligible binding kinetics. Therefore, washing and elution stages are not of interest and will be disregarded. Moreover, the only element of the process considered is the chromatographic module: all the effects of fluid dynamics in the other parts of the chromatographic system are not taken into account. With the simple model proposed, it will be possible to obtain a breakthrough curve and to calculate the dispersion coefficient, when a solution of a generic solute $i$ flows through a membrane column, under non-binding conditions.

### 5.2.1 Membrane column model and transport mechanism

The membrane column is considered as an ideal porous medium with uniform porosity, in particular, the module is composed of one membrane disc of known diameter, $d_m$: for all the calculations that will follow the membrane diameter will be considered equal to 2.2 cm. The features of the membrane, in terms of thickness, void fraction and average pore size, refer to a commercial membrane of the Sartobind[®] family (Sartorius Stedim Biotech GmbH); the relevant data, according to the data sheet, are reported in Table 5.1.

**Table 5.1**     Sartobind[®] Q membrane specifications [19].

| Pore diameter | ε | Thickness |
|:---:|:---:|:---:|
| μm | % | μm |
| 3.00 | 80 | 275 |

The membrane pores are schematized as cylinders of radius equal to the average pore radius and length equal to the membrane thickness. Moreover, it is assumed that the pore size distribution of the membrane can be approximated to a Gaussian curve, as in Eq. (5.1). Indeed, measured pore size distribution of commercial membranes do not differ much from a Gaussian curve and the choice made is representative of real membrane systems.

$$f(r_p) = \frac{1}{\sqrt{2\pi}\sigma} \exp\left[ -\frac{1}{2}\left( \frac{r_p - \mu}{\sigma} \right)^2 \right] \tag{5.1}$$

Different Gaussian curves were arbitrarily chosen, as shown in Fig. 5.1, as pore size distributions. The values of the curve parameters, $\mu$ (average pore radius ) and $\sigma$ (standard deviation), used in the calculations are listed in Table 5.2.

**Table 5.2**    Pore size distribution parameters.

| μ (average pore radius) | σ | Minimum pore radius | Maximum pore radius |
|---|---|---|---|
| μm | μm | μm | μm |
| 1.50 | 0.10- 0.18- 0.26- 0.35 | 0.50 | 6.50 |
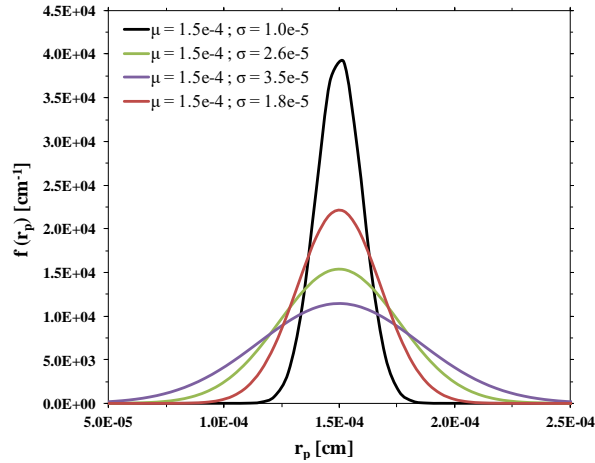


**Figure 5.1**    Gaussian pore size distributions hypothesized for the membrane disc; in the plot the pore radius range was cut at $2.5 \cdot 10^{-4}$ cm.

The interstitial flow velocity is assumed to be constant and uniform over the membrane column, in addition, an optimal flow distribution in the radial direction is considered. Therefore the variation of concentration of all species in the radial direction can be neglected and the problem reduces to a one-dimensional problem, simple to solve.

The model developed takes into account only axial convection and longitudinal dispersion, that is due to two simplifying assumptions: 1) the contribution of molecular diffusion to the motion of the generic solute $i$ is negligible; 2) the flow velocity of the solution inside each pore is considered constant over the cross section of the pores themselves and equal to the average velocity. This second hypothesis is particularly important, since it implies that the Taylor-Aris dispersion is not relevant and can be neglected.

### 5.2.2 Model equations

Before introducing the structure of the mathematical model it is necessary to list all the variables used and, in particular, the variables are reported in two tables, Table 5.3 and Table 5.4, and they are divided into *input data* and *output data*, respectively.

Some of the values of the variables used as input data were already introduced in Table 5.1 and Table 5.2. In addition to those data, for all calculations that follows, it was considered a constant flow rate, $F$, of 1 mL/min and an initial concentration, $c_{i,\text{in}}$, of 0.5 g/L.

**Table 5.3**   Input variables.

| | | |
|---|---|---|
| $d_m$ | cm | Membrane disc diameter |
| $r_{p,\min}$ | cm | Minimum value of the pore radius (for Gaussian pore size distribution) |
| $r_{p,\max}$ | cm | Maximum value of the pore radius (for Gaussian pore size distribution) |
| $L_m$ | cm | Membrane thickness |
| $\varepsilon$ | % | Void fraction |
| $\mu$ | cm | Average pore radius value for Gaussian pore size distributions |
| $\sigma$ | cm | Standard deviations for Gaussian pore size distributions |
| $F$ | mL/s | Flow rate |
| $c_{i,\text{in}}$ | g/L | Initial concentration of the solute $i$ in the solution |

**Table 5.4**   Output variables.

| | | |
|---|---|---|
| $A_m$ | cm$^2$ | Membrane surface |
| $A_{eff}$ | cm$^2$ | Effective membrane surface |
| $\langle v \rangle$ | cm/s | Average interstitial velocity through the module |
| $\langle t \rangle$ | s | Average time needed to let the solution flow through each pore |
| $v_m(r_p)$ | cm/s | Average velocity inside the pore of radius $r_p$ |
| $t_{r_p}$ | s | Time that the solution needs to flow through the pore of radius $r_p$ |
| $F(r_p)$ | mL/s | Flow rate inside the pore of radius $r_p$ |
| $F_i$ | mL/s | Auxiliary variable needed for the calculation of the flow rate exiting the module |
| $F_{out}$ | mL/s | Flow rate coming out from the module |
| $c_{i,\text{out}}$ | mg/mL | Concentration of solute $i$ in the solution coming out from the module |
| $z_{r_p}$ | cm | Axial coordinate covered by the solution for the pore of radius $r_p$ |
| $t$ | s | Time coordinate |
| $a$, $b$, $c$ | mg/mL, s$^{-1}$, s | Adjustable parameters used in equation (5.15) |
| $t_{lag}$ | s | Parameter used in equation (5.15) |
| $\mu_1$ | s | First absolute moment |
| $\bar{\mu}_2$ | s$^2$ | Second central moment |
| $D_L$ | cm$^2$/s | Dispersion coefficient |

Starting from the input data of the model, it is possible to fully characterize the membrane module, calculating the following parameters:

$$A_m = \pi \frac{d_m^2}{4} \tag{5.2}$$

$$A_{eff} = A_m \varepsilon \tag{5.3}$$

$$\langle v \rangle = \frac{F}{A_{eff}} \tag{5.4}$$

$$\langle t \rangle = \frac{L_m}{\langle v \rangle} \tag{5.5}$$

At this point it is possible to calculate the velocity and the flow rate associated to each pore of the medium, as well as the time needed by the solution to cover the total length of the membrane module. It is worth noticing that this time is different for pores of different radius and this is the reason why the response to a concentration step function is a breakthrough curve.

$$F(r_p) = F \frac{\pi r_p^4}{A_m \varepsilon} \frac{\int_0^{+\infty} r_p^2 \cdot f(r_p) dr_p}{\int_0^{+\infty} r_p^4 \cdot f(r_p) dr_p} \tag{5.6}$$

$$v_m(r_p) = F \frac{r_p^2}{A_m \varepsilon} \frac{\int_0^{+\infty} r_p^2 \cdot f(r_p) dr_p}{\int_0^{+\infty} r_p^4 \cdot f(r_p) dr_p} \tag{5.7}$$

$$t_{r_p} = \frac{L_m}{v_m(r_p)} \tag{5.8}$$

The construction of the breakthrough curve starts from the calculation of the flow rate through the fraction of pores that have radius between $r_p$ and $r_p + dr_p$:

$$F(r_p; r_p + dr_p) = \int_{r_p}^{r_p + dr_p} F(r_p) \cdot f(r_p) \cdot n_p dr_p \tag{5.9}$$

$$n_p = \frac{\varepsilon A_m}{\pi \int_0^{+\infty} r_p^2 \cdot f(r_p) dr_p} \tag{5.10}$$

Considering a generic time coordinate $t$, it is possible to calculate the position of the concentration front inside each pore; comparing the variable $z_{r_p}$ (for each pore dimension) to the membrane thickness it is possible to establish if the solution is actually coming out from the pore considered or not. In this way it is possible to calculate the flow rate exiting the column as a function of time, and to obtain the concentration profile.

$$z_{r_p} = v_m(r_p)t \tag{5.11}$$

$$\begin{cases} \text{if } \left( z_{r_p} \leq L_m \right) \text{then } F_i = 0 \\ \text{else } F_i = F(r_p; r_p + dr_p) \end{cases} \tag{5.12}$$

$$F_{out}(t) = \sum F_i(t) \tag{5.13}$$

$$c_{i,out}(t) = F_i(t) \frac{c_{i,in}}{F} \tag{5.14}$$

where $F_{out}(t)$ is the flow rate exiting the membrane column as a function of time and $c_{i,out}(t)$ is the concentration profile, as a function of time, that describes the breakthrough curve.

The obtained breakthrough curve derives from a finite discretization of the pore radius: it has to be regularized by fitting the data with an appropriate relation. A sigmoid function properly modified, Eq. (5.15), was chosen to fit, and smoothen, the breakthrough curve:

$$\begin{cases} t \leq t_{lag} & c_{i,out} = 0 \\ t > t_{lag} & c_{i,out} = \dfrac{a}{1 + \exp\left\{ -b\left[ \left( t - t_{lag} \right) - c \right] \right\}} - \dfrac{a}{1 + \exp(b \cdot c)} \end{cases} \tag{5.15}$$

The fitting equation has three adjustable parameters, $a$, $b$ and $c$, plus another parameter, $t_{lag}$, that represents the time up to which, the concentration exiting the membrane module is equal to zero. $t_{lag}$ can be measured, therefore it is not an adjustable parameter of the model.

The method of moments was applied to calculate the dispersion coefficient: to this aim it was necessary to study the response of the membrane column to a concentration pulse [20-23]. It is useful to remind that the response to a pulse is a peak, that can be easily obtained as the derivative of the breakthrough curve.

$$\begin{cases} t \leq t_{lag} & \dfrac{dc_{i,out}}{dt} = 0 \\ t > t_{lag} & \dfrac{dc_{i,out}}{dt} = \dfrac{a \cdot b \cdot \exp\left\{ -b\left[ \left( t - t_{lag} \right) - c \right] \right\}}{\left\{ 1 + \exp\left\{ -b\left[ \left( t - t_{lag} \right) - c \right] \right\} \right\}^2} \end{cases} \tag{5.16}$$

Finally, the last step of the proposed model is the application of the method of moments for the determination of the dispersion coefficient. This method was developed for bead-based chromatography [20-23], but in the case of membrane columns it can be simplified, so that the first absolute moment ($\mu_1$) and the second central moment ($\overline{\mu}_2$) are defined as follows (see Chapter 2, paragraph 2.6.2.2):

$$\mu_1 = \frac{L_{TOT}}{\langle v \rangle} \tag{5.17}$$

$$\bar{\mu}_2 = 2L_{TOT}\frac{D_L}{\varepsilon\langle v\rangle^3} \tag{5.18}$$

where $D_L$ represents the dispersion coefficient.

Equations (5.1) - (5.18) were implemented in Microsoft Excel® and solved to obtain the breakthrough curves and the dispersion coefficient.

## 5.3 Model validation

The path followed to validate the simple model proposed is a theoretical comparison with a rigorous mathematical model, that was previously developed and validated in our research group [14]. In particular, a physical model for membrane chromatography has been used, that considers all transport and kinetic phenomena involved in the process:

$$\begin{cases}\dfrac{\partial c_{i,out}}{\partial t}\left[1+\dfrac{(1-\varepsilon)}{\varepsilon}\dfrac{q_m K_d}{(c_{i,out}+K_d)^2}\right]+\langle v\rangle\dfrac{\partial c_{i,out}}{\partial z}=D_L\dfrac{\partial^2 c_{i,out}}{\partial z^2}\\ t=0 \qquad c_i=0\end{cases} \tag{5.19}$$

where $q_m$ and $K_d$ represent the Langmuir isotherm parameters.

Although, the assumptions made for the development of this simple model focus on the breakthrough curve under non-binding conditions and reduce the physical model governing equation as the following:

$$\begin{cases}\dfrac{\partial c_{i,out}}{\partial t}+\langle v\rangle\dfrac{\partial c_{i,out}}{\partial z}=D_L\dfrac{\partial^2 c_{i,out}}{\partial z^2}\\ t=0 \qquad c_i=0\end{cases} \tag{5.20}$$

The partial differential equation was solved using Aspen Custom Modeler™, imposing the same input data used for the simplified model. The dispersion coefficient calculated with the simplified model was also used as input data for the physical model and the new developed theory was proved by comparing the breakthrough curves obtained with the two models.

## 5.4 Results

The breakthrough curves obtained for the hypothetical polydispersed membranes are shown in Fig. 5.2. As expected, the breakthrough curves are steeper for membranes with a narrow pore size distribution, corresponding to a low value of the standard deviation $\sigma$, and broaden as the pore size distribution broadens, that is at higher values of the standard deviation.

Fig. 5.2b shows the regularized breakthrough curves with a sigmoid function properly modified, according to Eq. (5.15).

The fitting parameters and the lag time related to the breakthrough curves shown in Fig. 5.2b are reported in Table 5.5.



a)                                                    b)
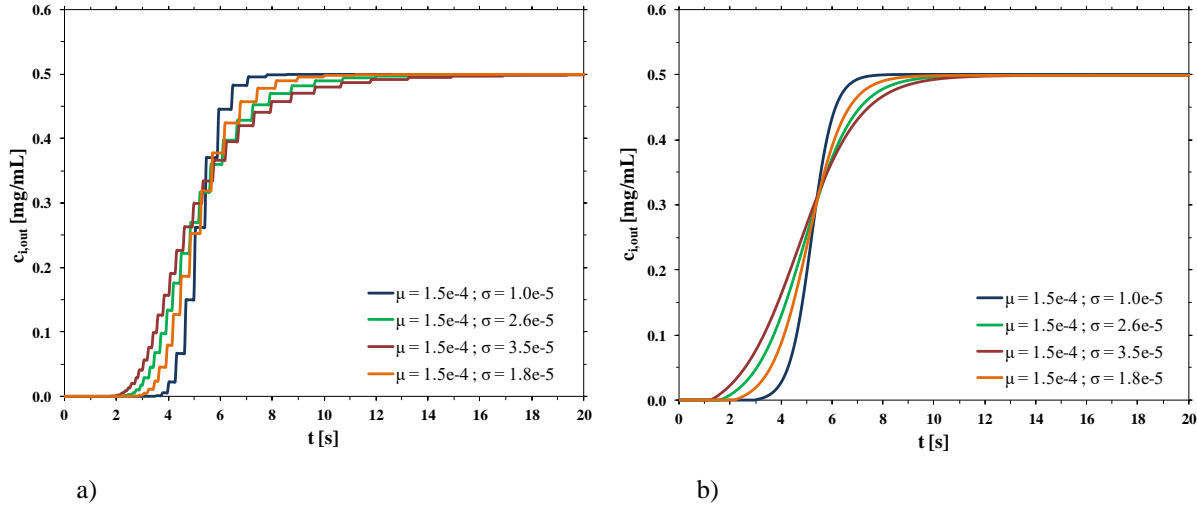
**Figure 5.2**    a) dimensional breakthrough curves as a function of the pore size distribution; b) fitting of dimensional breakthrough curves as function of the pore size distribution.

**Table 5.5**    Fitting parameters of the breakthrough curves in Fig. 5.2b.

| Pore size distribution | | Fitting parameters and $t_{lag}$ | | | |
|---|---|---|---|---|---|
| $\mu = 1.5 \cdot 10^{-4}$ $\sigma = 1.0 \cdot 10^{-5}$ | $a = 0.50$ | $b = 2.32$ | $c = 2.26$ | $t_{lag} = 2.94s$ |
| $\mu = 1.5 \cdot 10^{-4}$ $\sigma = 1.8 \cdot 10^{-5}$ | $a = 0.51$ | $b = 1.38$ | $c = 2.90$ | $t_{lag} = 2.16s$ |
| $\mu = 1.5 \cdot 10^{-4}$ $\sigma = 2.6 \cdot 10^{-5}$ | $a = 0.52$ | $b = 1.02$ | $c = 3.29$ | $t_{lag} = 1.62s$ |
| $\mu = 1.5 \cdot 10^{-4}$ $\sigma = 3.5 \cdot 10^{-5}$ | $a = 0.53$ | $b = 0.83$ | $c = 3.43$ | $t_{lag} = 1.26s$ |

To obtain the impulse response peaks it is necessary to take the derivative of the corresponding regularized breakthrough curves; for the case under investigation, the peaks derived from the curves of Fig. 5.2b are shown in Fig. 5.3.

As expected, the more the pore size is dispersed, the more the output peaks are broad, tailed and, consequently, short. All peaks show an irregular behaviour for times near $t_{lag}$, especially the peaks related to broad pore size distributions. The steps are due to the range of variation of the pore radius, shown in Table 1. In particular, the maximum value of the pore radius is responsible for an abrupt change in the flow exiting the membrane (breakthrough curve) and this causes an even more abrupt change in the impulse response peak (derivative of the breakthrough curve). However, it was demonstrated that if the maximum value of the range of

variation of the pore radius is increased from $2.5 \cdot 10^{-4}$ cm to $6.5 \cdot 10^{-4}$ cm , to limit the irregular behaviour near $t_{lag}$, the dispersion coefficient undergoes a variation of only 3.16% in the case of the broader pore size distribution (higher $\sigma$ value).
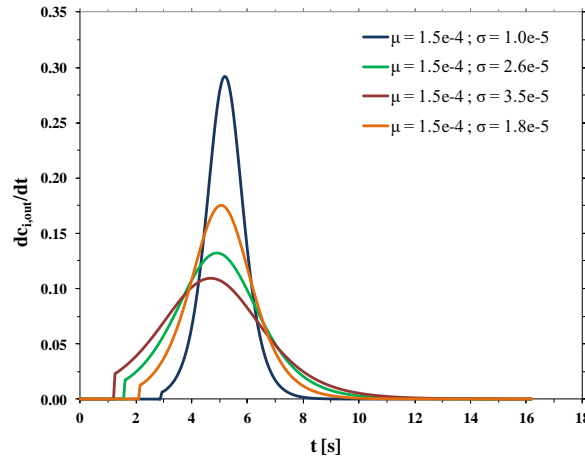


**Figure 5.3**    Impulse response peaks as a function of the pore size distribution.

By applying the method of moments to these curves and, in particular, by making use of the second central moment of Eq. (5.18), the relevant dispersion coefficients were calculated and summarized in Table 5.6.

**Table 5.6**    Dispersion coefficient for each pore size distribution.

| Pore size distribution | Dispersion coefficient |
|---|---|
| $\mu = 1.5 \cdot 10^{-4} \quad \sigma = 1.0 \cdot 10^{-5}$ | $D_L = 1.38 \cdot 10^{-6} \, \text{cm}^2/\text{s}$ |
| $\mu = 1.5 \cdot 10^{-4} \quad \sigma = 1.8 \cdot 10^{-5}$ | $D_L = 3.63 \cdot 10^{-6} \, \text{cm}^2/\text{s}$ |
| $\mu = 1.5 \cdot 10^{-4} \quad \sigma = 2.6 \cdot 10^{-5}$ | $D_L = 6.17 \cdot 10^{-6} \, \text{cm}^2/\text{s}$ |
| $\mu = 1.5 \cdot 10^{-4} \quad \sigma = 3.5 \cdot 10^{-5}$ | $D_L = 8.77 \cdot 10^{-6} \, \text{cm}^2/\text{s}$ |

The values of the dispersion coefficients, reported in Table 5.6, were used among the input data for the rigorous physical model for membrane chromatography. The breakthrough curves computed by the two mathematical models considered are compared side by side in Fig. 5.4.

In the case of a less broad pore size distribution, Fig. 5.4a, the contribution to the dispersion phenomenon is especially given by the parabolic profile of flow velocity inside each pore: this means that the Taylor-Aris dispersion is the dominant phenomenon. This is true in general: the dispersion phenomenon in a porous medium can be traced back to the Taylor-Aris dispersion when the pore size distribution is narrow.

On the other side, when the pore size distribution is broad, Fig. 5.4d, the contribution of Taylor-Aris to the overall dispersion phenomenon is not relevant, while the pore size distribution gives the major contribution to the dispersion phenomenon. In any case, the two models agree very well in all stages of breakthrough indicating that the physical model approach, that makes use of a dispersion coefficient, that is a characteristic parameter of the porous medium, is a more efficient way to describe the membrane chromatographic process. Indeed, the use of a polydispersed membranes and of a description in the microscopic scale is time consuming and does not give any additional information to the description of membrane chromatography.
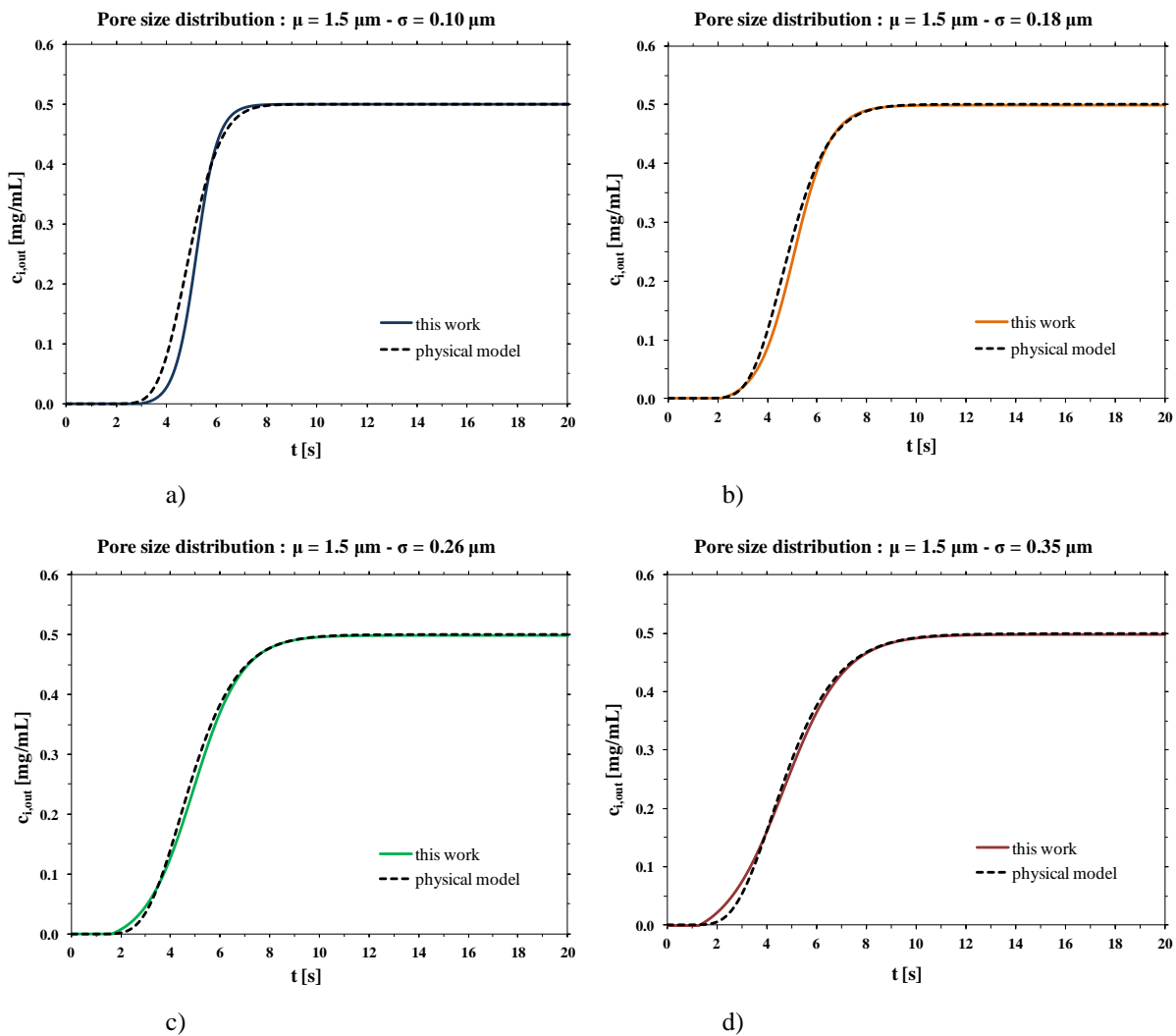


**Figure 5.4**    Comparison between the model proposed in this work and the physical model [14].

## 5.5 Conclusions

The dispersion coefficient is an important parameter for modelling of membrane chromatography processes. It is intrinsically linked to the porous nature of the stationary phase

used for this separation unit. The dispersion coefficient can be easily measured applying the method of moments, performing independent experimental tests, as pulse injections of small volumes of tracer molecules, under non binding conditions.

The development of a simplified model demonstrated that the breakthrough curve obtained hypothesizing a polydispersed membrane is the same breakthrough curve obtained using a physical model, that uses the dispersion coefficient as input parameter. The differences between the two models are mostly related to the fact that the model proposed in this work neglects the parabolic flow velocity profile inside each pore: however, this hypothesis is acceptable in the case of broad pore size distributions, that usually reflects the real structure of polymeric membranes.

# References

[1]     H. C. Thomas, *Heterogeneous ion exchange in a flow system*, Journal of the American Chemical Society 66 (1944) 1664-1666

[2]     H.C. Thomas, *Chromatography: a problem in kinetics*, Annals of the New York Academy of Sciences (1948) 161-182

[3]     S. Suen, M. Etzel, *A mathematical analysis of affinity membrane bioseparations*, Chemical Engineering Science 47 (1992) 1355-1364

[4]     P. Van Beijeren, P. Kreis, T. Zeiner, *Development of a generic process model for membrane adsorption*, Computers and Chemical Engineering 53 (2013) 86-101

[5]     K. Miyabe, G. Guichon, *Determination of the lumped mass transfer rate coefficient by frontal analysis*, Journal of Chromatography A 890 (2000) 211-223

[6]     G. Guichon, A. Felinger, D. G. Shirazi, A. M. Katti, *Fundamentals of preparative and nonlinear chromatography*, second edition, Elsevier, San Diego, 2006

[7]     D. Cecchini, J. Ganguli, J. Pieracci, J. Thommes, *Modeling of industrial scale purification processes using multivariate analysis and principal component analysis*, Recovery of Biological Products XIV Conference, Lake Tahoe, CA, 2010

[8]     P. Ghosh, K. Vahedipourm, M. Lin, J. H. Vogel, C. A. Haynes, E. Von Lieres, *Zonal rate model for axial and radial flow membrane chromatography. Part I: knowledge transfer across operating conditions and scales*, Biotechnology and Bioengineering 110 (2013) 1129-1141

[9]     P. Ghosh, M. Lin, J. H. Vogel, D. Choy, C. Haynes, E. Von Lieres, *Zonal rate model for axial and radial flow membrane chromatography. Part II: model-based scale-up*, Biotechnology and Bioengineering 111 (2014) 1587-1594

[10]    P. Ghosh, K. Vahedipour, M. Leuthold, E. Von Lieres, *Model-based analysis and quantitative prediction of membrane chromatography: Extreme scale-up from 0.08 ml to 1200 ml*, Journal of Chromatography A, 1332 (2014) 8-13

[11]    P. Ghosh, K. Vahedipourm, M. Lin, J. H. Vogel, C. A. Haynes, E. Von Lieres, *Computational fluid dynamic simulation of axial and radial flow membrane chromatography: mechanism of non-ideality and validation of the zonal rate model*, Journal of Chromatography A 1305 (2013) 114-122

[12]    S. Dimartino, C. Boi, G. C. Sarti, *A validated model for the simulation of protein purification through affinity membrane chromatography*, Journal of Chromatography A 1218 (2011) 1677-1690

[13]  A. Tejeda-Mansir, R. M. Montesinos, R. Guzmán, *Mathematical analysis of frontal affinity chromatography in particle and membrane configuration*, Journal of Biophysical Methods 49 (2001) 1-28

[14]  R. M. Montesinos, A. Tejeda-Mansir, R. Guzmán, J. Ortega, W. E. Schiesser, *Analysis and simulation of frontal affinity chromatography of proteins*, Separation and Purification Technology 42 (2005) 75-84

[15]  P. Van Beijeren, P. Kreis, T. Zeiner, *Ion exchange membrane adsorption of bovine serum albumin - Impact of operating and buffer conditions on breakthrough curves*, Journal of Membrane Science 415-416 (2012) 568-576

[16]  W. Shi, F. Zhang, G. Zhang, *Mathematical analysis of affinity membrane chromatography*, Journal of Chromatography A 1081 (2005) 156-162

[17]  D. Ge, W. Shi, L. Ren, F. Zhang, G. Zhang, X. Zhang, Q. Zhang, *Variation analysis of affinity-membrane model based on Freundlich adsorption*, Journal of Chromatography A 1114 (2006) 40-44

[18]  Y. Wei, Y. Li, C. Yang, E. L. Cussler, *More effective membrane chromatography*, AIChe Journal (2015) 1-8

[19]  www.sartorius.com

[20]  M. Kubin, *Theory of the chromatography. II. Effect of the external diffusion and of the adsorption on the sorbent particle*, Collection of Czechoslovak Chemical Communications 30 (1965) 2900–2907

[21]  E. Kučera, *Contribution to the theory of chromatography : Linear non-equilibrium elution chromatography*, Journal of Chromatography 19 (1965) 237–248

[22]  K. Miyabe, G. Guiochon, *Measurement of the parameters of the mass transfer kinetics in high performance liquid chromatography*, Journal of Separation Science 26 (2003) 155-173

[23]  H. Hong, A. Felinger, K. Kaczmarski, G. Guiochon, *Measurement of intraparticle diffusion in reversed phase liquid chromatography*, Chemical Engineering Science 59 (2004) 3399–3412

# CHAPTER 6
# Conclusions of Part I

The first part of this PhD thesis dealt with the characterization of cellulose affinity membranes functionalized with synthetic affinity ligands for the purification of antibodies. In particular, Chapter 3 describes the experimental protocols for the functionalization of the membranes and the experimental procedures for their characterization, while the results are presented in Chapter 4. Moreover, a simplified model for the prediction of breakthrough curves in membrane chromatography systems was developed and described in Chapter 5.

The results of the characterization of affinity membranes and of the model developed are discussed in the next paragraphs.

The performance of an affinity chromatographic support depends on many different factors, especially on the elements composing the support itself. As pointed out several times, the affinity membranes subject of the first part of this work were composed of the cellulose matrix, the affinity ligands and the spacer arm, a small molecule that acts as a linker between the membrane and the ligand. All chromatographic experiments performed aimed to the determination of the contribution that each element of the affinity membrane has on the overall chromatographic performance. In particular, the goal was to determine the binding capacity, the selectivity and the recovery for IgG associated to the two affinity ligands studied: A2P and the new HPTA. It was taken into account that both the membrane and the spacer arm could significantly influence the parameters listed above and, in particular, they can contribute to non-specific adsorption and hinder the target protein complete recovery. The results obtained from the experimental characterization will be summarized and discussed for each element of the chromatographic support.

At first the interaction between different protein and the membrane support, Sartobind® Epoxy, was evaluated.

The results obtained demonstrated that the native membranes showed a non-negligible interaction with proteins such as IgG, BSA and lysozyme, due to the presence of the highly reactive epoxy groups. Different protocols for the deactivation of these functional groups were tested to ensure that neither the membranes, nor the blocking agents, interacted with the tested proteins. It is useful to remind that the endcapping procedure has to be performed, after ligand immobilization, to ensure the complete deactivation of the residual epoxy groups.

In particular, endcapping procedures using 2-ethanolamine, 2-mercaptoethanol and acidic hydrolysis were employed for the deactivation of epoxy groups. It was found that all the three endcapping strategies were able to significantly reduce the interactions between the cellulose support and the proteins. In particular, the acidic hydrolysis and 2-mercaptoethanol were able to prevent any protein adsorption, however, since acidic hydrolysis could damage the ligand structure, it was decided not to proceed further with this method.

The role of the cellulose membrane in the context of non-specific adsorption was definitely excluded, when an appropriate endcapping strategy was adopted. Moreover, the very low interaction that 2-ethanolamine exhibited towards BSA became negligible once the ligand was immobilized on the surface, meaning that the influence that the spacer arm and the affinity ligand have on the overall performance is much higher than that of the endcapped cellulose matrix.


Once assured that the membrane support was not responsible for non-specific interactions with the target protein IgG or with other contaminant proteins, the work continued by studying the spacer arm used to immobilize the ligands: the 2LP (1,2-diaminoethane) molecule.

2LP-membranes (with no ligand immobilized), properly endcapped, were used to perform batch and dynamic chromatographic experiments using solutions of pure IgG and pure BSA in PBS.

The obtained results in batch experiments showed that the quantity of protein adsorbed in the presence of the spacer arm 2LP was not negligible, while it was negligible for the original unmodified membrane, as discussed above. These results were confirmed by dynamic experiments; therefore, it is possible to conclude that the contribution of the spacer 2LP to non-specific protein adsorption was relevant and must be taken into account when analyzing the performance of the affinity membranes. In fact, from the results obtained it was clear that when the spacer 2LP was used as a linker for ligand immobilization it influenced the performance of the affinity membrane, in terms of non-specific adsorption and low protein recovery. In particular, the limited recovery of the IgG adsorbed on A2P-membranes and HPTA-membranes was not only due to the strong binding between protein and ligands, but also to an irreversible

binding on the 2LP spacer, since it was not possible to recover any protein adsorbed on 2LP-membranes using the standard elution protocol.

Finally, batch tests and dynamic experiments were performed to determine the binding capacity, the selectivity and the recovery with respect to IgG of affinity A2P and HPTA membranes.

HPTA-membranes showed binding capacities comparable to those exhibited by the supports modified with A2P ligand. No excessive reduction of the maximum binding capacity during consecutive affinity cycles was measured for the two ligands, suggesting that ligand leakage was not an issue. On the other hand, the values of recovery that were measured were always higher for HPTA with respect of A2P, indicating its superiority concerning this aspect. However, even for this new ligand the elution capacities could still be improved: the recovery decreased from ~75% measured with a pure IgG solution, to 59% calculated with a mixture of IgG and lysozyme, to 33% determined with a mixture of IgG and BSA.

In fact, the presence of bovine serum albumin appeared to be a critical issue for the purification of antibodies both for HPTA- and A2P-membranes. It was observed that BSA could bind substantially to the affinity supports, while at the same time the amount of bound and eluted immunoglobulin decreased, resulting in an important loss of efficiency of the separation process. This aspect was clearly confirmed by the results of batch experiments carried out using HPTA-membranes and human serum solutions; among all the contaminant proteins present in the serum, BSA was the only one detected by SDS-PAGE analysis in the elution samples of the chromatographic cycles.

A more effective elution was the only great difference pointed out between HPTA- and A2P-membranes. However, while A2P was already characterized by many other authors who coupled it with different spacer arms and chromatographic supports, almost always with very poor results, the same cannot be said regarding HPTA ligand. This new affinity ligand was tested in the present work for the first time, coupled with a benchmark spacer arm, 2LP, and with a commercial support, Sartobind® Epoxy membranes. The present study had the aim of obtaining important information for understanding what aspects should be changed to improve the functionalized membranes.

More specifically, future research should consider the replacement of 2LP with a different spacer arm, to better understand the influence that HPTA ligand has on non-specific binding of impurities and elution performances.

A complete dynamic characterization has to be performed to determine the dynamic binding capacity of this new ligand, using pure solutions of IgG and more complex solutions, such as mock mixtures containing IgG, human serum or cell culture supernatants.

In the last chapter of the first part of this work a simple model for the prediction of breakthrough curves in membrane chromatography systems was presented and discussed. The model vas validated using a rigorous mathematical model developed in a previous work. The comparison of the two models confirmed that the use of the simple model was sufficient for the prediction of breakthrough curves without the need of a great computational capacity. In particular, it was demonstrated that:1) the axial dispersion coefficient is the only parameter needed for the prediction of breakthrough curves and, since it is a property of the porous medium, it can be easily determined in independent dynamic experiments; 2) the model based on the hypothesis of polydispersed membranes is not efficient and leads to incomplete and misleading mathematical theories.

# PART II


# Ceramic Monoliths Chromatography

# CHAPTER 7

# Monoliths design and characterization

## 7.1 Introduction

The second part of this PhD thesis begins with the description of the design and characterization of cellular ceramic monoliths to be used as stationary phase for chromatographic processes. This interesting aspect of the work was done in Portugal, during a research period abroad, at Universidade de Aveiro under the supervision of Dr. Andrei Kovalevsky.

## 7.2 Design of $Al_2TiO_5$-$Al_2O_3$ cellular ceramic monoliths

### *7.2.1 $Al_2TiO_5$ properties and applications*

High melting point and excellent thermal shock resistance, provided by rare combination of low thermal conductivity, thermal expansion and Young´s modulus, render aluminium titanate ($Al_2TiO_5$) attractive for many technological applications as a thermal insulating material [1-4]. Ceramics based on $Al_2TiO_5$ possess poor wettability and good erosion resistance in contact with molten metals, making them appropriate for use in foundry technology and metallurgical melting [3-5]. Very recently, $Al_2TiO_5$ was found to improve the average efficiency of planar perovskite solar cells [6]. Due to high refractoriness, shock and corrosion resistance, aluminium titanate ceramics was also proposed for filtration and separation applications including soot traps for diesel engines, filters for hot gas clean-up systems [3-7] and even for water purification [8, 9]. These applications require flexible design of highly porous materials with controlled microstructures, as pointed out in the relevant literature [10].

However, severe limitations on potential applications are imposed by strong anisotropy of the crystal lattice expansion, which, although resulting in attractively low thermal expansion, also promotes the formation of microcracks and general decrease of the mechanical strength [1, 7, 11, 12]. Another challenge in processing of these materials is related to the fact that $Al_2TiO_5$ is thermodynamic stable only at high temperatures, often requiring high temperature reactive firing

for microstructural control [8] or reactive sintering to seek densification [13]. Consequently, there is a need in effective strategies to induce meta-stabilization on cooling, preventing structural instability of $Al_2TiO_5$ ceramics at temperatures below ~1553 K [1, 2, 7, 14, 15] this may lead to decomposition to denser rutile and corundum phases, also contributing to microcracking. Several known approaches to tackle these issues include various substitutions to suppress the structural effects and grain growth [2, 7, 13, 16-20], and implementation of composite concepts for microstructural engineering [7, 21-24].

Thus, rational design of $Al_2TiO_5$ ceramics for filtration and separation applications requires both optimization of the processing conditions to minimize negative effects of the highly-anisotropic expansion and phase decomposition, and flexible tuning of the porous structure to counter significant pressure drops and to provide the desired functionalities. From an economical viewpoint, reactive firing directly from the oxide precursors appears to be a suitable method and was already applied for the preparation of $Al_2TiO_5$ ceramics [8, 13, 17, 25, 26]. On the contrary, literature on processing the porous $Al_2TiO_5$ ceramics is scarce [8, 27, 28], and none of these references dealt with designing the porosity with specific pore shapes, sizes and pore interconnectivity.

The present work takes the advantages of a recently developed processing method for preparation of porous cellular ceramics through emulsification of ceramic suspensions [29-32]; Taguchi experimental design [33, 34] was used to assess the effects of firing conditions on phase composition and to obtain some guidelines for the microstructural evolution in $Al_2TiO_5$ and $Al_2TiO_5$-$Al_2O_3$ composite ceramic monoliths. The firing procedure was based on a two-step firing method [35, 36], relying on activation of reactive firing by heating to the highest temperature without dwell time, and subsequent dwell at a lower temperature to increase the conversion and promote ceramic consolidation without undue grain growth and/or loss of the deigned porosity. Suppressing the grain growth was pointed out as particularly important for preventing microcracking of aluminium titanate ceramics [7, 13, 17, 18, 23].

The guidelines for porosity design have an emphasis on potential catalytic and separation applications, including chromatographic systems [37]. Indeed, there is a growing interest in the development of new stationary phases for chromatography such as monolithic supports, due to their structure and convective flow properties that are promising for bioseparations [38].

### 7.2.2 Preparation of the cellular ceramic monoliths

Cellular $Al_2TiO_5$ and $Al_2TiO_5/TiO_2/Al_2O_3$ composite monoliths were prepared through suspension emulsification and reactive ceramic consolidation, using a combined methodology

derived from those applied in recent works [29-31] for the preparation of alumina based ceramics with designed porosity.

Titanium oxide (TiO$_2$, Anatase) was purchased from Sigma Aldrich and aluminium oxide (Al$_2$O$_3$) (Alcoa CT3000) were used as precursor powders for material preparation. The precursor were mixed in nominal titania:alumina molar ratios $r$ = 1:1, 0.5:1 and 0.25:1. Anatase precursor readily transforms to rutile already at 850-900 K [39]. Thus, for further discussion rutile is assumed as the main titania phase reacting with alumina.

The resulting precursor mixtures were used to prepare aqueous suspensions with 50% v/v solids loading, and Dolapix PC-67, purchased from Zschimmer&Schwarz, was added as a dispersion agent to stabilize the suspensions of mixed precursors, in the amount equal to the 10% v/v of the total volume of suspension prepared. The suspensions were mixed at 1300 rpm for 40-60 minutes, until they became smooth.

Liquid paraffin (Vencilab) was then used as an organic phase for oil in water emulsification of the powder suspension. Various paraffin:suspension volume ratios were accessed (1.5:1, 1:1 and 0.6:1). Table 1 lists the chemical compositions of solid loads and corresponding organic phase to suspension volume ratios used.

A solution of sodium lauryl sulfate (Sigma-Aldrich L-6026) with a concentration of 1 mg/mL was added in the amount equal to 6% v/v of the volume of the emulsion and was used as emulsifier; collagen (Oxoid LP0008) in proportions of 5% relative to water volume in the emulsion, was added for subsequent shape-stabilization on casting. The emulsions were stirred at 1000 rpm for 10 min at 348 K, and then casted inside containers of the appropriate shape, previously lubricated with grease to easily remove the monolith once dried.

It is very important not to stir the emulsion for more than 10 minutes, otherwise the aqueous and organic phase will separate and it will not be possible to emulsify the suspension anymore.

The green monoliths were dried at room temperature for 48 h and then in the oven at 341 K for 48 h, to prepare them for the subsequent thermal treatments, performed using specific high temperature furnaces.

The consolidated and dried monoliths were subjected to a preliminary heat treatment, called *burnout*, needed to eliminate the organic phase under delicate conditions, avoiding fast evolution of burnout gases and disintegration of the samples. This was performed by heating up to 573 K at a rate of 1 K/min, followed by a 3 h dwell, and further heating up to 773 K at 1 K/min, with a second dwell for 1 h, and final cooling down to room temperature at 10 K/min.

The second and final important thermal treatment is the *sintering* step, also called *firing*. Conventional firing, with a single isothermal plateau was found ill-suited to attain high

conversion of the oxide precursors to $Al_2TiO_5$ while retaining crack-free cellular microstructures, as demonstrated in Fig. 7.1.

**Table 7.1**  Chemical composition of ceramic suspensions and liquid paraffin/suspension volume ratio, used for the preparation of various samples sets for implementation of the Taguchi planning. The correlation matrix for the effects of firing parameters on weight fraction of $TiO_2$ and porosity of the monoliths is also shown.

| Samples set | r* | p** | Correlation matrix | | | |
|---|---|---|---|---|---|---|
| | | | Parameter | $T_{peak}$ | $T_{iso}$ | $t_{iso}$ |
| 1 | 1.0:1.0 | 1.5 | $x(TiO_2)$, %wt. | -0.327 | -0.327 | 0.302 |
| | | | porosity | -0.238 | 0.087 | 0.567 |
| 2 | 0.5:1.0 | 1.5 | $x(TiO_2)$, %wt. | -0.639 | -0.365 | -0.120 |
| | | | porosity | -0.345 | -0.769 | 0.022 |
| 3 | 0.5:1.0 | 1.0 | $x(TiO_2)$, %wt. | -0.399 | -0.399 | -0.435 |
| | | | porosity | -0.025 | -0.331 | 0.607 |
| 4 | 0.5:1.0 | 0.6 | $x(TiO_2)$, %wt. | -0.352 | -0.282 | -0.677 |
| | | | porosity | 0.230 | -0.166 | -0.088 |
| 5 | 0.25:1.0 | 1.5 | $x(TiO_2)$, %wt. | 0.218 | -0.436 | -0.571 |
| | | | porosity | 0.192 | 0.247 | -0.235 |

\* r = titania/alumina molar ratio

\*\* p = liquid paraffin/suspension volume ratio

Note that a sudden loss of the cellular microstructures occurs on raising the isothermal plateau from 1673 K to 1723 K, suggesting very strong dependence of microstructural changes on temperature of reactive firing. It is noteworthy that microstructures similar to that shown in Fig. 7.1C were previously pointed out in other works [40,41] and attributed to significant difference between the treatment and recrystallization temperatures.

Thus, non-conventional 2-step firing procedures were designed with relatively fast heating to a peak temperature, to trigger the reactivity, and then immediately dropping the temperature to a lower temperature plateau to increase the fraction reacted and to attain ceramic bonding while retaining the cellular microstructures.
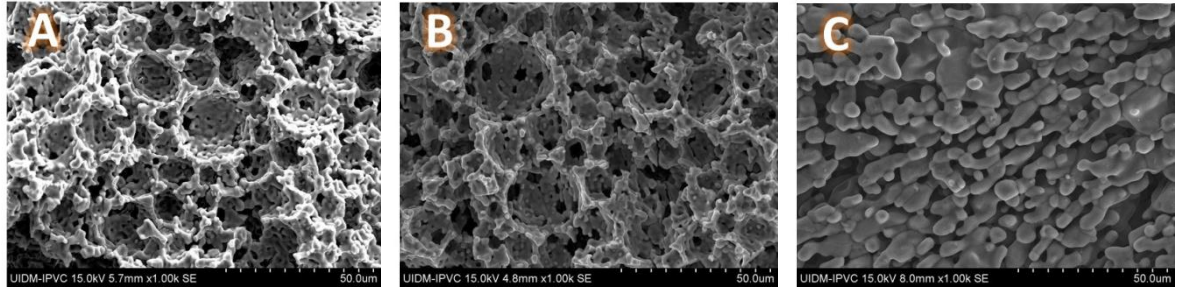
**Figure 7.1** SEM microstructures of $Al_2TiO_5$ samples with nominal stoichiometric composition (p=1.5) obtained by conventional firing at 1673 K (A,B) and 1723 K (C) for 2 h, with relatively fast cooling (20 K/min, A,C) or quenching (B).

### 7.2.3 Taguchi experimental design and analytical techniques

A Taguchi plan was implemented to assess the impact of two-step firing conditions on phase composition, porosity and other microstructural features. The method involved three variable parameters, namely, peak temperature ($T_{peak}$), isothermal treatment temperature ($T_{iso}$) and time ($t_{iso}$), with three levels for each variable, as shown in Fig. 7.2.
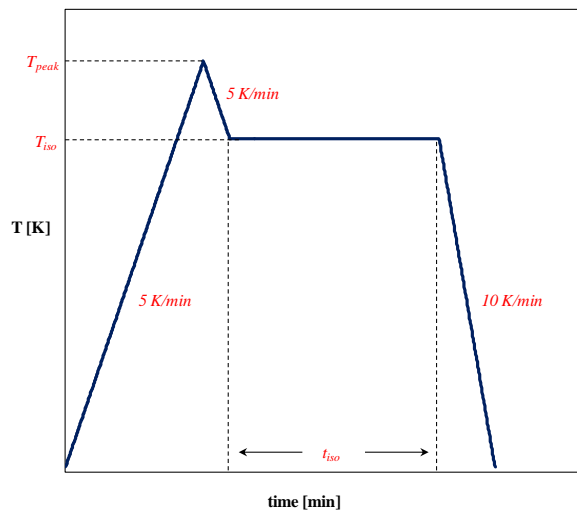


**Figure 7.2** Qualitative diagram of the two-step thermal treatment used as sintering procedure.

Although some minor effects depending on the cooling rate from $T_{peak}$ to $T_{iso}$ on the phase composition and density may still be expected, this parameter was not considered for the Taguchi experimental plan; the cooling rate was kept constant and equal to 5 K/min in all experiments, to avoid an excessive number of experiments and to avoid to increase the complexity in the interpretation of the correlations among different parameters.

Phase composition of the fired monoliths was studied by XRD, x-ray diffraction, using the instrument Bruker D8 Advance Da Vinci, in the rang $2\theta = 10-80°$; the analysis were

performed after crushing the samples to powder using a mortar. The software Panalytical HighScore Plus 4.1 (PDF-4) was used for data elaboration to obtain quantitative results from this analysis; the reference intensity ratio (RIR) method was used [42] and corundum was set as reference standard.

Factorial design was employed to reduce the number of experiments. An L9 orthogonal array of the experiments (Table 7.2) was chosen to assess the effects of the firing parameters on two distinct properties, namely, the residual weight fraction of titanium dioxide $x_t$ and porosity of the fired ceramics.

**Table 7.2**    An example of L9 orthogonal array of the samples with initial $r = 0.5:1.0$, prepared using 1.5:1.0 p = 1.5:1.0 (set 2 in the Table 1), and Taguchi plan for effects of the firing paramters on the final phase composition, namely, weight fractions of titania ($x_t$) and aluminium titanate ($x_{at}$), porosity volume fraction ($y$) and density ($\rho$).

| Experiment | $T_{peak}$ [K] | $T_{iso}$ [K] | $t_{iso}$ [h] | $x_{at}$ [%wt] | $x_t$ [%wt] | $\varepsilon$ | $\rho$ [g/cm$^3$] |
|---|---|---|---|---|---|---|---|
| E1 | 1873 | 1673 | 4 | 62.0 | 0.0 | 0.558 | 1.18 |
| E2 | 1873 | 1623 | 2 | 59.0 | 2.0 | 0.568 | 1.25 |
| E3 | 1873 | 1573 | 8 | 53.0 | 1.0 | 0.581 | 1.27 |
| E4 | 1823 | 1673 | 2 | 64.0 | 0.0 | 0.565 | 1.12 |
| E5 | 1823 | 1623 | 8 | 65.0 | 1.0 | 0.563 | 1.20 |
| E6 | 1823 | 1573 | 4 | 65.0 | 1.0 | 0.589 | 1.17 |
| E7 | 1773 | 1673 | 8 | 63.0 | 3.0 | 0.576 | 1.21 |
| E8 | 1773 | 1623 | 4 | 61.0 | 2.0 | 0.571 | 1.19 |
| E9 | 1773 | 1573 | 2 | 50.0 | 5.0 | 0.586 | 1.16 |

The estimated values of the fraction of the two precursors reacted were derived from the results of XRD quantitative analysis, assuming ideal stoichiometry for the overall reaction:

$$rTiO_2 + Al_2O_3 \rightarrow zAl_2TiO_5 + (1-z)Al_2O_3 + (r-z)TiO_2 \qquad (7.1)$$
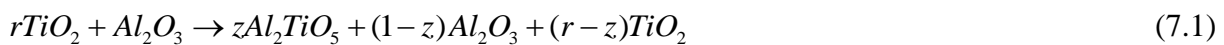
Since 1 mole of alumina was taken as a basis of calculations, one may deduce the relevant relation between the fraction of reacted $TiO_2$ ($z$), the measured weight fractions of titania ($x_t$) and aluminium titanate ($x_{at}$), and molecular weights of aluminium titanate ($M_{at}$), titania ($M_t$) and alumina ($M_a$):

$$\frac{z}{r} = \frac{x_{at}M_t}{x_t M_{at} + x_{at}M_t} \qquad (7.2)$$

In addition, the reacted fraction $z/r$ allowed to re-estimate the ideal molar ratios $z:(1-z):(r-z)$ of aluminium titanate: alumina: titania in the resulting ceramics, and to recalculate the corresponding ideal weight fraction of alumina ($\varphi_a$), as follows:

$$\varphi_a = \frac{(1-z)M_a}{zM_{al} + (1-z)M_a + (r-z)M_t} \qquad (7.3)$$

This ideal fraction was based on the assumption of ideal stoichiometry for $Al_2TiO_5$, and by neglecting mutual solubility of alumina in the rutile phase and of titania in corundum. Thus, the predictions for ideal stoichiometry $\varphi_a$ may differ significantly from the nominal fraction obtained by combining the measured fractions of the aluminium titanate and residual titania.

$$x_a = 1 - x_{at} - x_t \qquad (7.4)$$

The second property dependent on processing conditions evaluated in Taguchi planning was the density ($\rho$) or the corresponding void fraction ($\varepsilon$) of fired cellular monoliths; these parameters were assessed by the Archimedes method, based on a combination of weight measurements of the dried sample ($wt_1$), water impregnated sample ($wt_2$) and sample immersed in water ($wt_3$), as follows:

$$\varepsilon = \frac{wt_2 - wt_1}{wt_2 - wt_3} \qquad (7.5)$$

$$\rho = \frac{wt_1}{wt_2 - wt_3}\rho_w \qquad (7.6)$$

where $\rho_w$ is the density of water. Note that though density differences are expected to be mainly related to the pore-forming contribution of paraffin, this may also be substantially changed by microstructural changes occurring on firing, as illustrated in Fig.7.1, and also quantified in Table 7.2.

Both fractured fired and green samples were characterized by scanning electron microscopy, using the instrument SEM - Hitachi SU-70 to inspect relevant microstructural features and their evolution depending on the processing conditions. Complementary EDS analyses were performed for the same samples using Bruker Quantax 400 detector, to confirm the phase composition and assess the distribution of various phases.

### *7.2.4 Results of the experimental design*

The formation of a well defined cellular ceramic structure was verified by SEM/EDS analysis of the green monoliths, that are the samples after suspension emulsification, drying and burnout of the organic phase; some representative examples are shown in Fig. 7.3.
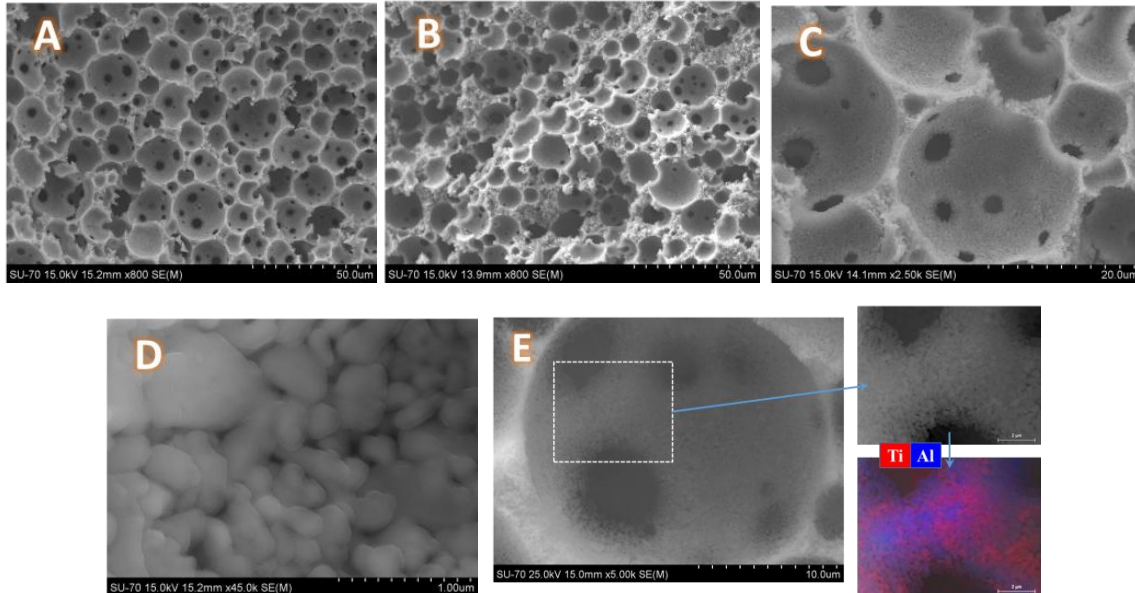


**Figure 7.3**    SEM micrographs of the green fractured samples after removing the organic phase: $r$=0.5, $p$=1.5 (A); $r$=0.5, $p$=0.6 (B); $r$=0.25, $p$=1.5 (C); $r$=0.5, $p$=1.5 (D,E) and EDS mapping results for selected area of the sample (E).

A moderate decrease in the cavity size and formation of thicker cell walls are notable for the samples prepared from emulsified suspensions with lower paraffin contents (Fig. 3A,B), in agreement with the results previously observed for $Al_2O_3$-based cellular ceramics [30, 32]. Most cells are well-interconnected by multiple windows, Fig. 7.3C, highly desirable for applications requiring significant liquid or gas transport fluxes through porous ceramics. The precursor powders develop tight necking after burning out the dispersed organic phase, Fig. 7.3D, forming the intended cellular skeleton, and EDS mapping at high resolutions in various local areas, Fig. 7.3E, demonstrate homogeneous distribution of the $Al_2O_3$ and $TiO_2$ components. In general, these results for green samples provide clear evidence that the described processing method allows the formation of desired porous frameworks, and is highly flexible for emulsification-based processing with various organic phase:suspension volume ratio, and for different $TiO_2$:$Al_2O_3$ reactants ratios. Cell sizes and their interconnections can be tuned by proper selection of the suspension/emulsion processing parameters, in a similar way with previous processing of cellular $Al_2O_3$ ceramics [29, 30, 32]; this flexibility allowed optimization of

cellular ceramics by Taguchi planning and, most likely, this is also the case for the actual materials processed by reactive firing.

However, preliminary experiments showed that the complex dynamics of reactive firing of $Al_2TiO_5$ imposes difficulties to flexible microstructural design under classical firing cycles (Fig. 7.1), and also risks of phase instability on cooling below 1173-1553 K [1, 2, 7, 14], or collapse of cellular microstructures, due to wall cracking. Thus, non-conventional firing conditions was used to design the porosity of $Al_2TiO_5$-based monoliths, in addition to the expected prevailing effect of paraffin contents, acting as pore former. Note that the correlation factor between porosity and the paraffin to suspension ratio for all samples (R=0.883) exceeds the corresponding correlation matrixes for the effects of processing parameters on individual sets (Table 7.1). The firing conditions within every set of samples are listed in Table 7.2 and the corresponding results are also shown for each of those sets.
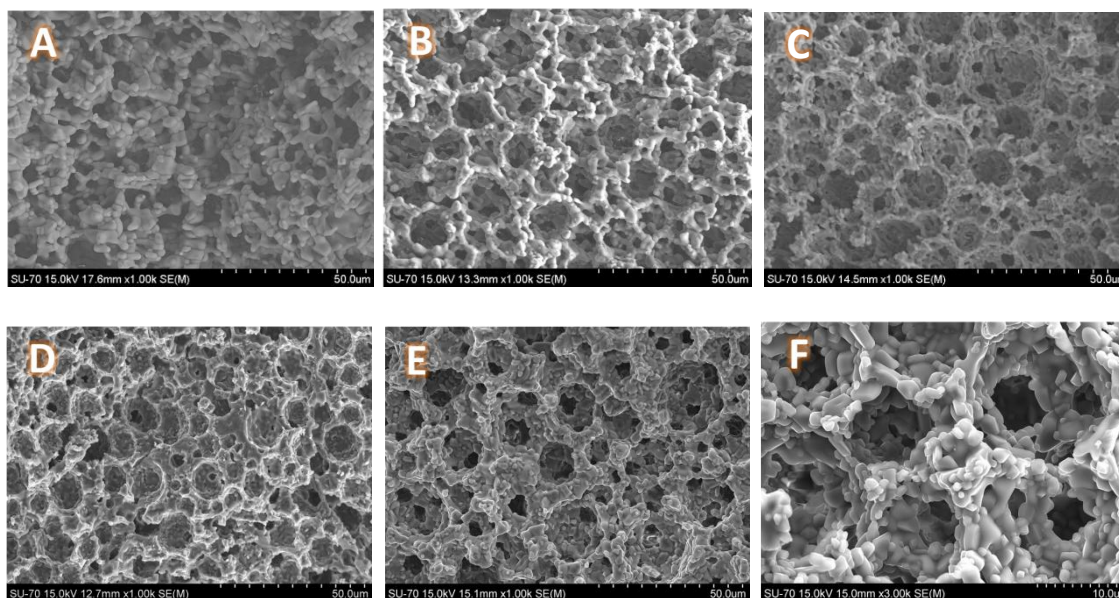


**Figure 7.4**   SEM micrographs of the fractured monoliths after firing: *r*=1.0, *p*=1.5, E5 (A); *r*=0.5, *p*=1.5, E6 (B); *r*=0.5, *p*=1.5, E5 (C); *r*=0.5, *p*=0.6, E9 (D); *r*=0.25, *p*=1.5, E2 (E); *r*=0.25, *p*=1.5, E5 (F).

Fig. 7.4 shows typical microstructures of the cellular monoliths after firing under various conditions. Stable cellular porous microstructures were obtained mainly in the cases of composite materials, containing nominal $Al_2O_3$ excess, as shown in Fig. 7.4B,F, whereas samples with nominal stoichiometric ratio $TiO_2:Al_2O_3$=1:1 (*r*=1.0) showed porosity with irregular shape and size, see Fig. 7.4A. These samples were also mechanically weak and readily disintegrate on handling. In fact, low mechanical strength is a known disadvantage of $Al_2TiO_5$ materials, usually ascribed to microcracking on cooling from firing temperatures, due to highly-anisotropic thermal expansion of the crystal lattice [1, 7, 11, 12]. Failure has also be related to

eutectoid decomposition of $Al_2TiO_5$ to rutile and corundum at temperatures below ~1553 K [1, 2, 7, 14].

In addition, other authors indicated that titania might dissolve significant fractions of alumina and showed evidence that microstructural defects may be present in contact with residual rutile phase [43]. Thus, one may consider the correlation matrix between residual fraction of rutile and processing parameters (Table 7.1) as a guideline for optimization, by seeking complete conversion. Still, correlation factors for individual sets of samples (Table 7.1) remain also inferior to the overall correlation between the residual fraction of $TiO_2$ and reactants ratio $r=TiO_2/Al_2O_3$ for all the samples (R=0.790).

XRD studies of the fired samples with stoichiometric $TiO_2:Al_2O_3=1:1$ ratio confirm the presence of noticeable amounts of $TiO_2$ and $Al_2O_3$, as demonstrated by Fig. 7.5A.
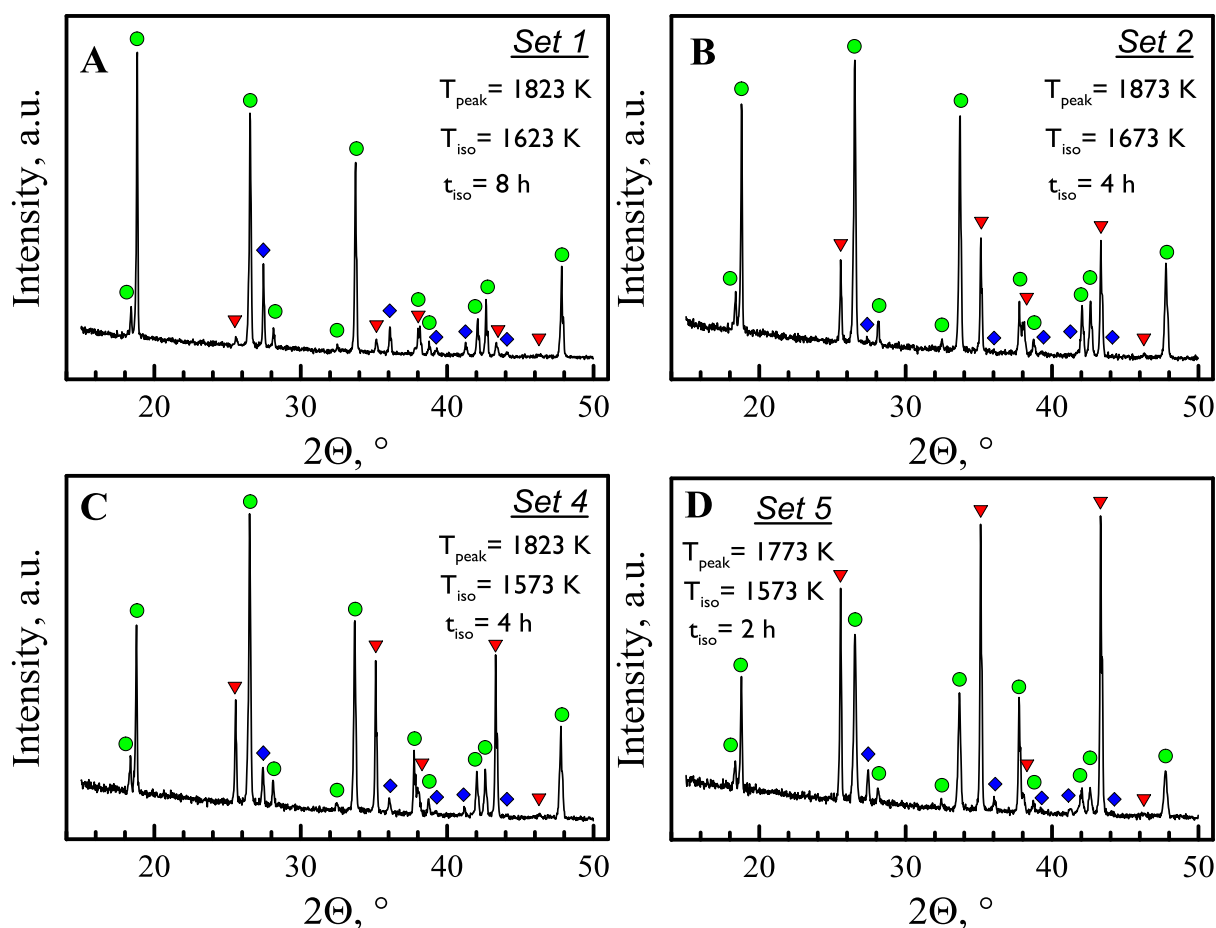


**Figure 7.5** XRD patterns of the powdered monoliths samples after firing using a Taguchi planning: r=1.0, *p*=1.5, E5 (A); r=0.5, *p*=1.5, E1 (B); r=0.5, *p*=0.6, E6 (C); r=0.25, *p*=1.5, E9 (D). Green circles, red triangles and blue diamonds denote $Al_2TiO_5$, $Al_2O_3$ and $TiO_2$ phases, respectively.

The distribution of $TiO_2$ and $Al_2O_3$ phases in stoichiometric *r*=1.0 was additionally analysed by EDS mapping, the results are shown in Fig. 7.6A,B.

Although the capabilities of the EDS analysis for the samples possessing significant topography, as in the case of the samples under investigation, are limited due to shielding effects, the results are informative enough to confirm random distribution of unreacted inclusions with sizes $\geq 2$ μm, which is about one order of magnitude larger than the size of precursor´s agglomerates, as indicated by EDS in the bottom inset of Fig. 7.3E.
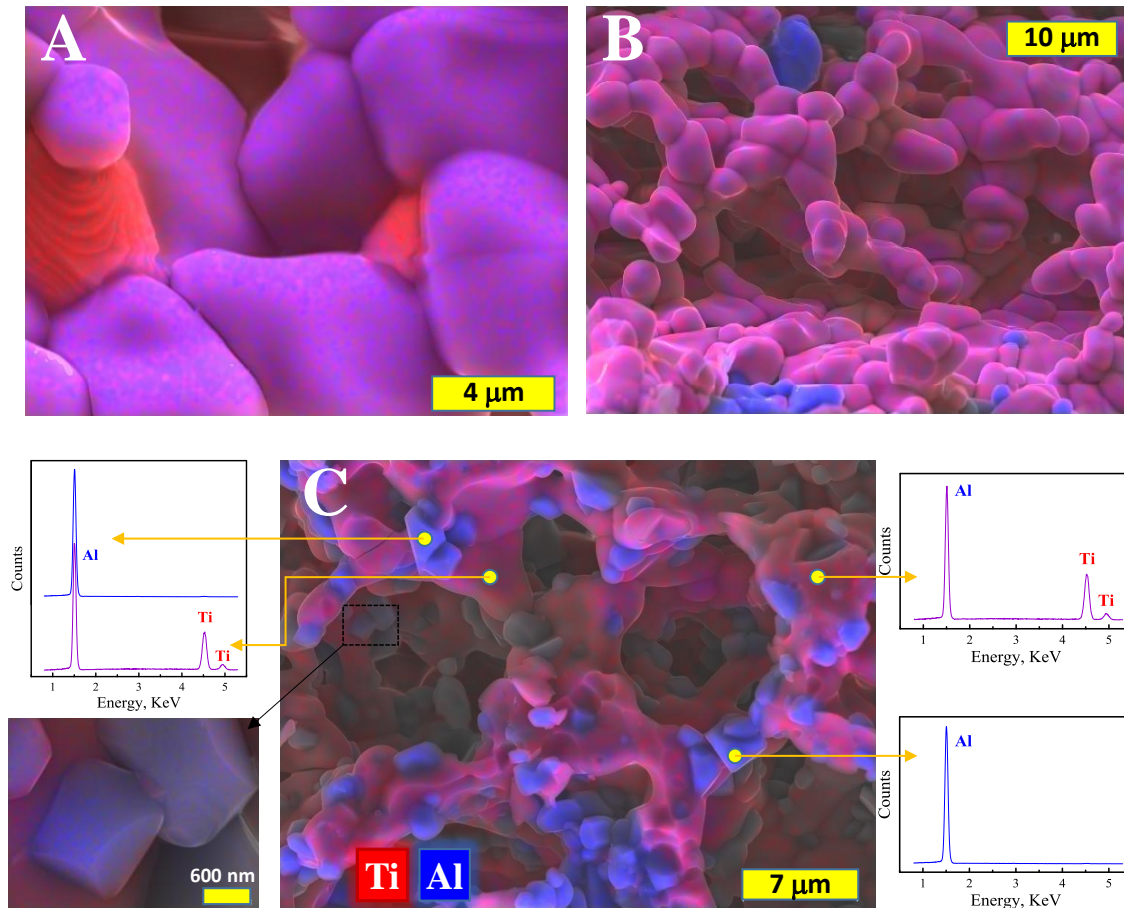


**Figure 7.6**   EDS mapping results of the fractured fired monoliths: $r$=1.0, $p$=1.5, E4 (A,B) and $r$=0.5, $p$=1.5, E5 (C). The insets for image (C) show corresponding EDS spectra in selected points and EDS mapping of the selected area of a cavity interior at high magnification.

Thus, incomplete reaction is revealed by $Al_2O_3$ and $TiO_2$ inclusions, mostly tightly bonded to the aluminium titanate matrix, but also undergoing coarsening, and tendency for clustering of $Al_2O_3$ inclusions during reactive firing. Moreover it might not be possible to detect close proximity between Ti-rich and Al-rich inclusions, which should be expected by decomposition of the aluminium titanate matrix. Therefore, it was assumed that the residual reactants are mostly due to incomplete reaction. As an example, the work of Singh *et al*. suggests that the size of alumina precursor powder may have a noticeable effect on the phase evolution of aluminium titanate [44]. In addition, it was not possible to detect any close relation between microcracks and those

inclusions, indicating that undue changes in cellular microstructures and collapse of cell walls is due to the complex dynamics of reactive firing [25, 43].

Another contribution to local strain may be provided by the overall expansion on converting the reactants particles to $Al_2TiO_5$, or contraction upon its decomposition on cooling, as the $Al_2TiO_5$ density (3.7 $g/cm^3$) is significantly lower than that of equimolar $Al_2O_3/TiO_2$ mixture (4.1 $g/cm^3$) [13]. Still, the relatively low elastic modulus of highly porous cellular ceramics contributes to enhance their tolerance to relatively high strain. Thus, risks of collapse were found mainly for the nominal stoichiometric ratio (i.e. $r$=1.0), which leads to almost complete conversion to $Al_2TiO_5$, and is also more likely to undergo undue evolution of the intended cellular microstructures. On the contrary, the formation of an appropriate cellular framework was successful for most composite samples, both for $r$=0.5 and 0.25 nominal $TiO_2$ to $Al_2O_3$ molar ratios, as evidenced by SEM results, Fig. 7.4(B,F). For the same initial chemical composition, the interconnection between pores and wall thickness vary depending on the firing conditions. The cellular structure becomes better distinguishable when shifting from $r$=0.5 to 0.25, as expected on diminishing the $Al_2TiO_5$ phase. Thus, the observed behaviour can be attributed a combination of expected effects of excess of alumina, namely: i) impact on the ability to retain highly porous cellular microstructures (Fig.7.4), with lower rigidity and ability to sustain significant strain; ii) the contribution of $Al_2O_3$ to toughening of $Al_2O_3$-$Al_2TiO_5$ ceramics [19], by suitable mechanisms such as crack bridging or crack path deflection mechanisms [21, 45]; iii) its contribution to seek nearly complete conversion of the residual fraction of rutile, which may cause undue microstructural changes [43]. Fig. 7.7 demonstrates the ability to suppress the residual content of rutile by the use of an excess of alumina, for identical firing cycles (Table 7.2).

The observed differences between closed and open symbols in Fig. 7.7 may indicate deviations from nominal stoichiometry.

For example, defect chemistry modelling predicted possibilities for titania excess in Al-sites $(Al_{2-4x-2\delta}Ti_{3x+2\delta})TiO_{5+\delta}$, with mixed charge compensation by cation vacancies and interstitial oxygen ions [46]; this is also consistent with results reported by other groups [43]. Thus, the residual fraction of the alumina phase ($x_a$) should remain higher than for the corresponding conversion of titania with ideal stoichiometry, i.e. $x_a > \varphi_a$, except possibly for conditions when the aluminium titanate might be exposed to reducing atmospheres, inducing partial reduction to $Ti^{3+}$ and its incorporation in $A^{3+}$ sites [47]. Nevertheless, the actual results in Fig. 7.7 suggest that this only occurs for relatively high conversion of titania, i.e., when its residual fraction is relatively low. On the contrary, results for higher residual fractions of titania indicate that the

residual contents of alumina still remains lower than predicted by the mass balance for ideal stoichiometry. A plausible explanation for this difference may rely on a non-negligible solubility of alumina in the rutile phase, as already emphasized [43].
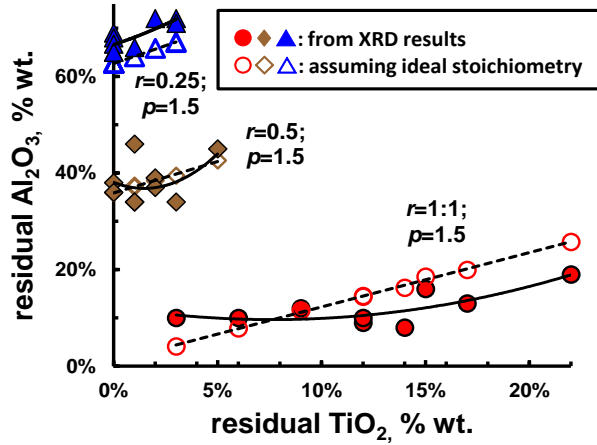


**Figure 7.7**    Interdependence of residual contents of the corundum and rutile phases for different combinations of reactants ratio ($r$=1.0, 0.5, 0.25) and paraffin to suspension ratio ($p$=1.5, 1.0). Closed symbols were obtained from combined experimental XRD results, taking into account that sum of weight fractions of $Al_2O_3$, $TiO_2$ and $Al_2TiO_3$ correspond to 100%. Open symbols are the corresponding predictions on assuming ideal stoichiometry (Eq. 7.3).

Microstructural features and phase compositions are also dependent on a complex combination of processing parameters, from emulsification to firing schedules, as emphasized by differences in porosity and contents of aluminium titanate, as shown in Fig. 7.8. The main effect on porosity is, indeed, exerted by the pore forming ability of paraffin droplets in the emulsified suspensions ($p$), whereas the reactants ratio ($r$) is the main factor governing $Al_2TiO_5$ formation. Thus, the upper limits for design of porosity $\varepsilon_{\lim}$ and contents of $Al_2TiO_5$ $x_{at,\lim}$ (open symbols at the end of pointing arrows) were computed on combining the initial volume of paraffin and the corresponding volumes of solid phases, assuming complete conversion of titania:

$$\varepsilon_{\lim} = \frac{\left(\dfrac{p}{1-x_{sl}}\right)\left[\left(\dfrac{M_a}{\rho_a}\right)+r\left(\dfrac{M_t}{\rho_t}\right)\right]}{\left(\dfrac{p}{1-x_{sl}}\right)\left[\left(\dfrac{M_a}{\rho_a}\right)+r\left(\dfrac{M_t}{\rho_t}\right)\right]+r\left(\dfrac{M_{at}}{\rho_{at}}\right)+(1-r)\left(\dfrac{M_a}{\rho_a}\right)} \tag{7.7}$$

$$x_{at,\lim} = \frac{M_{at}r}{M_{at}r+(1-r)M_a} \tag{7.8}$$

where $x_{sl}$ denotes the solid load in the precursors suspension, $\rho_a$, $\rho_t$ and $\rho_{at}$ are the phase densities of alumina (corundum), titania (anatase) and aluminium titanate, respectively.
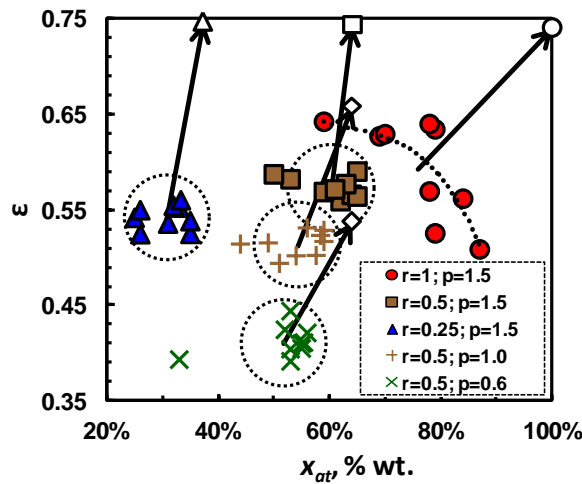
**Figure 7.8**   Porosity and $Al_2TiO_5$ content for different sets of cellular materials prepared with paraffin to suspension ratio ($p$=1.5, 1.0, 0.6) and reactants ratio ($r$=1.0, 0.5, 0.25). Open symbols show the corresponding upper limits for porosity $\varepsilon_{lim}$ and aluminium titanate content $x_{at,lim}$ (Eqs. 7.7 and 7.8).

All samples sets in Fig. 7.8 show significant gaps between the actual results and the corresponding upper limits (Eqs. 7.7 and 7.8) and significant spreading, mainly for samples with nominal stoichiometry ($r$=1). Though spreading may be mainly ascribed to the differences in firing conditions shown in Table 7.2, the correlation factors in Table 7.1 are somewhat low to clarify the prevailing factors. Some of these coefficient are also counter-intuitive, namely, for the samples which show positive dependence of residual fraction of titania or final porosity on $T_{peak}$, $T_{iso}$ or $t_{iso}$. These effects are analysed in more detail in Fig. 7.9, where $\varepsilon_{ij}$ or $x_{t,ij}$ denote averaged results for 3 experiments performed with factor $i$ at level $j$.
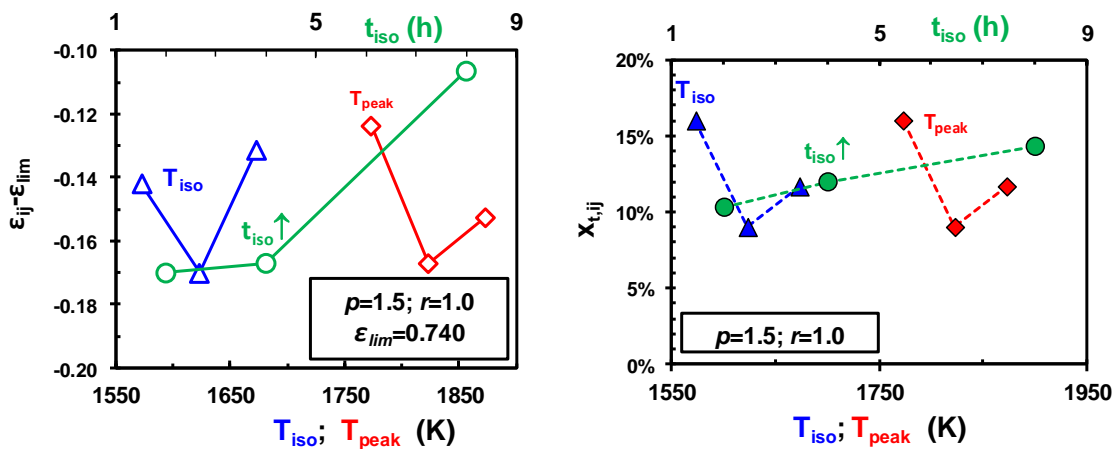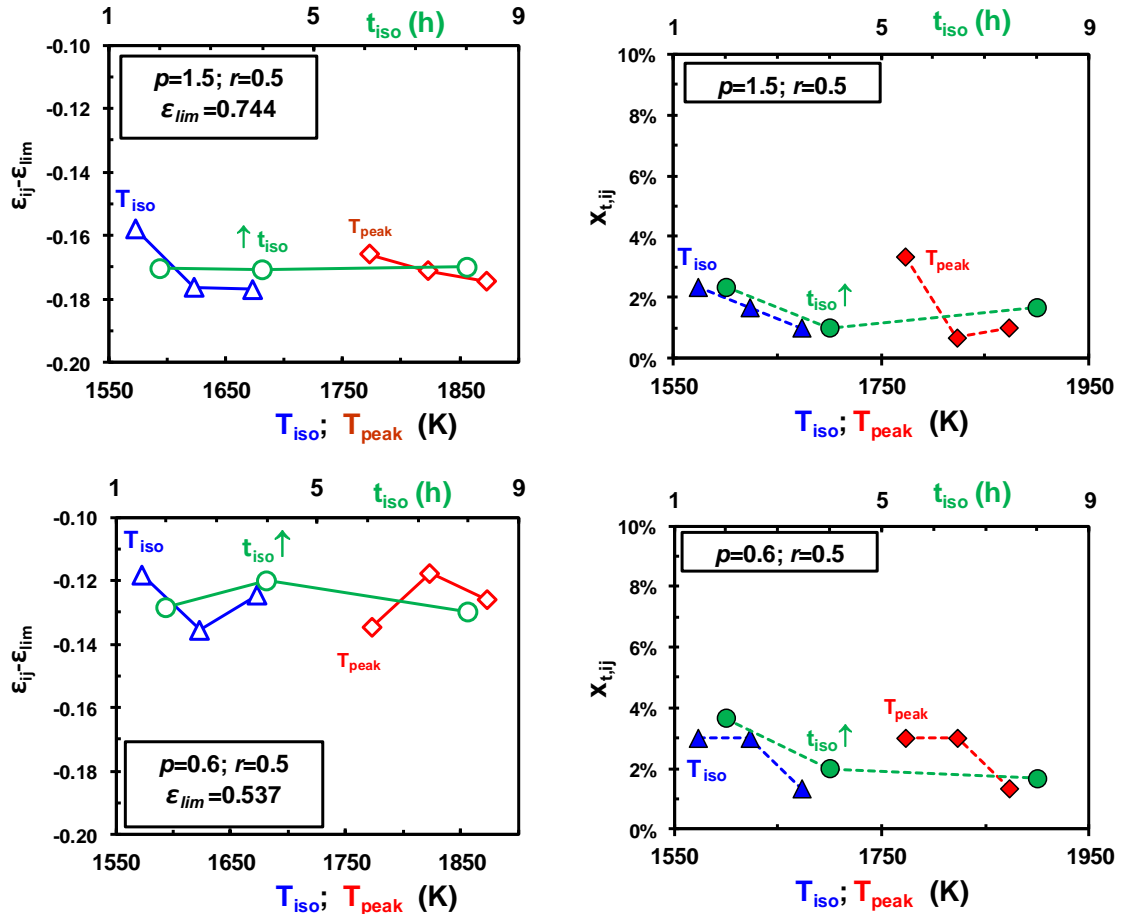
**Figure 7.9** Effects of firing parameters ($T_{peak}$, $T_{iso}$ and $t_{iso}$) on changes in porosity and content of residual titania $x_t$.

For example, $\varepsilon_{12}$ denotes the averaged porosity obtained for experiments E4, E5 and E6, corresponding to the first factor at its second level, i.e., $T_{peak}$=1823 K.

Fig. 7.9 shows that part of the unexpected trends suggested by the correlation matrix (Table 7.1) may be due to low signal to noise ratio, mainly for samples with stoichiometric composition; this is consistent with known difficulties in avoiding undue microstructural changes and their impact on mechanical failure. Composite compositions with lower titania:alumina ratio ($r<1$) show much lower changes on varying the firing conditions and, thus, greater ability to process materials with porosity and phase composition within narrow deviations from the designed characteristics. In addition, simultaneous changes in reactants ratio ($r$) and paraffin contents ($p$) allow greater flexibility in microstructural design, as found on comparing the results of porosity for samples ($p$=1.5; $r$=0.5) and ($p$=0.6; $r$=0.5).

### *7.2.4.1 Multivariate linear regression*

Multivariate linear regression was also performed to evaluate relevant coefficients for the effects of those firing parameters on residual fraction of titania ($x_t$), an porosity ($y$), as follows:

$$x_t = \alpha' T_{peak} + \beta' T_{iso} + \gamma' t_{iso} + \Theta' \qquad (7.9)$$

$$y = \alpha'' T_{peak} + \beta'' T_{iso} + \gamma'' t_{iso} + \Theta'' \qquad (7.10)$$

These coefficients for the relative effects of peak temperature, isothermal plateau temperature and time are shown in Tables 7.3 and 7.4, and provide further evidence for combined effects of reactants ratio, paraffin contents and firing conditions.

Coefficients for peak temperature and isothermal plateau temperature were multiplied by a factor of 100, to allow ready inspection of expected effects on increasing these temperatures by $\Delta T_{peak}$=100 K or $\Delta T_{iso}$=100 K, i.e., from their lowest to highest levels in the Taguchi plans.

**Table 7.3**    Multivariate linear regression coefficients for the effects of 2-step firing conditions on the residual fraction of titania in the fired cellular ceramics (Eq. 7.9)

| $r$ | $p$ | $\alpha' \times 10^2$ | $\beta' \times 10^2$ | $\gamma'$ | $\theta'$ | R |
|-----|-----|------|------|------|------|------|
| 1 | 1.5 | -0.043 | -0.043 | 0.0065 | 1.348 | 0.552 |
| 0.5 | 1.5 | -0.023 | -0.013 | -0.0007 | 0.562 | 0.746 |
| 0.25 | 1.5 | 0.007 | -0.013 | -0.0029 | 0.100 | 0.751 |
| 0.5 | 1 | -0.017 | -0.017 | -0.0030 | 0.522 | 0.712 |
| 0.5 | 0.6 | -0.017 | -0.013 | -0.0052 | 0.485 | 0.813 |

**Table 7.4**    Multivariate linear regression coefficients for the effects of 2-step firing conditions on porosity (Eq. 7.10)

| $r$ | $p$ | $\alpha'' \times 10^2$ | $\beta'' \times 10^2$ | $\gamma''$ | $\theta''$ | R |
|-----|-----|------|------|------|------|------|
| 1 | 1.5 | -0.029 | 0.011 | 0.0113 | 0.845 | 0.621 |
| 0.5 | 1.5 | -0.009 | -0.019 | 0.0001 | 0.833 | 0.843 |
| 0.25 | 1.5 | 0.006 | 0.007 | -0.0011 | 0.361 | 0.391 |
| 0.5 | 1 | -0.001 | -0.010 | 0.0029 | 0.642 | 0.692 |
| 0.5 | 0.6 | 0.009 | -0.006 | -0.0005 | 0.363 | 0.297 |

For example, $\alpha' \times 10^2$=-0.049 indicates that a change in residual content of titania of -4.9% wt. is attained on increasing the peak temperature from 1773 K to 1873 K ($\Delta T_{peak}$=100K), for samples with $p$=1.5 and $r$=1.0. Similarly, $\alpha'' \times 10^2$=-0.029 indicates the corresponding decrease in porosity

(-2.9 %). This confirms that the strongest effects of firing conditions are exerted on samples with nominal stoichiometry ($r$=1), including effects on residual fraction of unreacted titania (Table 7.3) and porosity (Table 7.4), in line with evidence of drastic microstructural changes occurring in small temperature intervals (Fig. 7.1), and its correlation with the reactivity.

These effects decrease in cellular composites ($Al_2TiO_5$-$Al_2O_3$), obtained by decreasing the reactants ratio. Actually, the effects of peak temperature may even be reverted if alumina becomes the prevailing phase in the final composites (for $r$=0.25); this may be ascribed to onset of a relatively stable $Al_2O_3$ skeleton at the earliest stage of firing, hindering subsequent microstructural rearrangement of reactants and their reactivity. This rigid skeleton may prevent the rearrangements required to accommodate volume changes in the cellular walls, and to sustain faster paths for the diffusion controlled process [25] with faster diffusion of aluminium cations in $TiO_2$ than in the reaction product $Al_2TiO_5$ itself [13]. Thus, these results are also consistent with evidence that risks of undue microstructural changes are related to the presence of residual titania, including its ability to dissolve significant fractions of alumina and to provide alternative diffusion mechanisms to overcome limitations of sluggish diffusion in aluminium titanate. The effects of $T_{peak}$ on reactivity and porosity also vary with paraffin contents, probably because this is the prevailing effect on porosity, with impact on rigidity of cellular materials and their ability to prevent undue microstructural rearrangements. The independent coefficients $\theta'$ and $\theta''$ in the dependence on firing conditions (Eqs. 7.9 and 7.10) confirm that paraffin content and reactants ratio still play the significant roles for effective design of cellular materials with controlled microstructures and phase composition.

The work related to the design of $Al_2TiO_5$-$Al_2O_3$ cellular ceramic monoliths is published in the paper *Flexible design of cellular $Al_2TiO_5$ and $Al_2TiO_5$-$Al_2O_3$ composite monoliths by reactive firing*, Materials and Design [48].

## 7.3 Fluid dynamic characterization

The designed cellular $Al_2TiO_5$-$Al_2O_3$ composite ceramics were characterized to assess their use as novel monolithic columns in affinity chromatographic processes. The interstitial porosity and the axial dispersion coefficient were experimentally determined using the moment analysis. Pressure drops through the monolithic columns were measured to determine the permeability of these new chromatographic media. Interesting results were also obtained from mercury intrusion porosimetry (MIP) analysis.

### *7.3.1 Moment analysis*

As already introduce in Chapter 2, the method of moments is a powerful tool to be used to determine important characteristics of the stationary phase. In particular it was used to measure the porosity and the axial dispersion coefficient of the cellular ceramic monoliths. The values of porosity obtained were also compared with the results of mercury porosimetry (see paragraph 7.3.3).

The moment analysis was performed by performing 10 and 50 µL pulse injections to three ceramic columns of different length, under non-binding conditions. Details related to the ceramic column used can be found in Table 7.5.

**Table 7.5**     Dimensions of the ceramic columns used for the moment analysis.

| | Samples | | |
|---|---|---|---|
| | **A** | **B** | **C** |
| **diameter [cm]** | 1.035 | 1.170 | 1.000 |
| **length [cm]** | 0.445 | 1.174 | 1.365 |

Injections were performed at four different flow rates: 1, 2.5, 5 and 7.5 mL/min. For each tracer, flow rate and pulse volume, three injections were performed to ensure the reproducibility of the results. For flow rates higher than 1 mL/min, only 50 µL pulses were injected. In the first moment measurement, contributions from extra column volumes were taken into account, by performing the same number of injections with the empty column holder.

As a reminder, the tracers used were: acetone (5% v/v), glycine (400 mM), arginine (8 mg/mL), dextran sulfate sodium salt (4000 Da, 8 mg/mL), LYS (4 mg/mL) and BSA (4 mg/mL) to cover a wide range of molecular weights. All tracers were dissolved in a 20 mM phosphate buffer containing 250 mM NaCl and 5% v/v of ethanol, to avoid interactions with the ceramic material.

The first moment measured for each tracer molecule at different flow rates was plotted against the theoretically calculated residence time (length of the column divided by the superficial velocity): the porosity was obtained from linear regressions that were, in all cases characterized by a coefficient of determination $R^2 > 0.98$. Contributions from extra column volumes were taken into account performing the same analysis to effluent peaks at the exit of the empty column.

a)                                    b)
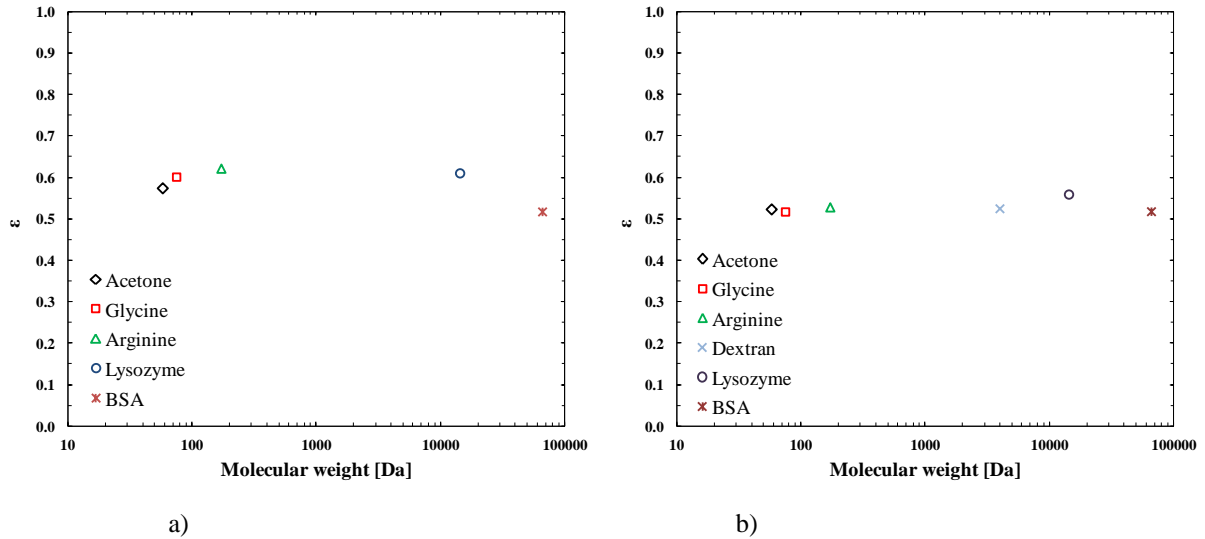
**Figure 7.10**   Void fraction of the ceramic monolithic column as a function of the tracers molecular weight;
a) sample B; b) sample C (Tab. 7.5).

Fig. 7.10 shows the results of the measured void fraction as a function of the molecular weight of the tracer molecules: results are shown for samples B and C. The total porosity measured for all the samples is reported in Table 7.6.

**Table 7.6**   Average porosity for the samples used for the moment analysis.

| | **Samples** | | |
|---|---|---|---|
| | **A** | **B** | **C** |
| **Porosity [%]** | 58.25 | 58.43 | 52.83 |

As shown in Table 7.6, using samples A and B, it was possible to obtain approximately the same average porosity, while, when using sample C, the porosity value obtained was lower. The use of short columns may lead to a non-accurate and more difficult estimation of the monolith parameters, because the presence of defects may heavily affect the results. On the one hand, the use of long columns ensure a good reproducibility of large amount of data, but it could be more likely to have structure defects inside the column that might not be seen, due to the method of production of the ceramics, and those may affect the physical characteristics measurements, such as porosity. For these reasons, it would be preferable to work with columns of maximum 1 cm height.

Moreover, according to the data represented in Fig. 7.10, the molecular weight of the tracers seems not to have an important influence on the measured porosity, as opposed to what was found by Herigstad *et al*. in the case of polymeric monoliths [49]. However, in the case of sample B, a slight porosity decrease with increasing tracer molecular weight can be observed:

this phenomenon has been already observed and reported in the literature [49,50]. Comparing the results of this analysis with studies of pore size distribution (see paragraph 7.3.3) performed on similar ceramic samples, it is possible to conclude that the pore structure of the ceramic monoliths is very well defined and all pores are accessible to the majority of biomolecules of interest. This might explain the fact that an evident trend of porosity as a function of the molecular weight of the tracers used can not be observed.

The axial dispersion coefficient determined for each tracer, normalized to the respective molecular diffusion coefficient, is reported in Fig. 7.11 as a function of the reduced velocity, also called the Péclet number:

$$Pe = \frac{vd_p}{D_m} \tag{7.11}$$

where $D_m$ is the molecular diffusion coefficient and $d_p$ is the particle diameter. In this case, the average pore diameter used was obtained from mercury porosimetry analysis and it is equal to 6.35 μm.
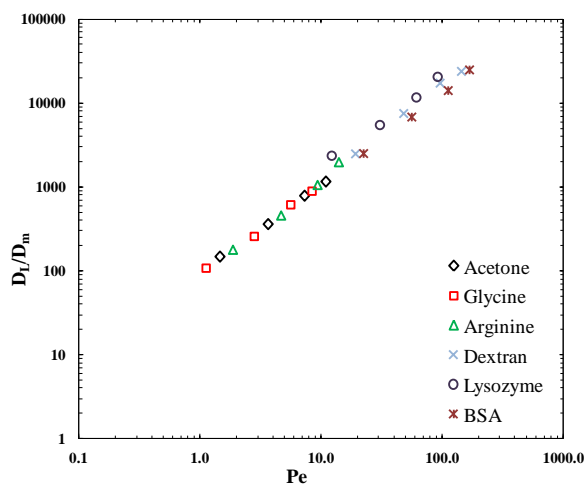


**Figure 7.11** Axial dispersion coefficient normalized with respect to the molecular diffusion against the Péclet number for different molecular weight tracers; sample C.

Fitting of the data in Fig. 7.11 demonstrates that the normalized axial dispersion coefficient is directly proportional to the Péclet number; therefore, the axial dispersion coefficient scales linearly with the superficial velocity:

$$D_b \propto Pe \propto v \tag{7.12}$$

Considering that the height equivalent to a theoretical plate (HETP) for a chromatographic column can be experimentally evaluated using the method of moments, according to the following equation:

$$HETP = \frac{\mu_2^* L}{\mu_1} \tag{7.13}$$

where $\mu_2^*$ is the second centred moment of a non-retained tracer, and comparing this relationship with the results shown in Fig. 7.11, it is possible to conclude that, under non-binding conditions, the HETP of the monolith does not depend on the superficial velocity. This result confirms what has been observed for monoliths and membranes [51, 52] and represents the potentiality of these convective media: the performance of these material, in terms of binding capacity, does not depend on the on the flow rate.

### 7.3.2 Permeability

Pressure drops across monoliths of different heights were measured using demineralised filtered water at room temperature, to obtain the permeability of the ceramic columns considered. The results were corrected with the pressure drops given by the empty column holder.

Considering the values of the flow rate used to carry out the experiments, the water density equal to 1000 kg/m$^3$, the water viscosity equal to 0.001 Pa·s, the size of the monoliths, as well as their average pore diameter, it is possible to conclude that conditions of the measurements fell underneath a viscous flow regime, so the pressure drop in porous media follows the Darcy's law [53]:

$$\Delta P = \frac{\mu L}{B_0} v \tag{7.14}$$

where $\Delta P$ represents the pressure drop across the column length $L$, $\mu$ the viscosity of the fluid and $B_0$ the superficial velocity based permeability of the medium.

Fig. 7.12 shows the results obtained for the sample B; as expected, the pressure drops increase as the superficial velocity increases. The slope of the curve in the plot allowed to calculate the permeability of the ceramic monolith, that is equal to $2.06 \cdot 10^{-13}$ m$^2$. The experiments performed on sample C gave a value for the permeability of the same order of magnitude. In both cases, the permeability is much higher than those of commercial polymeric monoliths (CIM discs; $B_0 = 5.74 \cdot 10^{-12}$ m$^2$; porosity = 0.6) [49]; moreover, if this measured value of permeability is compared to literature data related to a Protein A resin packed column ($B_0 = 9.50 \cdot 10^{-12}$ m$^2$), MabSelect (porosity = 0.3), it is confirmed that the lower pressure drops in the monolithic columns are not related to higher permeability, but to the fact that the bed height of a monolithic column is usually smaller than those of a packed bed column [49].
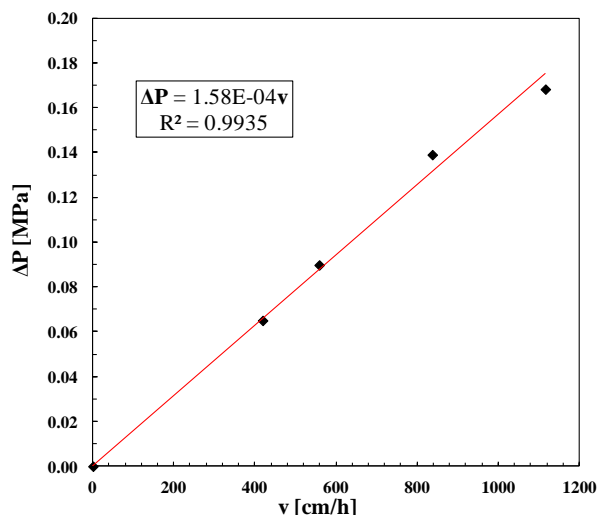
**Figure 7.12** Pressure drops through the monolithic column (sample B) against the superficial velocity.

### 7.3.3 Mercury Intrusion Porosimetry

MIP analysis was performed on small pieces of ceramic material; the aim was to measure the porosity and the pore size distribution. The instrument used was an AutoPore IV 9500 V1.09 (Micrometrics Instruments Corporation).

The results obtained are shown in Fig. 7.13 and in Table 7.7. As pointed out in paragraph 7.3.1, the mercury porosimetry results are in good agreement with the results obtained from the moment analysis.
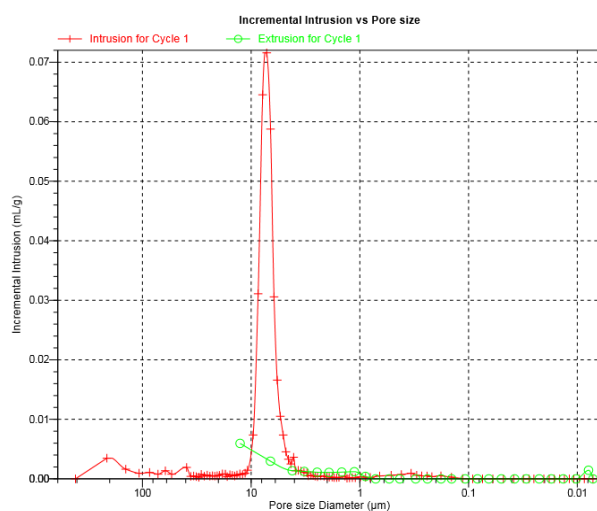


**Figure 7.13** Pore size distribution of the ceramic monoliths obtained with MIP technique

**Table 7.7** Results of MIP analysis.

| Porosity [%] | Median Pore Diameter [µm] |
|---|---|
| 58.45 | 6.3478 |

# References

[1] H.A.J. Thomas, R. Stevens, *Aluminium titanate - a literature review. Part 1. Microcracking phenomena*, (Journal Seek) British Ceramic Transaction 88 (1989)

[2] G. Tilloca, *Thermal stabilization of aluminium titanate and properties of aluminium titanate solid solutions*, Journal of Material Science 26 (1991)

[3] A. Tsetsekou, *A comparison study of tialite ceramics doped with various materials and tialite-mullite composites: microstructural, thermal and mechanical properties*, Journal of the European Ceramic Society 25 (2005) 335–348

[4] K. Moritz, C.G. Aneziris, *Enhancing the thermal shock resistance of alumina-rich magnesium aluminate spinel refractories by an aluminum titanate phase*, Ceramic International 42 (2016) 14155–14160

[5] M. Tanaka, K. Kashiwagi, N. Kawashima, S. Kitaoka, O. Sakurada, Y. Ohya, *Effect of grain boundary cracks on the corrosion behaviour of aluminium titanate ceramics in a molten aluminium alloy*, Corrosion Science. 54 (2012) 90–96

[6] B. Zhao, X. Wen, M. Jiang, J. Wu, F. Lan, J. Wang, et al., *The application of $Al_2TiO_5$ at the $TiO_2$/perovskite interface to decrease carrier losses in solar cells*, Journal of Material Chemistry A 5 (2017) 3691–3698

[7] I.J. Kim, *Thermal stability of $Al_2TiO_5$ ceramics for new diesel particulate filter applications-a literature review*, Journal of Ceramic Processing Research. 11 (2010)

[8] T. Hono, N. Inoue, M. Morimoto, Y. Suzuki, *Reactive sintering and microstructure of uniform, openly porous $Al_2TiO_5$*, Journal of Asian Ceramic Society. 1 (2013) 178–183

[9] P. Hristov, A. Yoleva, S. Djambazov, R. Vladov, A. Gigova, *Ceramic membranes on the basis of aluminium titanate*, Journal of Chemical Technology and Metallurgy 47 (2012) 471–475

[10] X. Guo, W. Zhu, X. Cai, S. Liu, H. Yang, *Preparation of monolithic aluminium titanate with well-defined macropores via a sol-gel process accompanied by phase separation*, Materials and Design. 83 (2015) 314–319

[11] B. Morosin, R.W. Lynch, *Structure studies on $Al_2TiO_5$ at room temperature and at 600 °C*, Acta Crystallographica Section B: Structural Crystallography and Crystal Chemistry. 28 (1972) 1040–1046

[12] R.D. Skala, D. Li, I.M. Low, *Diffraction, structure and phase stability studies on aluminium titanate*, Journal of the European Ceramic Society 29 (2009)

[13] V. Buscaglia, P. Nanni, G. Battilana, G. Aliprandi, C. Carry, *Reaction sintering of aluminium titanate: I-effect of MgO addition*, Journal of the European Ceramic Society 13 (1994) 411–417

[14] I.M. Low, Z. Oo, *Reformation of phase composition in decomposed aluminium titanate*, Material Chemistry and Physics 111 (2008)

[15] M. Ilatovskaia, G. Savinykh, O. Fabrichnaya, *Thermodynamic description of the TiAl-O system based on experimental data*, Journal of Phase Equilibra and Diffusion 38 (2016) 1–10

[16] X. Luo, Z. Xie, L. Zheng, K. He, M. Li, *Effect of adding $Cr_2O_3/Fe_2O_3$ on aluminum titanate properties*, Refractories and Industrial Ceramics. 56 (2015) 337–343

[17] M. Nagano, S. Nagashima, H. Maeda, A. Kato, *Sintering behaviour of $Al_2TiO_5$ base ceramics and their thermal properties*, Ceramic International 25 (1999) 681–687

[18] R. Maki, Y. Suzuki, *Microstructure and mechanical properties of MgO-doped $Al_2TiO_5$ prepared by reactive sintering*, JCS-Japan 121 (2013) 568–571

[19] Y. Ohya, S. Yamamoto, T. Ban, M. Tanaka, S. Kitaoka, *Thermal expansion and mechanical properties of self-reinforced aluminum titanate ceramics with elongated grains*, Journal of the European Ceramic Society 37 (2017) 1673–1680

[20] C.C. Guedes-Silva, F.M. de S. Carvalho, T. dos S. Ferreira, L.A. Genova, *Formationof aluminum titanate with small additions of MgO and $SiO_2$*, Journal of Material Research 19 (2016) 384–388

[21] S. Bueno, M.H. Berger, R.Moreno, C. Baudín, *Fracture behaviour of microcrack-free alumina-aluminium titanate ceramics with second phase nanoparticles at alumina grain boundaries*, Journal of the European Ceramic Society 28 (2008)

[22] S. Bueno, R. Moreno, C. Baudín, *Design and processing of $Al_2O_3$-$Al_2TiO_5$ layered structures*, Journal of the European Ceramic Society 25 (2005) 847–856

[23] A. Borrell, M.D. Salvador, V.G. Rocha, A. Fernández, T. Molina, R. Moreno, *Enhanced properties of alumina-aluminium titanate composites obtained by spark plasma reaction-sintering of slip cast green bodies*, Composites Part B: Engineering 47 (2013) 255–259

[24] M. Sobhani, T. Ebadzadeh, M.R. Rahimipour, *A comparison study on the R-curve behavior of alumina/aluminum titanate composites prepared with different $TiO_2$ powders*, Theoretical and Applied Fracture Mechanics 85 (2016) 159–163

[25]  B. Freudenberg, A. Mocellin, *Aluminum titanate formation by solid state reaction of coarse Al₂O₃ and TiO₂ powders*, Journal of the American Ceramic Society 71 (1988) 22–28

[26] L. Stanciu, J.R. Groza, L. Stoica, C. Plapcianu, *Influence of powder precursors on reaction sintering of Al₂TiO₅*, Scripta Materialia 50 (2004) 1259–1262

[27] G. Xu, Y. Ma, G. Ruan, H. Cui, Z. Zhang, B. Bai, *Preparation of porous Al₂TiO₅ ceramics reinforced by in situ formation of mullite whiskers*, Materials Design 47 (2013) 57–60

[28] H. Nishijima, R. Maki, Y. Suzuki, *Microstructural control of porous Al₂TiO₅ by using various starches as pore-forming agents*, Journal of the Ceramic Society of Japan 122 (2014) 565–569

[29] N. Vitorino, J.C.C. Abrantes, J.R. Frade, *Cellular ceramics processed by paraffin emulsified suspensions with collagen consolidation*, Materials Letters 98 (2013) 120–123

[30] M.F. Sanches, N. Vitorino, J.C.C. Abrantes, J.R. Frade, J.B. Rodrigues Neto, D. Hotza, *Effects of processing parameters on cellular ceramics obtained by paraffin emulsified suspensions*, Ceramic International 40 (2014) 9045–9053

[31] N. Vitorino, C. Freitas, A.V. Kovalevsky, J.C.C. Abrantes, J.R. Frade, *Cellular MgAl₂O₄ spinels prepared by reactive sintering of emulsified suspensions*, Materials Letters 164 (2016) 190–193

[32] M.F. Sanches, N. Vitorino, C. Freitas, J.C.C. Abrantes, J.R. Frade, J.B. Rodrigues Neto, D. Hotza, *Cellular ceramics by gelatin gelcasting of emulsified suspensions with sunflower oil*, Journal of the European Ceramic Society 35 (2015) 2577–2585

[33]  G. Taguchi, S. Chowdhury, Y. Wu, *Quality engineering: the Taguchi method*, Taguchi's Quality Engineering Handbook, John Wiley&Sons, Inc., Hoboken, NJ, USA, 2004, pp. 56–123

[34]  L.N. Harris, Philip J. Ross (Ed.), Taguchi Techniques for Quality Engineering, 5 (1989) McGraw-Hill Book Company, 1988, p. 249

[35]  I.-W. Chen, X. Wang, *Sintering dense nanocrystalline ceramics without final-stage grain growth*, Nature 404 (2000) 168–171

[36] K. Maca, V. Pouchly, P. Zalud, *Two-step sintering of oxide ceramics with various crystal structures*, Journal of the European Ceramic Society 30 (2010) 583–589

[37] P. Gagnon, *Monoliths open the door to key growth sectors*, Bioprocess International 8 (2010) 20–23

[38] M.O. Herigstad, S. Dimartino, C. Boi, G.C. Sarti, *Experimental characterization of the transport phenomena, adsorption and elution in a protein A affinity monolithic medium*, Journal of Chromatography A 1407 (2015) 130-138

[39]  D.A.H. Hanaor, C.C. Sorrell, *Review of the anatase to rutile phase transformation*, Journal of Material Science 46 (2011) 855–874

[40] V.V. Atuchin, T.A. Gavrilova, J.C. Grivel, V.G. Kesler, I.B. Troitskaia, *Electronic structure of layered ferroelectric high-k titanate $Pr_2Ti_2O_7$*, Journal of Solid State Chemistry 195 (2012) 125–131

[41] V.V. Atuchin, T.A. Gavrilova, J.-C. Grivel, V.G. Kesler, *Electronic structure of layered ferroelectric high-k titanate $La_2Ti_2O_7$*, Journal of Physics D: Applied Physics. 42 (2009) 35305

[42] C.R. Hubbard, R.L. Snyder, *RIR-measurement and use in quantitative XRD*, Powder Diffraction Journal 3 (1988) 74–77

[43] B. Freudenberg, A. Mocellin, *Aluminium titanate formation by solid state reaction of $Al_2O_3$ and $TiO_2$ single crystals*, Journal of Material Science 25 (1990) 3701–3708

[44]  V. Singh, G. Jayarao, R. Mazumder, *Phase evolution and stability of aluminium titanate prepared by solid-state route: effect of two different particle size of $Al_2O_3$*, Transactions of the Indian Ceramic Society 75 (2016) 170–174

[45] Q.H. Qin, *Introduction to the composite and its toughening mechanisms*, Toughening Mechanisms in Composite. Materials (2015)1–32

[46]  R.W. Grimes, J. Pilling, *Defect formation in $\beta$-$Al_2TiO_5$ and its influence on structure stability*, Journal of Material Science 29 (1994) 2245–2249

[47] R. Naghizadeh, H.R. Rezaie, F. Golestani-fard, *The influence of composition, cooling rate and atmosphere on the synthesis and thermal stability of aluminum titanate*, Material Science and Engineering B 157 (2009) 20–25

[48] E. Lalli, N.M.D. Vitorino, C.A.M. Portugal, J.G. Crespo, C. Boi, J. R. Frade, A.V. Kovalevsky, *Flexible design of cellular $Al_2TiO_5$ and $Al_2TiO_5$-$Al_2O_3$ composite monoliths by reactive firing*, Materials and Design 131 (2017) 92-101

[49] M.O. Herigstad, S. Dimartino, C. Boi, G.C. Sarti, *Experimental characterization of the transport phenomena, adsorption and elution in a protein A affinity monolithic medium*, Journal of Chromatography A 1407 (2015) 130-138

[50] A. Zöchling, R. Hahn, K. Ahrer, J. Urthaler, A. Jungbauer, *Mass transfer characteristics of plasmid in monoliths*, Journal of Separation Scince 27 (2004) 819-827

[51] A. Jungbauer, R. Hahn, *Polymethacrilate monoliths for preparative and industrial separation of biomolecular assemblies*, Journal of Chromatography A 1184 (2008) 62-79

[52] S. Brandt, R.A. Goffe, S.B. Kessler, J.L. O' Connor, S. Zale, *Membrane-based affinity technology for commercial scale purification*, Nature Biotechnology 6 (1988) 779-782

[53] H. Darcy, *Les fontaines publiques de la ville de* Dijon, Victor Dalmont, Paris 1856

# CHAPTER 8

# Surface activation and protein adsorption

## 8.1 Introduction

This last chapter presents the experimental activity performed to functionalize the surface of cellular $Al_2TiO_5$-$Al_2O_3$ composite ceramic monoliths, whose design and characterization where the subject of the previous chapter. Moreover, preliminary results related to protein adsorption tests will be presented to evaluate the possible use of this ceramic monolith as a novel chromatographic support for IgG purification.

## 8.2 Chemical modification of the surface

The processing method for the production of cellular $Al_2TiO_5$-$Al_2O_3$ ceramic and its design are based on one important thermal treatment, the firing procedure, for the formation of aluminium titanate and the mechanical consolidation of the material. After this step of the processing method, the surface of the ceramics is completely inert, due to the very high temperature reached during the two-step sintering procedure described in Chapter 7.

It is necessary to create a high number of active sites on the surface, to immobilize affinity ligands or for direct binding of proteins, to use these ceramic monoliths as affinity chromatographic supports. Therefore, an important part of the work related to the production of cellular ceramic materials, to be used as chromatographic stationary phases, is related to the modification of their surface. To this aim, different reagents and the hydrothermal process were used to obtain functional groups, like amine or epoxy groups, and to make the surface more hydrophilic, respectively.

The next paragraphs will be dedicated to the description of the chemicals used, the modification protocols implemented, the surface characterization using different analytical techniques and the relevant results.

### 8.2.1 Experimental procedures

All the samples subjected to modification without performing the hydrothermal process were produced according to the following parameters: the molar ratio between alumina and titania in the initial suspension was 0.25; the volume ratio between the organic phase and the suspension for the emulsification step was 1. The ceramic material was consolidated through a two-step firing procedure, using the following conditions: $T_{peak}$=1550°C, $T_{iso}$=1300°C and $t_{iso}$=4 h (corresponding to experiment E6 in the Taguchi plan, Table 7.2, described in the previous chapter).

On the other hand, studies regarding the hydrothermal process were carried out before chemical modification of the surface, using samples of different composition: details regarding the molar ratio between alumina and titania, as well as the volume ratio between liquid paraffin and suspension will be given once the results are presented. Moreover, the samples prepared with different two-step firing conditions were used to study the effects of the hydrothermal process: all the sintering conditions used corresponded to a specific experiment in the Taguchi plan (see Table 7.2, Chapter 7).

All the ceramic samples were casted in the shape of cylindrical columns that were cut into small discs, 0.5 cm thickness and 1.2 cm diameter approximately, to perform the chemical modification and the hydrothermal process.

### 8.2.1.1 Chemicals

Poly(ethylene glycol) diglycidyl ether (PEGDE, 500g/mol), 1,4-Butanediol diglycidyl ether (1,4-BDE), (3-glycidyloxypropyl)trimethoxysilane (GPTMS), (3-aminopropyl)triethoxysilane (APTES), acetone 99.5%, dimethyl sulfoxide (DMSO) 99.5% and 1,2-propanediol were purchased from Sigma Aldrich. Hydrogen peroxide 30% was purchased from PanReac AppliChem, absolute ethanol was purchased from Scharlab, sodium acetate and sodium hydroxide 1M were purchased from Merck. The chemical structure of the reagents used for the surface modification is shown in Fig. 8.1.



| PEGDE | 1,4-BDE | GPTMS | APTES |
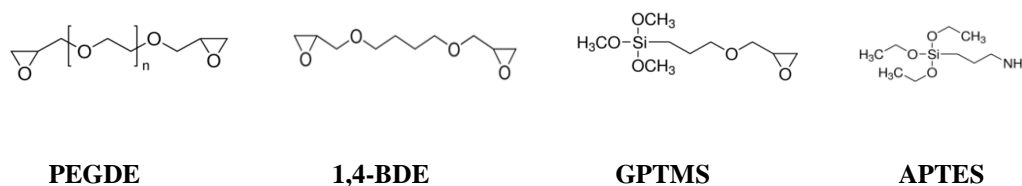
**Figure 8.1** Chemical structure of poly(ethylene glycol) diglycidyl ether (**PEGDE**), 1,4-Butanediol diglycidyl ether (**1,4-BDE**), (3-glycidyloxypropyl)trimethoxysilane (**GPTMS**), (3-aminopropyl)triethoxysilane (**APTES**).

### 8.2.1.2 Cleaning of the surface

It is a good practice to clean the surface of the materials with an appropriate procedure before modification of the ceramic monoliths, to remove any organic contaminant and make the surface more hydrophilic. In the case of samples treated with the hydrothermal treatment, this cleaning procedure was performed after this process, before chemical functionalization of the surface.

Hydrogen peroxide was chosen as cleaning agent. The samples were immersed in hydrogen peroxide 30% v/v under gentle agitation and they were kept under vacuum at 80°C for 4 h. After this cleaning procedure, the samples were washed several times with demineralised water and kept in water overnight. Finally, the samples were dried at 70°C.

### 8.2.1.3 Hydrothermal process

The hydrothermal treatment was carried out using a stainless steel reactor, whose inner part was made of Teflon; the total internal volume of the Teflon part was 92 mL.

This treatment combines the use of high temperature, high pressure and aggressive chemical conditions to induce the partial degradation of $Al_2TiO_5$, exploiting the fact that aluminium titanate is metastable below 1200°C [1], as introduced in Chapter 7. Hydrothermal treatment represents a self-functionalization process of the material itself: the degraded part of the surface precipitates due to extreme process conditions and re-depose on the surface creating characteristic active structures.

A 1M NaOH solution was used to induce the partial degradation of the surface of the aluminium titanate phase of the composite monolith. This process was based on interesting results recently obtained on cellular ceramic alumina [2, 3]. In these studies, it was demonstrated through FTIR analysis that the density of the hydroxyl groups on the surface increased after the hydrothermal process and the characteristic structures were mostly composed of boehmite, AlO(OH). Another important consequence of the use of the hydrothermal process is the increase of the surface area per unit volume, due to the formation of the boehmite structures, that can assume different shapes.

The volume of the sodium hydroxide solution that was poured inside the reactor was maximum 40% of the volume of the Teflon part of the reactor. It is really important not to exceed the maximum volume of solution inside the reactor, because the very high pressure reached during the process may lead to the explosion of the reactor itself. One or maximum two discs of the sintered cellular ceramic monoliths were immersed in the solution and the reactor

was kept inside a oven at 190°C for 24 h. After the reactor was cooled down naturally, the samples were washed several times with demineralised water, to remove any sodium trace. The samples were finally dried before any chemical modification was performed.

### *8.2.1.4 Chemical modification protocols*

The reagents chosen for the surface modification allowed to obtain monoliths functionalized with epoxy groups (PEGDE, 1,4-BDE and GPTMS) and amine groups (APTES). The modification protocols used were adapted from procedures found in literature.

**- PEGDE**: 25 mL of solution of PEGDE in acetone were prepared, varying the concentration of the reagent ($4 \cdot 10^{-5}$M, 0.01M, 0.05M and 0.10M). The sample disc was kept in this solution for 6 h, on the orbital shaker at 140 rpm, and for 2 h in the sonicator, in the same solution. The sample was washed several times with acetone and dried at 70°C overnight [4].

**- 1,4-BDE**: For each sample, 6.5 mL of DMSO were mixed with 3.5 mL of 1N NaOH. 1,4-BDE was added in the amount of 3.5 mL, to reach a concentration of 1.4 M. The sample was immersed in the solution for 3 h and 20 min, at room temperature. After the reaction, the ceramic disc was washed using demineralised water and then, it was dried at 70°C overnight [5].

- **GPTMS**: The step for the preparation of the sol-gel is crucial: 30 mL of absolute ethanol were mixed with 2 mL of sodium acetate buffer (50 mM, pH 5); then, 5 mL of GPTMS were added drop-wise under vigorous stirring. After that, the solution was stirred for three hours. The device used to prepare the sol-gel and carry out the reaction was made of Teflon. The ceramic sample was soaked into the sol-gel and the reaction for surface modification was performed under vacuum for three hours, then the sample was washed using ethanol and it was subjected to a thermal treatment at 100°C for 1 hour [6].

Moreover, a systematic experimental plan was adopted to investigate the effect of different parameters affecting the sol-gel process, such as the effect of concentration of GPTMS and the effect of pH. In particular, three different values for GPTMS concentration and pH were chosen, as reported in Table 8.1.

The functionalization was also carried out in dynamic conditions, using a plastic cell and a peristaltic pump, to further improve the modification of the surface using this epoxy-silane reagent. Each sample was allocated into the cell, that was connected to the pump, to force the modification solution to flow through the porous material. In this case, the modification reaction

was carried out for at least 6 hours. After that, the samples were subjected to a thermal treatment at 100°C for 1 hour, following the same protocol described before.

Finally, a few samples were subjected to two or three subsequent modifications, in order to increase the density of the epoxy groups on the surface of the ceramic material. This samples were used only to perform preliminary batch adsorption experiments and were not subjected to any kind of analytical investigation.

**Table 8.1**     Values of the sol-gel process parameters.

| C [mol/L] | pH |
|---|---|
| 0.5 | 6 |
| 1.0 | 10 |
| 1.5 | 14 |

- **APTES**: for each sample disc, 25 mL of solution containing 19.15 mL of ethanol, 100 μL of NaOH (1 N, the catalyst) and 5.85 mL of APTES were prepared (APTES final concentration of 1 M). APTES was added to the solution of ethanol and NaOH drop wise, mixing vigorously. The sample was immersed in the prepared solution for 2 h and it was kept at 60°C under vacuum and gentle agitation. After the reaction the sample was dried at room temperature for 1 h and then, it was dried at 70°C overnight [7].

### 8.2.1.5 Samples characterization

The samples treated with the hydrothermal process and subjected to the chemical modification of the surface were characterized by scanning electron microscopy (SEM - Hitachi SU-70 instrument), to investigate relevant microstructural evolution. EDS analyses (Bruker Quantax 400 detector) were performed on a few samples after the hydrothermal process to confirm the composition of the structures created after the thermal treatment.

Fourier Transform Infrared Spectroscopy (FTIR, Vertex 70, Bruker, Germany) was performed to observe chemical changes on the surface of the cellular ceramic monoliths. Pellets for FTIR were prepared mixing the monolith reduced to powder with KBr (ratio sample:KBr=1:100). The two component mixture was grinded in a pestle to obtain a fine powder and a small amount of the powder was then pressed into a very thin and transparent pellet.

The analysis was performed placing the pellet inside a spectrometer disc holder mounted inside the spectrometer: the pellet was then scanned for wavenumber ranging from 400 to 4000 cm$^{-1}$, resolution 4 cm$^{-1}$, registering the transmittance.

TGA analysis (Thermo Gravimetric Analysis) was performed using a TA TGA Q-50 analyser (TA Instruments, USA); it was performed only on the samples modified with PEGDE, to further investigate the surface degree of modification. The analysis was carried out under nitrogen flow (40 mL/min), placing a small amount of the dried samples reduced to powder (approximately 18 mg) into the aluminium samples pan and performing a temperature ramp from room temperature up to 600°C, 10°C/min. Unfortunately, due to the composition of the sample holder it was not possible to exceed the temperature of 600°C during the analysis.

Finally, elemental analysis was carried out using some of the modified samples, to quantitatively estimate the density of the functional groups on the surface, after chemical modification. The samples were reduced to powder to perform this analysis. The instrument used to perform the elemental analysis was an Elemental analyzer, Thermo Finnigan-CE Instruments, Flash EA 1112 CHNS series.

### 8.2.2 Results

#### 8.2.2.1 Hydrothermal process

SEM images in Fig. 8.2 represents very good results obtained performing the hydrothermal process on the cellular ceramic monoliths. All pictures were taken from the surface of the sample, that was the one directly in contact with the aggressive solution during the hydrothermal process (it means that the sample was not crushed after the treatment with NaOH).

As it can be observed from Fig. 8a, the wire-like structures grown during the thermal treatment are very homogeneously distributed on the entire surface of the sample analyzed. The other SEM images reported in Fig. 8.2 focus on specific zones in the material to point out the shapes of the structures as well as their dimensions. These wire-like structures have a diameter of the order of magnitude of nanometers, while their length is about a few micrometers.
Fig. 8.2d and 8.2e are an example of how interesting is to play with the SEM instrument: changing the focus is possible to see through pores and investigate if the same modification took place also inside the material, and not only on the surface. However, since the sample was not broken to investigate a fracture surface, it was not possible to evaluate the modification dept.
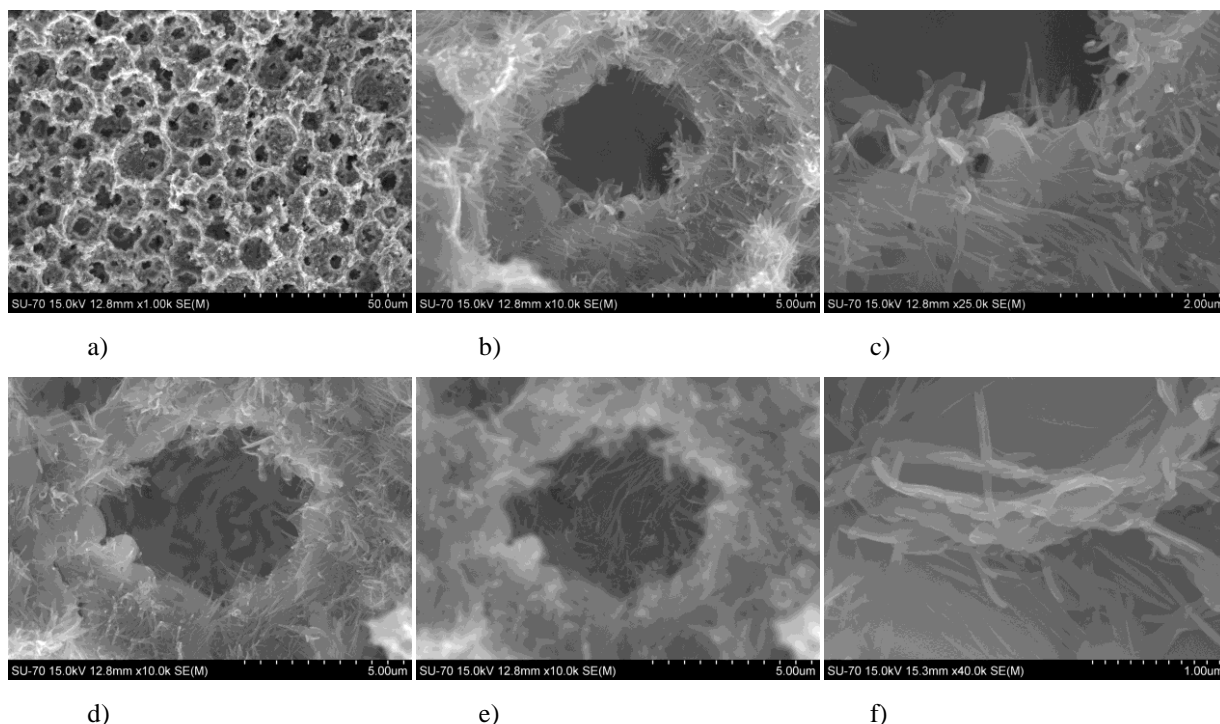
**Figure 8.2** SEM images for samples treated with the hydrothermal process; molar ratio between alumina and titania equal to 0.5; volume ratio between liquid paraffin and suspension equal to 1.5; firing conditions: $T_{peak}$=1550°C, $T_{iso}$=1300°C and $t_{iso}$=4h (corresponding to experiment E6 in the Taguchi plan).

The active wire-like structures can grow from $Al_2O_3$ phase degradation, as know from literature [2, 3], but the aim of this investigation was to demonstrate that they could also grow from the metastable phase, represented by aluminium titanate. About this, EDS mapping was performed and the results can be found in Fig. 8.3.

EDS studies showed that the most part of the wire-like structures grown from the $Al_2TiO_5$ phase: in fact, in Fig. 8.3a and 8.3b alumina grains in blue are quite visible and it is clear that the nice structures grown during the hydrothermal process come from the aluminium titanate phase. Moreover, it is possible to have an idea of the composition of those structures, as represented in Fig. 8.3c. It seems that the wire-like structures are rich in titania, and this was another goal of the experimental investigation: the aim of the hydrothermal treatment was to make the surface more hydrophilic, thanks to boehmite formation, and more active, thanks to presence of titania. Of course, titania in the wire-like structures is more active than $TiO_2$ on the surface after the sintering procedure.

Other samples, of different composition and prepared using different operating conditions, were characterized with the hydrothermal process. Some examples are shown in Fig. 8.4 and 8.5, through SEM images.

a)                                    b)                                    c)
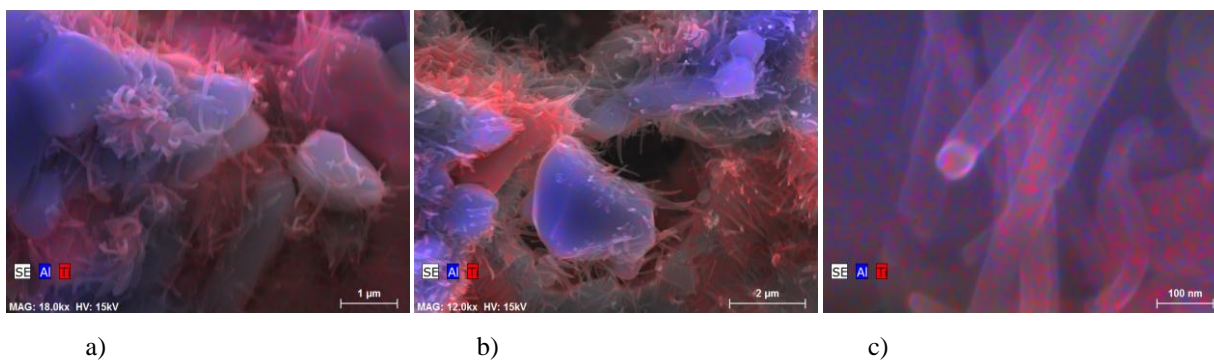
**Figure 8.3**  EDS mapping for samples treated with the hydrothermal process; molar ratio between alumina and titania equal to 0.5; volume ratio between liquid paraffin and suspension equal to 1.5; firing conditions: $T_{peak}$=1550°C, $T_{iso}$=1300°C and $t_{iso}$=4h (corresponding to experiment E6 in the Taguchi plan).



a)                                    b)                                    c)
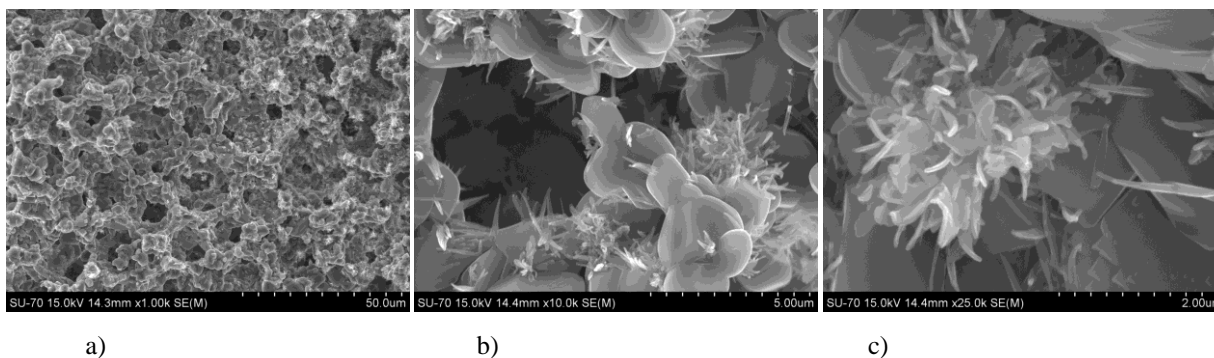
**Figure 8.4**  SEM images for samples treated with the hydrothermal process; molar ratio between alumina and titania equal to 0.25; volume ratio between liquid paraffin and suspension equal to 1.5; firing conditions: $T_{peak}$=1550°C, $T_{iso}$=1300°C and $t_{iso}$=4h (corresponding to experiment E6 in the Taguchi plan).



a)                                    b)
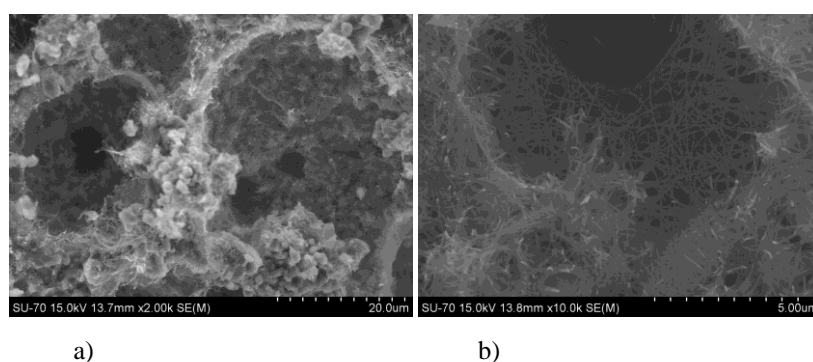
**Figure 8.5**  SEM images for samples treated with the hydrothermal process; molar ratio between alumina and titania equal to 0.25; volume ratio between liquid paraffin and suspension equal to 1; firing conditions: $T_{peak}$=1550°C, $T_{iso}$=1300°C and $t_{iso}$=4h (corresponding to experiment E6 in the Taguchi plan).

The pictures show how different can be the shape and the distribution of the structures grown during the hydrothermal treatment. For example, different structures are shown in Fig. 8.4 and 8.2: in this last case the wire-like structures grown in clusters are well distributed on the surface analyzed. On the other hand, from Fig. 8.5, it can be seen that surface of the sample is very rich in wire-like structures, that sometime create networks like cobwebs.

The SEM images in Fig. 8.5 refer to the sample that was also used to perform the chemical modification, described in the following paragraphs.

### *8.2.2.2 Chemical modification*

This paragraph will present the results related to the chemical modification of fired samples and of samples treated using the hydrothermal process.

For each chemical reagent used FTIR spectra will be shown, in which the wavenumber corresponding to the bonds of interest will be pointed out, as well as the results of TGA (that was performed only for the reagent PEGDE) and those of elemental analysis.

Finally, the results of the chemical modification of the hydrothermal samples will be illustrated through the use of SEM images and FTIR spectra.

### **PEGDE**

In Fig. 8.6 the FTIR results for ceramic samples functionalized using PEGDE with different concentration in the modifying solution can be found. All curves have to be compared to the control curve (in black), that corresponds to the fired unmodified sample.
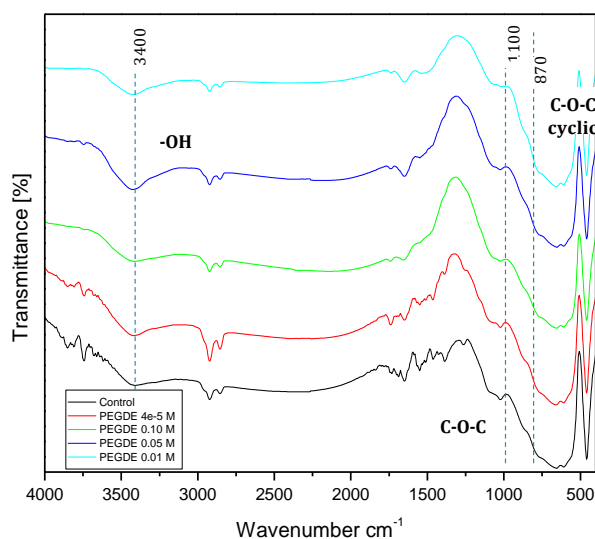


**Figure 8.6**    FTIR spectrum for ceramic samples modified using PEGDE solutions at different concentrations.

The comparison between the spectra of the modified samples and the control is only qualitative: the curves were translated to make the comparison easier. It can be observed that there is not a great difference between the spectra of the control and those of the functionalized samples, indicating that the modification was successful only in a small part.

This result was confirmed by the TGA and elemental analysis results, shown in Fig. 8.7 and in Table 8.2. TGA results show that the functionalization using PEGDE actually took place, because the degradation of the sample as a function of the temperature in the experiment is comparable to qualitative trends reported in literature [4], Fig. 8.7b. However, the degree of modification is very low: the percentage of material degraded during TGA is less than 0.03%, while the percentage of carbon found during the elemental analysis is less than 0.1% for almost all the analyzed samples.

To explain these results, it is important to consider that PEGDE is an organic compound and it is possible that the compatibility between this organic reagent and the inorganic surface is very low: for this reason it is difficult to create stable bonds between the two.



a)                                                                                    b)
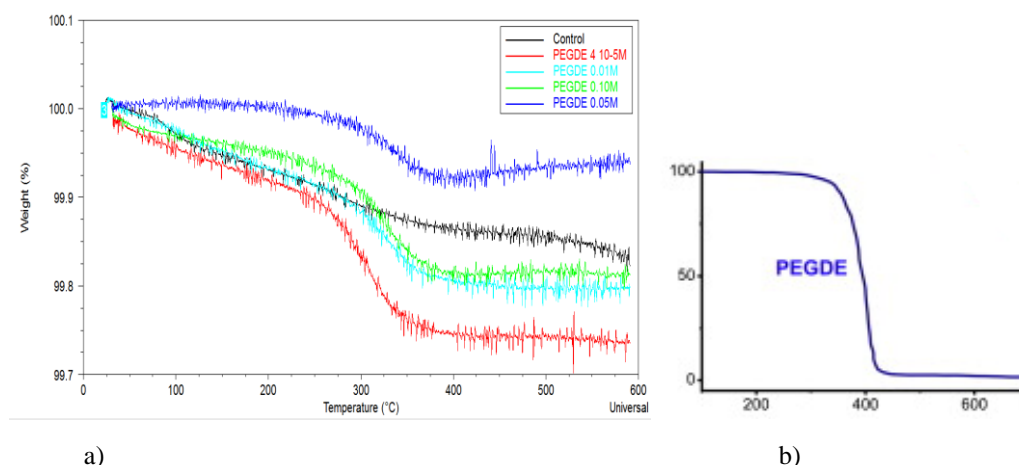
**Figure 8.7**   a)TGA results for ceramic samples modified using PEGDE solutions at different concentrations; b) TGA analysis for PEGDE [4].

**Table 8.2**   Elemental analysis results for fired ceramic samples and ceramic samples modified using PEGDE solutions at different concentrations.

|  | C | N | H |
|---|---|---|---|
| **control** | 0.07 % | - | - |
| **$4 \cdot 10^{-5}$ M** | 0.10 % | - | - |
| **0.10 M** | 0.09 % | - | - |
| **0.05 M** | 0.11 % | - | - |
| **0.01 M** | 0.06 % | - | - |

**1,4-BDE**

Similar conclusions can be drawn from the FTIR and elemental analysis results of the samples modified using 1,4-BDE; in fact, PEGDE and 1,4-BDE are very similar in terms of structure: the main difference is their molecular weight, 500 g/mol for PEGDE and 202.25 for 1,4-BDE.

The concentration of the modifying solution was 1.41 M, which seemed a quite high concentration. Looking at Fig. 8.8, the spectrum of the functionalized sample seems to be quite different from that of the control, however the two curves in correspondence of the wavenumber of interest (those corresponding to the typical bonds in the modifying reagent) are very similar.

The elemental analysis also confirmed the low degree of functionalization of the surface, even if the amount of carbon found is a bit higher with respect to that measured in samples treated with PEGDE. The low compatibility between the organic compounds and the inorganic ceramic surface can still explain the results obtained, while the slight increase in carbon content can be due to the lower molecular weight of 1,4-BDE that can be translated in a probable faster diffusion inside the pores of the material during the functionalization reaction.
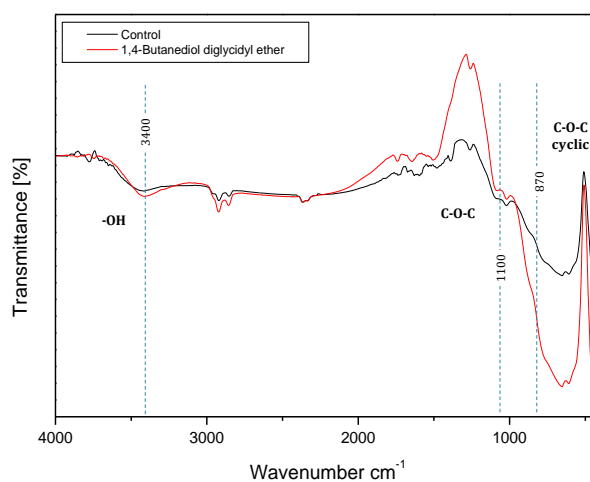


**Figure 8.8**    FTIR spectrum for ceramic samples modified using a 1,4-BDE solution at a concentration of 1.41 M.

**Table 8.3**    Elemental analysis results for fired ceramic samples and ceramic samples modified using a 1,4-BDE solution at a concentration of 1.41 M.

|         | C      | N | H |
|---------|--------|---|---|
| control | 0.07 % | - | - |
| 1,4-BDE | 0.27 % | - | - |

## GPTMS

GPTMS is an epoxy-silane composed by an inorganic part, containing Si, and an organic part. The nature of this reagent might improve the compatibility with the ceramic surface.

The degree of functionalization of the surface was found strongly dependent on the concentration of the reagent used during the chemical modification reaction. In Fig. 8.9 the FTIR spectrum of a sample treated with a solution of GPTMS 0.6M is shown. As already observed for the two previous epoxy reagents, it is apparent that the modification of the surface is quite low and the result is confirmed by the elemental analysis results in Table 8.4.
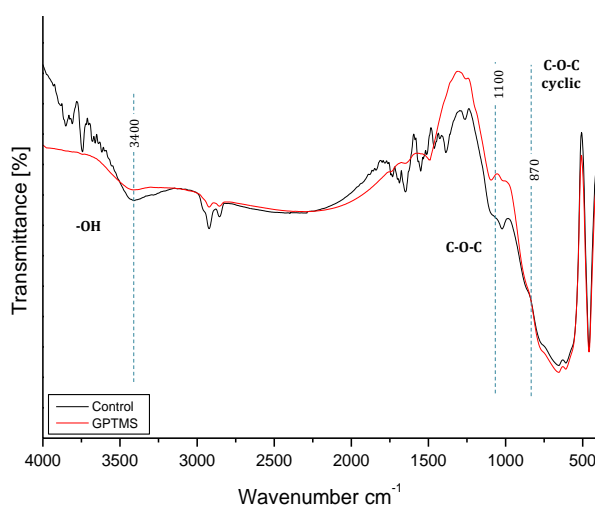


**Figure 8.9**    FTIR spectrum for ceramic samples modified using a GPTMS solution at a concentration of 0.6 M.

**Table 8.4**    Elemental analysis results for fired ceramic samples and ceramic samples modified using a GPTMS solution at a concentration of 0.6 M.

|  | **C** | **N** | **H** |
|---|---|---|---|
| **control** | 0.07 % | - | - |
| **GPTMS 0.6 M** | 0.36 % | - | - |

However, an investigation of the effect of GPTMS concentration and pH of the solution was carried out. Elemental analysis was not performed for these samples, but the FTIR spectra in Fig. 8.10 demonstrates that there is a positive influence of the concentration and pH on the functionalization of the ceramic monoliths using GPTMS. In fact, increasing the concentration in the modifying solution up to 1.5 M and increasing the pH to the value of 14, it was possible to obtain what was considered the best modification for GPTMS. These, of course, are only qualitative results, but they encouraged to continue the work using this epoxy reagent.
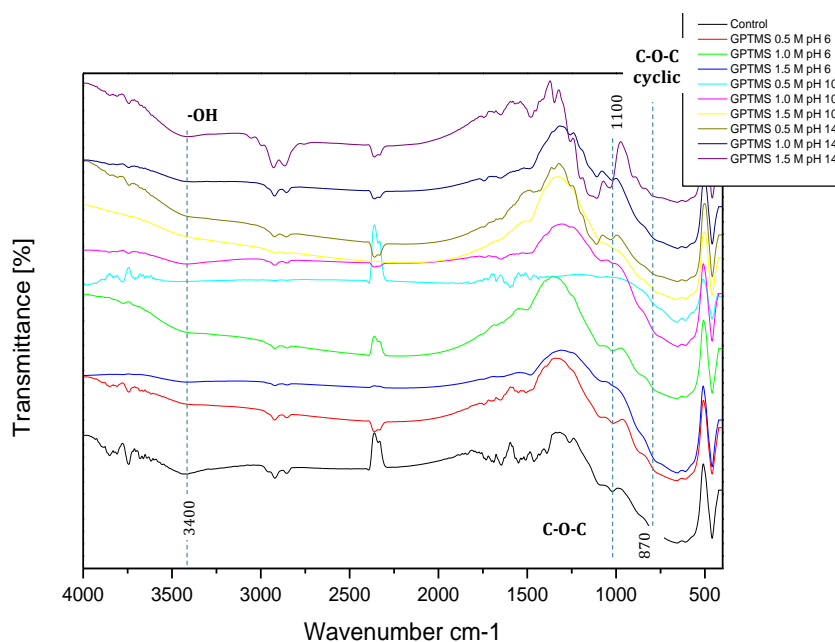
**Figure 8.10** FTIR spectrum for ceramic samples modified using GPTMS solutions at different concentrations and pH values.

## APTES

APTES was the only reagent used to functionalize the surface of the ceramic monoliths with amine groups. As for GPTMS, it is composed of an inorganic part, containing Si, and an organic part. Also in this case the compatibility between the reagent and the ceramic material was expected to be higher.

FTIR spectra show a strong influence of the APTES concentration on the degree of functionalization of the material, as illustrated in Fig. 8.11.



a)                                                      b)
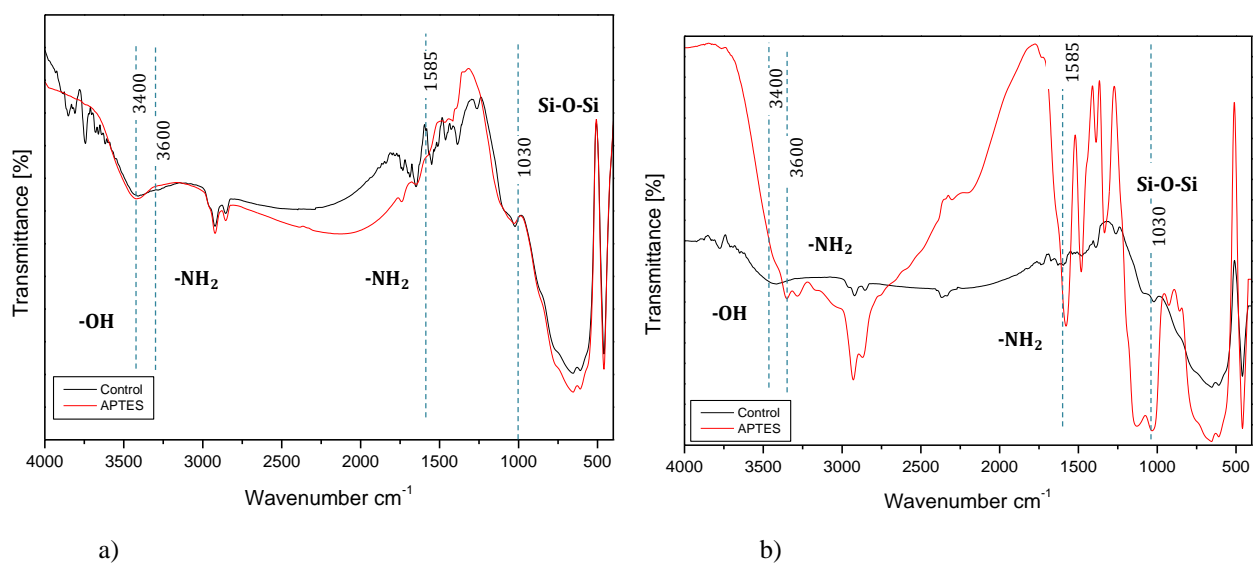
**Figure 8.11** FTIR spectrum for ceramic samples modified using APTES solutions at a concentration of a) 1% v/v; b) 1 M.

By changing the concentration from 1% v/v to 1 M it was possible to obtain a good degree of surface modification. In particular, the sample modified with the 1 M APTES solution presents a FTIR spectrum with clear differences, with respect to the control, in correspondence of the wavenumbers pointed out in the plot. This clearly indicates the presence of amine groups and Si-O-Si bonds in the analyzed sample.

In addition, elemental analysis results demonstrate the successful modification of the ceramic monoliths.

**Table 8.5** Elemental analysis results for fired ceramic samples and ceramic samples modified using an APTES solution at a concentration of 1 M.

|  | **C** | **N** | **H** |
|---|---|---|---|
| **control** | 0.07 % | - | - |
| **APTES 1 M** | 4.75 % | 1.71 | 0.84 |

However, since samples modified with APTES were not stable and readily degraded once immersed in water, it was decided to continue working with GPTMS as epoxy reagent for the chemical modification of the surface.

**Hydrothermal samples**

FTIR spectra of hydrothermal samples functionalized with different chemicals are shown in Fig. 8.12. No wavenumber corresponding to specific chemical bonds was pointed out, since they were already shown previously in the paragraph.
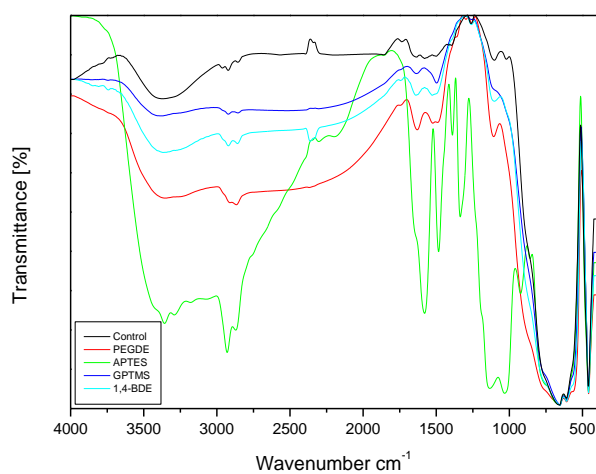


**Figure 8.12** FTIR spectrum for ceramic samples treated with the hydrothermal process and modified using all the chemical reagents considered.

The same conclusions drawn for the samples not treated with the hydrothermal process can be assumed valid even for the hydrothermal samples. The modification performed with the epoxy reagents is very poor, while a good modification was obtained using APTES, even if these samples were not stable in water as well as the samples not treated with the hydrothermal process.

Another interesting result is represented by the comparison between the unmodified fired ceramics and the hydrothermal unmodified ceramics, shown in Fig. 8.13. An increase of the hydroxyl groups is clear from the FTIR spectra, therefore the aim of the hydrothermal process was demonstrated.
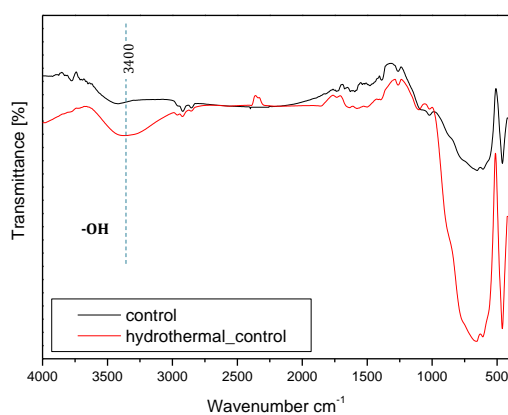


**Figure 8.13**   Comparison between FTIR spectra for fired samples and hydrothermal samples.

Examples of SEM images are reported below to show the structural modifications that occurred after the surface functionalization. It was not possible to perform EDS mapping on these type of samples because carbon, nitrogen and hydrogen cannot be detected with this analysis. Fig. 8.17 demonstrates that the APTES functionalization was the one that affected the material the most; indeed, the wire-like structures that were present in the unmodified hydrothermal sample (Fig.8.5) are completely lost.

a)                                        b)
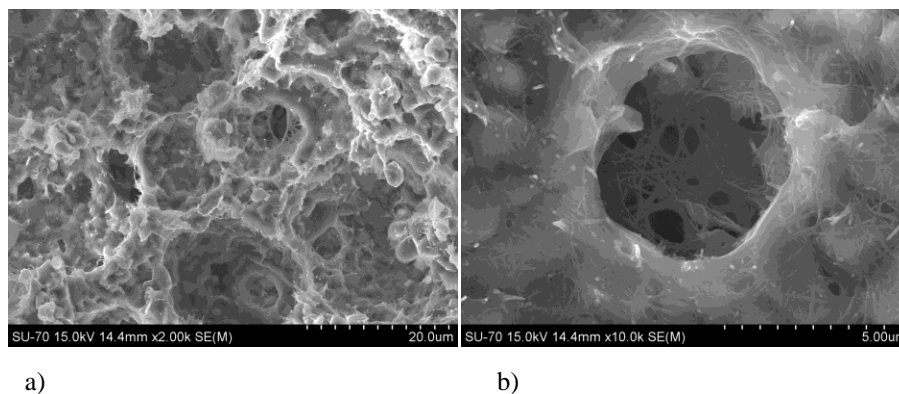
**Figure 8.14**  SEM images for samples treated with the hydrothermal process and modified using a solution of PEGDE at a concentration of 0.1 M; molar ratio between alumina and titania equal to 0.25; volume ratio between liquid paraffin and suspension equal to 1; firing conditions: $T_{peak}$=1550°C, $T_{iso}$=1300°C and $t_{iso}$=4h (corresponding to experiment E6 in the Taguchi plan).



a)                                        b)
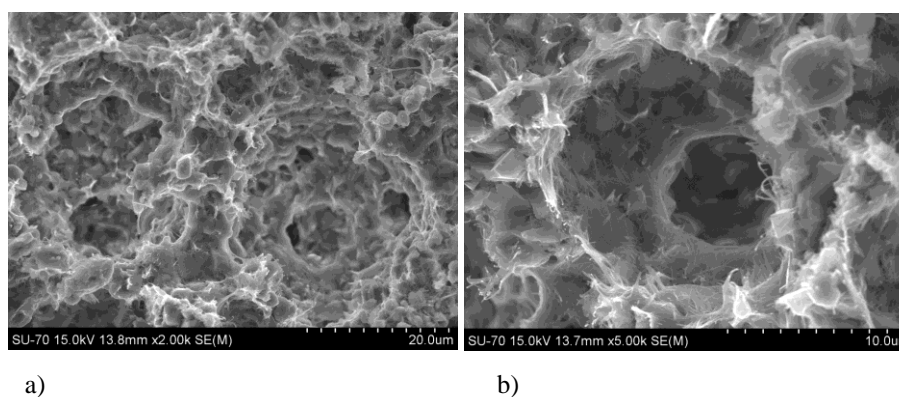
**Figure 8.15**  SEM images for samples treated with the hydrothermal process and modified using a solution of 1,4-BDE at a concentration of 1.41 M; molar ratio between alumina and titania equal to 0.25; volume ratio between liquid paraffin and suspension equal to 1; firing conditions: $T_{peak}$=1550°C, $T_{iso}$=1300°C and $t_{iso}$=4h (corresponding to experiment E6 in the Taguchi plan).



a)                                        b)
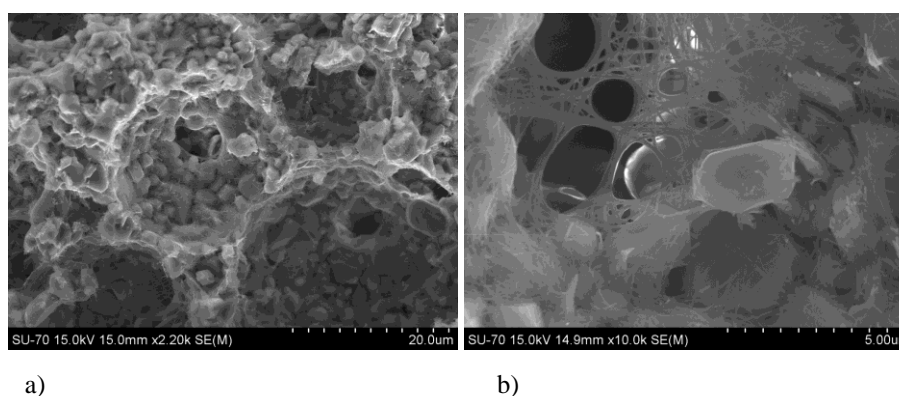
**Figure 8.16**  SEM images for samples treated with the hydrothermal process and modified using a solution of GPTMS at a concentration of 0.6 M; molar ratio between alumina and titania equal to 0.25; volume ratio between liquid paraffin and suspension equal to 1; firing conditions: $T_{peak}$=1550°C, $T_{iso}$=1300°C and $t_{iso}$=4h (corresponding to experiment E6 in the Taguchi plan).

a)                                                      b)
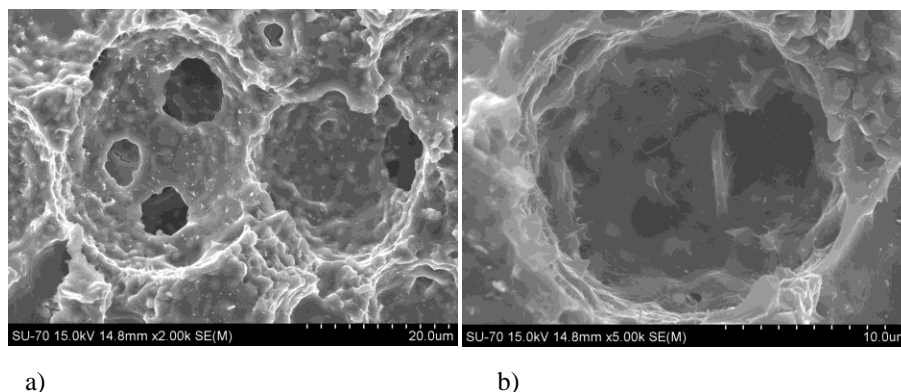
**Figure 8.17** SEM images for samples treated with the hydrothermal process and modified using a solution of APTES at a concentration of 1% v/v; molar ratio between alumina and titania equal to 0.25; volume ratio between liquid paraffin and suspension equal to 1; firing conditions: $T_{peak}$=1550°C, $T_{iso}$=1300°C and $t_{iso}$=4h (corresponding to experiment E6 in the Taguchi plan).

## 8.3 Preliminary protein adsorption tests

According to the chemical modification of the monoliths surface results, it was decided to work with chromatographic supports, not treated with the hydrothermal process, modified using the GPTMS reagent (concentration of 1.5 M, pH 14).

The use of ceramic monoliths activated with epoxy groups was reserved to preliminary BSA adsorptions experiments. The aim was to obtain information related to the density, distribution and availability of the active sites on the surface. Since the binding between BSA and epoxy groups is expected to be non-reversible, only the adsorption step was studied.

### *8.3.1 Batch experiments*

In the case of batch adsorption experiments, the ceramic material was used in small pieces and pieces crushed to powder to assess the effect of diffusion limitations and availability of the active sites on the surface.

Experiments were performed with ceramic material modified one, two and three subsequent times with GPTMS. The monolith sample was soaked in 4 mL pure BSA (0.5 mg/mL) diluted with PBS and kept under gentle agitation for 24 h. The protein concentration was measured at the beginning and at the end of this step, by absorbance reading at 280 nm. Fired ceramics samples (non-modified) were used as a control, to make sure the support itself did not interact with the proteins. Details related to characteristic of the samples used are shown in Table 8.6.

**Table 8.6**  Shape, degree of modification with GPTMS and amount of ceramic material used for batch adsorption experiments.

| Amount of material [g] | Piece | Powder |
|---|---|---|
| **No modification** | **blank 1** | **blank 2** |
| | 0.1193 | 0.1183 |
| **GPTMS I** | **a** | **b** |
| | 0.1104 | 0.1019 |
| **GPTMS II** | **c** | **d** |
| | 0.1092 | 0.1062 |
| **GPTMS III** | **e** | **f** |
| | 0.1013 | 0.1033 |

## 8.3.2 Dynamic experiments

To better understand the contribution of diffusion limitations and epoxy groups accessibility, dynamic studies were carried out in a chromatographic set-up, using the FPLC. The system dispersion curve was obtained in independent experiments under non-binding conditions, to account for the delay volumes and band broadening contributions from column holder, tubing and frits, as well as the axial dispersion in the ceramic column. The system dispersion curve was determined for a fired ceramics sample, identical to the modified one in terms of shape and dimensions, by feeding the same BSA solution. This curve was compared to the breakthrough curve: the experiments were performed at a constant flow rate of 1 mL/min, and the breakthrough curve was obtained using an epoxy activated monolith, modified one time with GPTMS, under dynamic conditions (using the cell and a peristaltic pump). In particular, three subsequent adsorption cycles were performed.

Information related to the dimensions of the columns used can be found in Table 8.7.

**Table 8.7**  Dimensions of the ceramic columns used for dynamic adsorption experiments, regarding the fired sample used as a control and the GPTMS modified column.

| | non-modified | modified |
|---|---|---|
| **diameter [cm]** | 0.990 | 0.990 |
| **length [cm]** | 1.360 | 1.360 |

### *8.3.3 Results and discussion*

#### *8.3.3.1 Batch experiments*

Batch adsorption experiments with pure solutions of BSA in PBS using fired ceramics samples (non-modified with the epoxy silane reagent) did not shown any adsorption of protein, both for pieces and powder. The results are reported in Table 8.8.

**Table 8.8**   Amount of BSA adsorbed per mg of ceramic material, as a function of the number of GPTMS subsequent modifications. Adsorption time = 24 h.

|  | Piece | | | Powder | |
|---|---|---|---|---|---|
|  |  | q mg/mg |  |  | q mg/mg |
| **Blank** | **blank1** | 0.00 | | **blank2** | 0.00 |
| **GPTMS I** | **A** | 0.47 | | **B** | 2.16 |
| **GPTMS II** | **C** | 0.81 | | **D** | 1.95 |
| **GPTMS III** | **E** | 2.85 | | **F** | 2.73 |

The results regarding the batch adsorption of BSA show that increasing the number of GPTMS modifications the amount of BSA adsorbed per mg of ceramic material increases (except for sample D, for which experimental errors might have occurred). Moreover, the samples in powder showed better performance with respect to the samples in small pieces: of course, diffusion limitations affected the experiments performed using the sample in pieces, while, crushing the samples to powder made the epoxy groups on the surface more accessible for BSA binding.

The fact that the unmodified samples did not show any adsorption of BSA was important to ensure that the ceramic material was completely inert towards the protein, and that the BSA captured by the modified samples was adsorbed due to the presence of the epoxy groups.

This result was encouraging, since the analysis performed to assess the modification of the surface did not give very encouraging results.

#### *8.3.3.2 Dynamic experiments*

Dynamic binding capacity of BSA measured during the three subsequent dynamic cycles are reported in Table 8.9.

**Table 8.9**     Amount of BSA adsorbed per mL of ceramic material during the dynamic adsorption experiments.

|  | Affinity cycle | DBC [mg/mL] |
|---|---|---|
|  | I | 0.155 |
| **BSA** | II | ~0.000 |
|  | III | 0.017 |

The highest value of DBC is obviously reached during the first cycle: in this experiment all the epoxy groups present on the surface of the pore of the ceramic monolith are saturated; the corresponding comparison between the system dispersion curve and the breakthrough curve can be observed in Fig. 8.18.
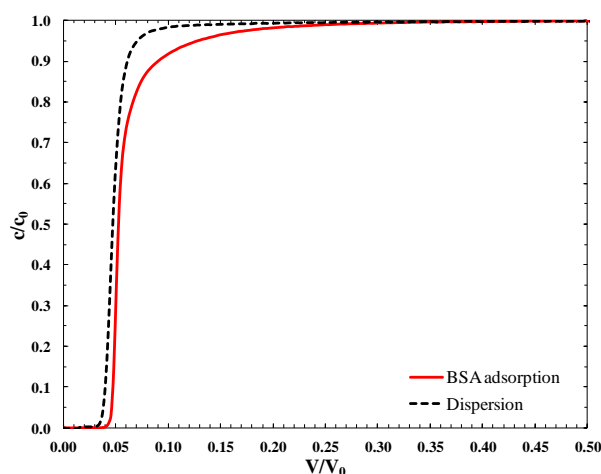


**Figure 8.18**   Comparison between system dispersion curve and BSA breakthrough curve; b) the plot is a zoom of the plot (a).

The second and third cycle did not show any significant adsorption of BSA: the binding between an epoxy group and BSA is supposed to be irreversible and this is confirmed by the obtained results. Indeed, by observing Fig 8.19 , where the complete first chromatographic cycle is illustrated, it is possible to notice that there is no elution peak: the noise visible in plot, at the end of the washing step (around 50 mL fed volume) is due to the buffer change, from PBS to the elution buffer (glycine). The absorbance reading of the first 4 mL of elution demonstrated that no protein was eluted from the monolith.

However, even if the modified monolith works as expected, the amount of BSA adsorbed is only 0.155 mg/mL; this low value represent an indication of the not efficient chemical modification of the surface. Due to lack of ceramic material, it was not possible to perform subsequent GPTMS modifications and repeat the dynamic experiments. This might have improved the dynamic binding capacity of the monolith, as it was shown for batch experiments.
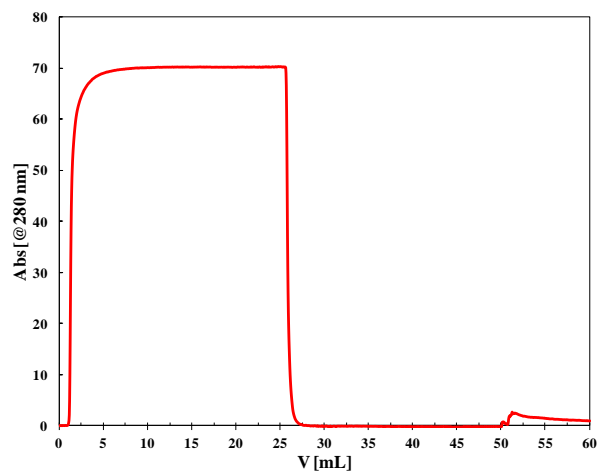
**Figure 8.19**  Complete chromatographic cycle for the GPTMS modified monolith.

The new recently designed monoliths are a promising novel chromatographic stationary phases, but the chemical modification of the surface must be improved, as well as the analytical techniques performed to quantify the amount of functional groups on the surface of the ceramic material.

# References

[1] Ik Jin Kim, *Thermal stability of Al₂TiO₅ ceramics for new diesel particulate filter applications-a literature review*, Journal of Ceramic Processing Research. 11, 4 (2010) 411-418

[2] N.M.D. Vitorino, A.V. Kovalevsky, J.C.C. Abrantes, J.R. Frade, *Hydrothermal synthesis of boehmite in cellular alumina monoliths for catalytic and separation application*, Journal of the European Ceramic Society 35 (2015) 3119-3125

[3] N.M.D. Vitorino, A.V. Kovalevsky, M.C.C. Azevedo, J.C.C. Abrantes, J.R. Frade, *Self-functionalization of cellular alumina monoliths in hydrothermal conditions*, Journal of the European Ceramic Society 36 (2016) 1053-1058

[4] J. Zhang, S. Hu, G. Zhan, X. Tang, Y. Yu, *Biobased nanocomposites from clay modified blend of epoxidized soybean oil cyanate ester resin*, Progress in Organic Coatings 76 (2013) 1683-1690

[5] W. Guo, E. Ruckenstein, *A new matrix for membrane affinity chromatography and its application to the purification of concanavalin A*, Journal of Membrane Science 182 (2001) 227-234

[6] W. Shi, Y. Shen, D. Ge, M. Xue, H. Cao, S. Huang, J. Wang, G. Zhang, F. Zhang, *Functionalized anodic aluminium oxide (AAO) membranes for affinity protein separation*, Journal of Membrane Science 325 (2008) 801-808

[7] A. Yamaguchi, F. Uejo, T. Yoda, T. Uchida, Y. Tanamura, T. Yamashita, N. Teramae, *Self-assembly of a silica-surfactant nanocomposite in a porous alumina membrane*, Nature Materials 3 (2004) 337-341

# CHAPTER 9

# Conclusions of Part II

The design and characterization of cellular ceramic monoliths, made of $Al_2TiO_5$ and $Al_2O_3$, to assess their use as novel chromatographic supports for the purification of antibodies, were described in the second part of this doctoral thesis. In particular, the experimental design and fluid dynamic characterization of the new chromatographic material were the subject of Chapter 7, while the chemical modification of the surface and the results of some preliminary adsorption tests were the subject of Chapter 8.

A combined method based on emulsification of ceramic suspensions and two-step firing procedure was applied to design the cellular ceramic monoliths: the obtain material was a cellular composite monolith with interconnected cellular microstructures.

The processing method applied allowed to change independently phase composition and porosity of the material: in particular, phase composition was adjusted by changing the ratio between the two precursors, alumina and titania, in the initial ceramic suspension; final microstructural features of the material were tuned changing the ratio between the organic phase and the suspension in the emulsification stage. These parameters provided guidelines for the upper limits of $Al_2TiO_5$ fraction and porosity of the composite cellular ceramics.

Taguchi experimental planning was used to study the impact of the two-step firing procedure parameters on phase composition, porosity and microstructural features of the final ceramic material. It was found that the excess of alumina, with respect to titania in the initial ceramic suspension, contributed to suppress the residual fraction of titania and to minimize the scattering of phase composition and porosity. This interesting aspect was found consistent with specific properties of titania, such as its ability to allow significant solubility of alumina and its faster diffusion.

Thus, it is possible to conclude that the flexible design of this material relies on the ability to take advantage of the key role of titania for enhanced solid state kinetics, while minimizing undue

microstructural changes during the reactive firing, and contributing to retain reproducible characteristics of the resulting cellular ceramics.

As far as the fluid dynamic characterization is concerned, it is possible to say that the method of moments was applied to obtain information regarding the void fraction and the axial dispersion coefficient of the ceramic monoliths, while the systematic measure of the pressure drops across this porous material allowed to obtain information regarding the hydraulic permeability.

In particular, pulse injections of different molecular weight tracers were performed under non binding conditions, to measure the void fraction and the axial dispersion coefficient, analyzing the effluent peaks using the method of moments.

The results obtained from the characterization of ceramic samples of different dimensions showed an average porosity of 58% approximately: this value was confirmed by mercury intrusion porosimetry measurements. Moreover, it was found that the void fraction did not shown a significant trend in function of the molecular weight of the tracers used; this can be explained observing that the pores of the material are quite large, with an average value of 6 μm approximately, and so the total pore volume is accessible also to large biomolecules. The average pore volume and the pore size distribution were obtained performing the mercury porosimetry analysis.

The method of moment allowed also to calculate the axial dispersion coefficient; in particular, it was found that the values of axial dispersion coefficient normalized with respect to the diffusion coefficient of each tracer presented a linear trend in function of the Péclet number: from this it was derived that the HETP of the material does not depend on the superficial velocity. This result was already reported for convective chromatographic materials and represents the potentiality of these new monolithic media, because it proves that the efficiency of the chromatographic separation does not depend on the flow rate used, as well as the dynamic binding capacity.

The measurement of the pressure drops varying the flow rate made it possible to determine the hydraulic permeability of the ceramic monoliths. This parameter was found equal to $2.06 \cdot 10^{-13}$ $m^2$, value that is much higher than those of commercial polymeric monoliths ($5.74 \cdot 10^{-15}$ $m^2$) and, if this measured value is compared to literature data related to columns packed with porous beads ($9.50 \cdot 10^{-12}$ $m^2$), it is confirmed that the lower pressure drops in the monolithic columns are not related to higher permeability, but to the fact that the bed height in the case of monoliths is

usually smaller than those of packed bed, since the permeability of packed column is usually sensibly higher.

The chemical modification of the surface was performed using different reagents to functionalize the ceramic monolith with epoxy or amine groups. This procedure was necessary to make the surface active, since after the firing procedure it was completely inert, due to the high temperatures reached. The reagents used were PEDGE, 1,4-BDE, GPTMS and APTES, Poly(ethylene glycol) diglycidyl ether, 1,4-Butanediol diglycidyl ether, (3-glycidyloxypropyl)trimethoxysilane and (3-aminopropyl)triethoxysilane respectively.

The chemical modification was performed both on fired ceramics and on samples treated with the hydrothermal process, which consist in a self-functionalising process using aggressive chemical and physical conditions. The hydrothermal process allowed to increase the hydrophilicity of the ceramic surface.

Both in the cases of hydrothermal and non-hydrothermal samples, the functionalization of the surface was found to be very poor, as demonstrated by FTIR and elemental analysis. In particular, the highest degree of modification with epoxy groups was obtained using the GPTMS reagent, with 0.36 % of carbon found on the surface, while the use of APTES allowed to obtain the highest degree of functionalization of the material, even if with amine groups.

However, since APTES samples were not stable in water and their use as chromatographic support would not have been possible, it was decided to continue the work using the GPTMS reagent, even if the degree of modification was not very high. This part of the work still needs improvements, both for the modification protocols and for the analytical techniques to quantify the density of functional groups on the surface of the ceramic monoliths.

Finally, preliminary adsorption tests were performed using samples modified with GPTMS and solutions of BSA in PBS to complete the characterization of the cellular ceramic monoliths. In particular, both batch and dynamic experiments were carried out; fired samples did not show any interaction with the protein solution, demonstrating that the protein adsorbed was due to the presence of epoxy groups on the surface of the samples.

Batch experiments were performed using ceramic samples in small pieces and in powder, modified with GPTMS one, two or three subsequent times. The results showed that increasing the number of chemical modification of the surface increased the amount of BSA adsorbed, especially for the samples in powder, demonstrating that diffusion is the controlling mass transport mechanism during batch tests.

Dynamic experiments were carried out using the FPLC and ceramic samples modified only one time with GPTMS. The amount of BSA adsorbed was very low, in the order of 0.16 mg per mL of ceramic material: this result can be explained probably by the very poor degree of modification of the surface.

As final remarks for the work regarding the design and characterization of cellular ceramic monoliths, it is possible to state that a new ceramic material was rationally designed and that it showed good properties in terms of porosity, microstructural features and permeability.

The results obtained lead to think that this new material could be easily used as a novel stationary phase for chromatographic separations, after a careful phase of sample preparation: the sintered ceramic cylinders have to be polished to remove imperfections that affect the external surface and have to be cut accurately to obtain monolithic columns of the desired dimensions. These operations are extremely important to adapt the shape and the size of the ceramic material to the those of the column holder that will be used to carry out the separation process. Moreover, it is important to ensure the hydraulic seal of the monolithic cell placing the ceramic column inside appropriate sealing elements, that will also guarantee, together with polymeric frits, the optimal flow distribution across the stationary phase.

If on the one hand, the design and preparation of the ceramic monoliths are well established, on the other hand the chemical modification of the surface represents the bottleneck of the work. It has to be improved to have many more functional and active groups that can react with the functional group of a spacer arm, with the aim of immobilizing affinity ligands for the purification of IgG.